Hua, Xiaoming

LINEAR AND NONLINEAR OPTICAL RESPONSE OF SMALL METALLIC PARTICLES AND ACCELERATED ENERGY TRANSFER OF DONOR AND ACCEPTOR MOLECULES NEAR THE SURFACE OF A SMALL PARTICLE AND A LONG FIBER

City University of New York PH.D. 1987

PLEASE NOTE:

In all cases this material has been filmed in the best possible way from the available copy. Problems encountered with this document have been identified here with a check mark __✓__.

1. Glossy photographs or pages _____
2. Colored illustrations, paper or print _____
3. Photographs with dark background _____
4. Illustrations are poor copy _____
5. Pages with black marks, not original copy _____
6. Print shows through as there is text on both sides of page _____
7. Indistinct, broken or small print on several pages ✓
8. Print exceeds margin requirements _____
9. Tightly bound copy with print lost in spine _____
10. Computer printout pages with indistinct print _____
11. Page(s) _____ lacking when material received, and not available from school or author.
12. Page(s) _____ seem to be missing in numbering only as text follows.
13. Two pages numbered _____. Text follows.
14. Curling and wrinkled pages _____
15. Dissertation contains pages with print at a slant, filmed as received ✓
16. Other _____

_____

_____

University
Microfilms
International

LINEAR AND NONLINEAR OPTICAL RESPONSE OF SMALL METALLIC PARTICLES AND ACCELERATED ENERGY TRANSFER OF DONOR AND ACCEPTOR MOLECULES NEAR THE SURFACE OF A SMALL PARTICLE AND A LONG FIBER

by

XIAOMING HUA

A dissertation submitted to the Graduate Faculty in Physics in partial fulfillment of the requirements for the degree of Doctor of Philosophy, The City University of New York.

1987

This manuscript has been read and accepted for the Graduate Faculty in Physics in satisfaction of the dissertation requirement for the degree of Doctor of Philosophy.

Oct. 30, 1986 — date — Chairman of Examining Committee

Oct. 30, 1986 — date — Executive Officer

Robert R. Alfano

Melvin Lax

Joseph L. Birman

Azriel Genack

Supervisory Committee

The City University of New York

Abstract

LINEAR AND NONLINEAR OPTICAL RESPONSE
OF SMALL METALLIC PARTICLES
AND
ACCELERATED ENERGY TRANSFER OF DONER
AND ACCEPTOR MOLECULES NEAR THE SURFACE
OF A SMALL PARTICLE AND A LONG FIBER

BY

XIAOMING HUA

Advisor: Prefessor Joel I. Gersten

In this thesis the following problems have been studied:

(a). for infrared absorption of a small metallic particle,
(b). second harmonic generation in a small metallic particle,
(c). enhanced energy transfer between a donor and acceptor molecule near a small prolate spheroidally shaped particle,
(d). enhanced energy transfer between a donor and acceptor molecule near a long fiber.

A classical model has been set up to combine the effects of electrons and acoustic phonons in metals. The ions are treated as an elastic jellium background and the electrons are treated hydrodynamically. The model has been used to calculate the far infrared absorption coefficient of a small metallic particle. The same model is also used to calculate the second harmonic generation of a small metallic particle in the frozen jellium limit. A simple dielectric model is used in the calculations of enhanced energy transfer . The materials of interest in the last two problems are not restricted to be metals.

The electric dipole absorption spectrum of a small metal particle is found to be oscillatory in the far infrared region. The magnetic dipole absorption is found to be stronger than the electric dipole absorption by a factor of 10^2.

The second harmonic generation of a small metal sphere is found to produce quadrupolar radiation as the response to an incident plane wave with positive helicity. The cross section for second harmonic generation has two resonant peaks, one corresponds to the linear dipole resonance, the other to the nonlinear quodrupole resonance.

The enhanced ratio of energy transfer between a donor

and acceptor molecule near a spheroidal particle is found to be a function of the frequency and the geometry of the system. When the molecules are inside the "active zone" and the frequency is close to the surface plasmon frequency the enhancement ratio is extremley high.

In a cylindrical configuration the long-range coupling between two molecules is found to be much stronger than the conventional dipole-dipole coupling. An excited surface mode provides a bridge for energy transfer between the two molecules.

ACKNOWLEDGEMENTS

I am greatly indebted to Prof. Joel I. Gersten for his continued help, encouragement, instruction and patient guidance during the course of this research. I am especially grateful to Mr. C. L. Wang for his continued and effective help in my use of the UNIX operating system. I thank Miss S. Das for her discussions.

My acknowledgement is also to the CUSPEA program, for without this program I might have not had a chance to write this thesis.

Contents

General Introduction

In recent years there has developed an interest in the properties of small particles. A variety of techniques have become available to prepare small particles ranging in size from what may be just called clusters of atoms to particles microns in size. Small particles differ from bulk matter in a number of important ways. Firstly they are composed of a finite number of atoms as opposed to the infinite number for bulk matter. Thus they are subject to substantial fluctuation effects, which may be either of a spatial or a temporal character. Secondly they have a non-negligible fraction of their atoms residing on the surface. Thus surface-specific effects can be more important than in a large piece of bulk solid. Thirdly the shape of the particle can be important in determining the optical properties of the system. This usually manifests itself in the depolarization field set up by the surface charge distribution. Finally quantum mechanical effects associated with the confinement of electrons into a small volume can lead to a variety of quantum size effects.

Research on the optical properties of small particles has a long history. Applications in many domains of chemistry, physics, meteorology, astronomy, and

atmospheric science have persisted.[1] In the current decade new interests have been arising in many problems involving small particles such as the work function[2], the electron scattering spectrum[3], the resonance optical response[4], the spontaneous electric dipole moments[5], the enhanced van der Waals force between small particles[6], the surface plasmon radiation[7] and so on. Lots of attention has been attracted to the anomalous far-infrared absorption of small metallic particles[8].

Interest in the nonlinear optical response of small particles is also increasing[9]. This is due to the fact that the local fields in the vicinity of a small particle would be modified strongly either by the resonance mechanism or by the morphology of the particle. The interest in studying the enhanced and quenching effects of some physical, chemical and biophysical processes when they occur near the surface of the small particle is highly appreciated[10]. Besides the single particle properties, research on the properties of the composition of small particles is very active. The percolation, cluster formation and fractal structure of systems composed of small particles have become some of the most tantalizing subjects in condensed matter research. On the other hand, research on the quantum properties of an isolated, very small cluster of atoms is progressing year by year.

In this thesis the linear and nonlinear optical response of a single, small, but macroscopic particle has been studied. Customarily a small particle is still considered macroscopic even if its size is much smaller than the wavelength of light it interacts with and the classical skin depth, if it is much larger than the lattice constant. In the linear response part of this thesis we emphasize the far-infrared absorption properties. The acoustic phonon exitation and screening effect are considered in combination with electronic effects. The difference between the traditional Mie solution and our results is obvious. In the nonlinear response part we emphasize the second harmonic generation (SHG) by the conduction electrons in a small metallic sphere. The difference between Jha's early work[9] and our results is given. The study of enhanced energy transfer between donor and acceptor molecules near the surface of a small particle and a infinitely long cylinder is also described in the thesis. In these calculations a simple dielectric model is used. The predicted enhancement ratio of energy transfer is so high that it is not difficult to be observed experimentally.

The thesis is arranged as follows. In chapter I a classical model of a small metallic particle is built up to study the linear optical response in the far-infrared region. The same model is used in chapter II to study SHG

of a small sphere. Chapter III is devoted to the enhanced energy transfer between the molecules near a solid spheroidal article. The calculation for the cylindrical geometry is presented in chapter IV.

References:

1. The early research results were well collected in books: see M. Kerker, "The Scattering of Light and Other Electromagnetic Radiation", (Acadamic, New York, 1965); H. C. van de Hulst, "Light Scattering by Small Particles", (Wiley, New York, 1957); N. C. Wickramasinghe, "Light Scattering Functions for Small Particles with Application in Astronomy", (Wiley, New York, 1973); and C. F. Bohren and D. R. Huffman, "Absorption and scattering of Light by Small Particles", (Wiley, New York, 1983).
2. W. Ekardt, Phys. Rev. B 29, 1558(1984).
3. P. C. Das and J. I. Gersten, Phys. Rev. B 27, 5412(1983)
4. J. I. Gersten and A. NItzan, Phys. Rev. B 29, 3852(1984)
5. P. C. Das and J. I. Gersten, J. Chem. Phys. 76, 3177(1982)

6. H. Burtscher and A. Schmidt-Ott, Phys. Rev. Lett. 48, 1734(1982)

7. J. W. Little, T. A. Callott, T. L. Ferrell and E. T. Arakawa, Phys. Rev. B 29, 1606(1984)

8. See the references in chapter I.

9. See the references in chapter II.

10. see the references in chapter III.

Chapter I Far Infrared Absorption of Small Metallic Particle

1.1 Introduction

In 1974 Granqvist and Buhrman[1] developed a technique, based on inert-gas evaporation, in which smaller and better characterized particles can be produced. They also found that the size dependence of a small particle sample has a log-normal distribution where the number of particles Δn per logarithmic diameter interval $\Delta(\ln x)$ is $\Delta n = f_{LN}\,\Delta(\ln x)$ with

$$f_{LN} = \frac{1}{\sqrt{2\pi}\,\ln \sigma_g} \exp\left[-\frac{1}{2}\left(\frac{\ln(x/x_M)}{\ln \sigma_g}\right)^2\right] , \qquad (1.1.1)$$

where x_M denote the statistical median of the diameters and σ_g is given experimentally by

$$\sigma_g = 1.48 \pm 0.12 \quad . \qquad (1.1.2)$$

The shape of inert-gas evaporated particles smaller than about 200 Å is almost spherical, while for larger sizes crystal faces are normally seen. According to the Gibbs-Wulff relation[10,11], the external shape is governed by

$$\Sigma_i \, \gamma_i \, A_i = \text{minimum} ,$$

where γ_i is the specific surface free energy of the

i^{th} face, whose area is A_i. This criterion predicts polyhedral shapes for crystalline particles. But for the particles smaller than 200 Å, this apparently fails.

As the technique for making small particle samples became available, Tanner et al.[3] and Granqvist et al.[4] made the first measurements of the far-infrared absorption of small particles. Their purpose was to check the Kubo formula[12] and the Gor'kov-Eliashberg (GE) theory[2].

Fröhlich[13] was the first to point out that the conduction electrons in small metallic particles occupy quantized energy levels. Kubo[12] showed that the mean energy level spacing at the Fermi surface is just the inverse of the density of states for one spin direction of the free electron gas

$$\Delta = 2\pi^2\hbar^2/Vm^*k_f = 4E_f/3N \quad , \qquad (1.1.3)$$

where V is the volume of the particle, m^* is the effective mass of the electrons, N is the number of free electrons in the particle, and k_f and E_f are the Fermi momentum and energy.

Gor'kov et al.[2] pointed out that the distribution of the conduction electron energy levels should be random even if the particles have the same volume and shape, because the electrons in the metal have a wavelength on the order of atomic dimensions. Therefore surface irregularities of atomic size are sufficient to make the energy level distribution perfectly random. They borrowed

the concept of level distribution based on complete randomness of interactions from Wigner[14] and Dyson[15,16]. They studied the distribution of eigenvalues of matricies whose matrix elements were random variables. These distribution were found to depend on gross symmetry properties of the matricies, such as on their being orthogonal, sympletic or unitary: 1). orthogonal, which describes systems that are invariant under time and space inversion, or with integer spin; 2). symplectic, invariant under time reversal; the total spin of the system is half-integer; 3). unitary, for systems that are not invariant under time reversal. The major prediction of the GE theory is the derivation of the electronic susceptibility of the small metal particles, which can be written as

$$\chi = \Lambda k_f x^2/(20\pi^2 a_B) + 139\Lambda A(\eta)/(1200\pi^2 a_B k_f)$$

where Λ is defined by $m^* = \Lambda m$ with m = free electron mass, and a_B is Bohr radius. Factor $A(\eta)$ depends on the ensembles,

$$A^{orth}(\eta) = A(w)$$
$$= 2 - w^{-1}\sin 2w - 2C_i(w)(\sin w/w - \cos w)$$
$$+ i[2w - 1/w + \cos 2w/w - S_i(w)(\sin w/w - \cos w)] \quad ,$$

$$A^{symp}(\eta)=A(z)$$
$$=2-(2z)^{-1}\sin 2z(\cos z/z+\sin z)[S_i(z)+\pi/2]$$
$$+i[z-\sin^2 z/z-(\sin z/z+\cos z)(S_i(z)+\pi/2)] ,$$

where $z=2w=(2\pi)^2 hc\tilde{\nu}/\Delta$, $\tilde{\nu}$ is the wave number of the external fields, and S_i and C_i are the sine and cosine integral. When the spin-orbit coupling is weak (light metals) the orthogonal ensemble applies, if it is strong (heavy metals) the symplectic ensemble would be used.

The first experimental measurement[4] and the following series of measurements[5-7] showed that the GE theory is not applicable to small metallic particles both because no multiple peaks have been found in the far-infrared absorption measurements and , more importantly, the absolute magnitude of the absorption coefficients is in a few orders higher than that predicted by GE theory.

Granqvist et al.[4] pointed out that the multiple-peak structure would be smeared if the parameter σ_g of size distribution function is larger than 1.1 . Until today no technique is available to prepare ultrafine particle samples with σ_g is as small as 1.1 . Even putting this aside, there is still a big gap between the GE theory and the experimental data.

The phenomenon that the finite size of a small particle splits the energy band structure of the conduction

electrons into a series discrete energy levels is now called the quantum size effect [55]. Many researchers contributed to the theory of the quantum size effect [26-30]. People discussed in detail under what conditions the quantum size effect would be important and the related problem of when the metal-insulator transition would occur. They did get enhanced far-infrared absorption when they applied their theory to the problem, but the magnitude of the absorption coefficients was still one or two orders lower than what observed experimentally. Besides, the experimental observations extended to particle radii up to 1 micron in radius[5] without a pronounced difference from the observations made at 24 Å. If quantum size effect were really important, one would perhaps have expected to see a qualitative change as the size of the particle was allowed to increase by 3 orders of magnitude.

The attempt to observe the quantum size effect is still going on, but a general belief exists today that the anomalous far-infrared absorption of small particles is not maily caused by it. In contrast to the quantum mechanical theories, a number of classical mechanisms leading to infrared absorption have also been studied. Simanek[31] and Ruppin[32] attributed the large far-infrared absorption to the oxide coating on the surface of the particles. In their calculation the

oxide-coated metal particles are aggregated into long cylinders, which enhance the absorption. (Electron microscopy of gas evaporated particles frequently shows that fine particles have clustered into long chains.)[1] Experimental measurements on palladium[5,6] (it does not oxidize) and directly on aluminum oxide particles[6] showed that the absorption by a thin oxide layer is negligible. But the existence of the oxide layer does reduce the volume fraction (or the filling factor) of metal, and when the volume fraction of metal is small this fact should be accounted for. The calculation by Sen et al.[33] also showed that the oxide absorption and long chain aggregation do not give an absorption large enough to explain the experiments.

Stroud and Pan[34] suggested that the effects of induced magnetic dipole should be considered to include the eddy current losses. Later Russell et al.[5], Carr et al.[6], and Devaty et al.[7] pointed out that when the radius of the particles is not very small (around 100 Å or less) the magnetic dipole term would dominate the electric dipole term or , at least, have equal importance. The calculation by Stroud and Pan[34] predicted a magnitude of the absorption coefficient about a factor of 10 smaller than that actually observed.

Instead of the electron contribution Glick and Yorke[35] proposed that the strong infrared absorption

arises from the direct excitation of phonon modes by the field acting on unscreened surface ions. Monreal et al.[36] found that for frequencies ranging from 100 cm^{-1} to 200 cm^{-1} phonon absorption dominates over the contribution coming from electric excitations or Joule heating. Shen[37] showed that in contrast to bulk metal, the phonon absorption by small metal spheres can be fairly appreciable because the spherical surfaces not only break the momentum conservation requirement for absorption transitions (which forbids acoustic phonon absorption in bulk crystals), but also enhance the coupling between the phonon and the electromagnetic radiation through incomplete screening of the surface jellium-density modulations arising from elastic vibrations. Hua and Gersten[38] presented a classical theory to combine the effects of electrons and phonons, and found that while the electric dipole absorption is stronger than what it was previously thought to be, the magnetic dipole absorption is significantly altered by phonon effects.

As has been pointed out by Kreibig et al.[39] the single particle optical properties are often veiled in many particle systems by effective medium and clustering effects. Indeed, the morphology of the samples upon which the measurements have been performed[3-6] reveal the presence of complicated clustering patterns and nonuniform size distributions. Gerardy and Ausloos did concrete

calculations of the absorption spectrum of binary spheres in the optical region in their series of papers[40]. They showed explicitly that in a powder made of binary clusters of various sized spheres the absorption spectrum would consist of a rather broad absorption band with some smooth structure nevertheless .

Historically[41], two different theoretical approachs have been made to calculate the dielectric function of composities. The first, known as Maxwell-Garnett theory (MGT), was a molecular-field model due originally to Clausius and Mosotti and applied to optical properties by Garnett[42]. The second was a self-consistent embedding technique developed by Bruggeman[43] and studied quantitatively by Landauer[44], and recently by Stroud[45] and Liebsch et al.[50]. This is called the effective medium approximation (EMA).

In MGT, the metal particles are considered to be randomly embedded in the insulating medium. It is further assumed that the particles do not make contact so that the theory is restricted to very dilute systems. The MGT dielectric function, ϵ_G , is defined as the ratio of volume-averaged displacement to the volume-averaged electric field and is given by

$$\epsilon_G = \epsilon_i + 3f\epsilon_i \frac{\epsilon_m - \epsilon_i}{(1-f)\epsilon_m + (2+f)\epsilon_i} \quad , \qquad (1.1.4)$$

where ϵ_i is the dielectric function of the insulating host and ϵ_m that of the metallic inclusions and f is the filling factor.

In EMA, the dielectric function of the composite , ϵ_B, is defined to be equal to that of a self-consistent effective medium. The self-consistency condition is that the electric field (and, therefore, the current and polarization) in the effective medium equals the averaged field (and current and polarization) in the inhomogeneous medium. EMA treats each constituent of the mixure on an equal basis. A particular grain is chosen for consideration and outside this grain the material is assumed to have a homogeneous dielectric function, ϵ_B . Volume averaging the fields then gives a quadratic equation for ϵ_B :

$$f\frac{\epsilon_m - \epsilon_B}{\epsilon_m + 2\epsilon_B} + (1-f)\frac{\epsilon_i - \epsilon_B}{\epsilon_i + 2\epsilon_B} = 0. \qquad (1.1.5)$$

Of the two solutions to the equation the one with the positive imaginary part is physically significant. One can construct[5] the effective magnetic permeability similar to the above equations by using MGT and EMA respectively. It is easy to see that when $f << 1$, $\epsilon_B \sim \epsilon_i$, the EMA equation goes over to the MGT formula, i.e., at low concentrations MGT and EMA give identical results.

Both MGT and EMA were derived at zero frequency and

extended to a finite frequency in a naive manner. It is quite certain that for high frequencies they break down. Stroud et al.[34] developed a dynamic effective medium approximation (DEMA) also known as the coherent potential approximation. They showed that the self-consistency condition is rigorously equivalent to the requirement that the forward scattering amplitudes of the particles in the composite, measured relative to ϵ_{eff}, should vanish on the average. Cheylek et al. used DEMA and also considered the size distribution of the particles[46], and applied the formula to the far-infrared absorption problem[47]. They obtained a strong absorption and fitted the experimental data. Later people, including themselves, realized that an incorrect approximation made this happen[38,48,49].

Devaty et al.[7] were able to get a well-dispersed sample of particles by adding the desired volume fraction of gelatin into $AgNO_3$ to get a Ag hydrosol. The water is removed by successive dilutions with acetone or by freeze drying. They showed that the far-infrared absorption of well-dispersed metal particles is not enhanced by more than 10^2. Curtin et al.[8] used the heat treatment of the small Sn particles to get clustering of particles. Based on these two experiments Curtin and Ashcroft[51] declare that the anomalous absorption is due to a clustering effect. They have made three models for

clustering, i.e., the fused cluster, cluster percolation and cluster tunnel junction. Each of these models satisfies the experimental data well. Perhaps due to mathematical difficulties there is no further closed-form theoretical work on the clustering effect which has been published.

Recently research on the localization of electromagnetic waves by a randomly distributed dielectric system is also active[52,53]. A deep understanding of photon localization may also be helpful in solving the problem of the anomalous absorption of small particles in far-infrared as well as in the optical region.

In summary, for a full understanding of anomalous far-infrared absorption of small particles one should study the single particle properties as well as all the enviromental effects. For a very dilute and well-dispersed composite single particle absorption would be the dominant effect. As the volume fraction of the particles increases the multiple scattering, clustering and other possible mechanisms related to the topology of the whole system will become more and more important.

In this chapter a classical theory for far-infrared absorption of an isolated metal particle, taking into account the coupled electron-phonon modes of the system has been developed. The chapter is based on the work [38], and arranged as follows. In section II a classical model

is introduced to combine the effects of electrons and acoustic phonons and general theoretical relationships are presented. In section III and IV the electric polarizability and magnetic polarizability , respectively, are studied, both are under long wavelength approximation. The full electrodynamical treatment is given in Appendix B. In section V the infrared absorption spectrum of small particles is discussed and the results of the calculation are presented.

1.2. Theory

We will be concerned with the interaction of a metallic sphere of radius a with a long-wavelength electromagnetic wave. Thus we assume that $a \ll \lambda$, where λ is the wavelength. The problem then reduces to the study of the interaction of the sphere with externally imposed, uniform, time-varying electric and magnetic fields $E_0(t)$ and $B_0(t)$. We shall start by considering the response to the electric field and derive an expression for the electric polarizability. Then we will consider the response to the magnetic field and obtain the corresponding expression for the magnetic response. In terms of these expressions we can compute the absorption constant for an assembly of spheres.

A number of approximations will be made. The electrons will be treated as a classical continuum fluid. The background ions will be treated as an isotropic elastic jellium medium. This allows us to consider phonon effects, but obviously neglects the pointlike nature of the ions and ignores the lattice symmetry.

The basic equations governing the system are Gauss's law,

$$\nabla \cdot \vec{E} = 4\pi\rho \quad , \tag{1.2.1}$$

the ion continuity equation,

$$\partial_t n_+ + \nabla \cdot \vec{J}_+ = 0 \quad , \tag{1.2.2}$$

the electron continuity equation,

$$\partial_t n_- + \nabla \cdot \vec{J}_- = 0 \ , \qquad (1.2.3)$$

Gauss's law for magnetism,

$$\nabla \cdot \vec{B} = 0 \ , \qquad (1.2.4)$$

Faraday's law,

$$\nabla \times \vec{E} + c^{-1} \partial_t \vec{B} = 0 \ , \qquad (1.2.5)$$

Ampere's law,

$$\nabla \times \vec{B} - c^{-1} \partial_t \vec{E} = \frac{4\pi}{c} \vec{J}, \qquad (1.2.6)$$

the equation of motion of an electron,

$$m_e[d\vec{v}/dt + \vec{v}/\tau] = -e[\vec{E} + \vec{v} \times \vec{B}/c] - \nabla\mu \ , \qquad (1.2.7)$$

(the derivation of the equation of motion of an electron (1.2.7) from the Boltzmann equation under the relaxation time approximation is presented in appendix A.) The chemical potential accounts for the screening.

and the equation of motion for the ions,

$$\rho_i \left[\frac{d^2\vec{u}}{dt^2} + \gamma \frac{d\vec{u}}{dt}\right] = n_+ Ze\left[\vec{E} + \frac{1}{c}\partial_t \vec{u} \times \vec{B}\right] + \alpha \nabla^2 \vec{u} + \beta \nabla \nabla \cdot \vec{u}. \qquad (1.2.8)$$

In these equations, $\vec{E}$ and $\vec{B}$ denote the electric and magnetic fields, ρ is the charge density, $\vec{J}$ is the current density, $n_+(r)$ is the number of ions per unit volume, $\vec{J}_+$ is the ion flux vector, $n_-(r)$ is the number of electrons per unit volume, $\vec{J}_-$ is the electron flux vector, m_e is the electron's mass and e the magnitude of its charge, τ is the collisional relaxation time for the electron, $\vec{v}$ is the electron velocity field, μ is the

chemical potential, ρ_i is the ion mass density, $\vec{u}$ is the ion displacement vector field, γ is the ion relaxation rate, Z is the valence charge of the ion, and α and β represent elastic constants for the isotropic ionic medium. In terms of these quantities, we have

$$\rho = e(Zn_+ - n_-) \quad , \tag{1.2.9}$$

$$\vec{J} = e[\, Zn_+ \partial_t \vec{u} - n_- \vec{v} \,] \quad , \tag{1.2.10}$$

$$\vec{J}_+ = n_+ \partial_t \vec{u} \quad , \tag{1.2.11}$$

$$\vec{J}_- = n_- \vec{v} \quad , \tag{1.2.12}$$

In Thomas-Fermi-Dirac theory the chemical potential is

$$\mu = (\hbar k_f)^2/2m_e - e^2(3n_-/\pi)^{1/3} \quad , \tag{1.2.13}$$

where k_f is the Fermi wave vector,

$$k_f = (3\pi^2 n_-)^{1/3} \quad . \tag{1.2.14}$$

The first term in Eq.(1.2.13) results from the kinetic energy of the electrons, while the second term is the exchange energy contribution. Correlation energy contributions are much smaller and will be neglected.

For metals, where the conductivity is high, the conduction current dominates the displacment current. Thus in place of Eq.(1.2.6), we will use

$$\nabla \times \vec{B} \cong (4\pi/c)\vec{J} \quad . \tag{1.2.6'}$$

Since $|\vec{v}| << c$ and $|\partial_t \vec{u}| << c$, we will neglect the magnetic force contribution to Eqs.(1.2.7) and (1.2.8).

We will be interested in the linear response of the sphere to the fields $\vec{E}_o$ and $\vec{B}_o$, which will be taken to have the harmonic time behavior $\exp(-i\omega t)$, where ω is

the angular frequency of the radiation. Thus, we let

$$n_+ = Z^{-1}(n_o + \nu_+) \quad , \tag{1.2.15}$$

$$n_- = n_o + \nu_- \quad , \tag{1.2.16}$$

where n_o is the mean number of electrons per unit volume and $\nu_\pm$ are density fluctuations. We will assume $\nu_\pm \ll n_o$ and linearize the preceding equations. The above equations then reduce to

$$\nabla \cdot \vec{E} = 4\pi e(\nu_+ - \nu_-) \quad , \tag{1.2.17}$$

$$\nabla \cdot \vec{B} = 0 \quad , \tag{1.2.18}$$

$$\nabla \times \vec{E} = i\frac{\omega}{c}\vec{B} \quad , \tag{1.2.19}$$

$$\nabla \times \vec{B} = -4\pi e n_o(i\omega\vec{u} + \vec{v})/c \quad , \tag{1.2.20}$$

$$\nabla \cdot \vec{u} = -\nu_+/n_o \quad , \tag{1.2.21}$$

$$\nabla \cdot \vec{v} = i\omega\nu_-/n_o \quad , \tag{1.2.22}$$

$$m_e[-i\omega + 1/\tau]\vec{v} = -e\vec{E} - \chi_o \nabla \nu_- , \tag{1.2.23}$$

$$-\rho_i(\omega^2 + i\gamma\omega)\vec{u} = n_o e\vec{E} + \alpha\nabla^2\vec{u} + \beta\nabla\nabla\cdot\vec{u}, \tag{1.2.24}$$

where the constant that results from linearizing the chemical potential is

$$\chi_o = (\hbar k_f)^2/3m_e n_o - e^2 k_f/3\pi n_o \quad . \tag{1.2.25}$$

The Fermi wave vector in Eq.(1.2.25) is now evaluated using the mean electron density n_o, Eqs.(1.2.17)-(1.2.24) will be solved analytically in the next sections for the electric and magnetic response.

1.3. Electric Polarizability

In studying the electric polarizability let us neglect the magnetic field altogether and disregard Eq.(1.2.20). In place of Eq.(1.2.19) we then introduce the scalar potential so that

$$\vec{E} = -\nabla\phi \quad . \tag{1.3.1}$$

Eq.(1.2.17) is replaced by

$$\nabla^2\phi = -4\pi e(\nu_+ - \nu_-) \quad , \tag{1.3.2}$$

Eq.(1.2.23) may be solved for $\vec{v}$,

$$\vec{v} = i[m_e(\omega + i/\tau)]^{-1}(e\nabla\phi - \chi_o\nabla\nu_-) \quad . \tag{1.3.3}$$

Taking the divergence of Eqs.(1.3.3) and (1.2.24), and combining them with Eqs.(1.2.21) and (1.2.22), yields

$$[\omega(\omega + i/\tau)\omega_p^{-2} - 1]\nu_- + \lambda^{-2}\nabla^2\nu_- = -\nu_+ \tag{1.3.4}$$

$$[\omega(\omega + i\gamma)\Omega_p^{-2} - 1]\nu_+ + \Lambda^{-2}\nabla^2\nu_+ = -\nu_- \tag{1.3.5}$$

Here we have introduced the electron plasma frequency

$$\omega_p = [4\pi n_o e^2/m_e]^{1/2} \quad , \tag{1.3.6}$$

the ion plasma frequency

$$\Omega_p = n_o e(4\pi/\rho_i)^{1/2} \quad , \tag{1.3.7}$$

the Thomas-Fermi-Dirac electronic screening constant

$$\lambda = \omega_p[m_e/\chi_o n_o]^{1/2} \quad , \tag{1.3.8}$$

and what will be termed the "ion screening constant",

$$\Lambda = \Omega_p/c_\ell \quad . \tag{1.3.9}$$

In place of the elastic constants α and β, it is convenient to introduce two other constants with the dimensions of velocity

$$c_\ell = [(\alpha+\beta)/\rho_i]^{1/2} \quad , \tag{1.3.10}$$

and

$$c_t = [\alpha/\rho_i]^{1/2} \quad . \tag{1.3.11}$$

These represent the unrenormalized longitudinal and transverse sound velocities.

Eqs.(1.3.4) and (1.3.5) represent second-order partial differential equations for the electron and ion density fluctuations. Let us choose the z axis to be along the direction of the external electric field $\vec{E}_o$. We will look for a dipolar fluctuation, i.e.,

$$\nu_\pm = A_\pm j_1(kr)\cos\theta \quad , \tag{1.3.12}$$

where A_+ and A_- are constants to be determined, r is the radial distance from the center of the sphere, $j_1(kr)$ is a spherical Bessel function, and θ is the polar angle. Eqs.(1.3.4) and (1.3.5) reduce to

$$[\omega(\omega+i/\tau)/\omega_p^2 - 1 - (k/\lambda)^2]A_- = -A_+ , \tag{1.3.13}$$

and

$$[\omega(\omega+i\gamma)/\Omega_p^2 - 1 - (k/\Lambda)^2]A_+ = -A_- , \tag{1.3.14}$$

There are two possibilities for a solution to Eqs.(1.3.13) and (1.3.14). The first corresponds to the

"trivial" case $A_+=A_-=0$. The second corresponds to the case where

$$[\omega(\omega+i\gamma)/\Omega_p^2-1+(k/\Lambda)^2] \times [\omega(\omega+i/\tau)/\omega_p^2-1-(k/\lambda)^2] = 1 \ . \qquad (1.3.15)$$

We start by considering the nontrivial case first. The solutions to Eq.(1.3.15) may be written as

$$k_+^2=k^2 = 0.5\left\{\lambda^2\epsilon(1-\epsilon)^{-1}+\Lambda^2\epsilon_i(1-\epsilon_i)^{-1} + \sqrt{[\lambda^2\epsilon(1-\epsilon)^{-1}-\Lambda^2\epsilon_i(1-\epsilon_i)^{-1}]^2+(2\lambda\Lambda)^2}\right\} \qquad (1.3.16)$$

and

$$k_-^2=-p^2 = 0.5\left\{\lambda^2\epsilon(1-\epsilon)^{-1}+\Lambda^2\epsilon_i(1-\epsilon_i)^{-1} - \sqrt{[\lambda^2\epsilon(1-\epsilon)^{-1}-\Lambda^2\epsilon_i(1-\epsilon_i)^{-1}]^2+(2\lambda\Lambda)^2}\right\} \qquad (1.3.17)$$

where ϵ is the Drude dielectric function and ϵ_i, the so named "ion dielectric function", they are defined as

$$\epsilon = 1 - \omega_p^2/\omega(\omega+i/\tau) \ , \qquad (1.3.16')$$

$$\epsilon_i = 1 - \Omega_p^2/\omega(\omega+i\gamma) \ . \qquad (1.3.17')$$

The general solution to Eqs.(1.3.4) and (1.3.5) may therefore be written as a linear combination of spherical Bessel functions,

$$\mathcal{V}_{\pm}=[A_{\pm}j_1(kr)+B_{\pm}i_1(pr)+C_{\pm}n_1(kr)+D_{\pm}k_1(pr)]\cos\theta \tag{1.3.18}$$

From Eq.(1.3.14) and its analogs, we have

$$A_-=A_+[1-(k/\Lambda)^2-\omega(\omega+i\Gamma)/\Omega_p^2]=Q_1A_+, \tag{1.3.19}$$

$$B_-=B_+[1-(p/\Lambda)^2-\omega(\omega+i\Gamma)/\Omega_p^2]=Q_2B_+, \tag{1.3.20}$$

In order for $\mathcal{V}_+$ and $\mathcal{V}_-$ to remain finite as r approaches 0, it may be shown that $C_+=C_-=D_+=D_-=0$.

Insertion of Eqs.(1.3.18) into (1.3.2) and then searching for a dipolar solution to the resulting Poisson equation gives

$$\Phi(r)=[C_0r+C_1j_1(kr)+C_2i_1(pr)]\cos\theta \quad , \quad r<a \tag{1.3.21}$$

and

$$\Phi(r)=[-E_0r+\mu_s/r^2]\cos\theta \quad , \quad r>a \tag{1.3.22}$$

Here, C_0, C_1 and C_2 are constants to be determined. The electric dipole moment of the sphere, μ_s, is also to be determined. Since the matter that the sphere is composed of consists of ions and electrons, the boundary conditions are that the potential be continuous at r=a, and also that the radial component of the electric field, E_r, be likewise continuous. These result in the relations

$$C_0=-E_0-(C_1x/3a)j_0(x)-(C_2z/3a)i_0(z), \tag{1.3.23}$$

and

$$\mu_s=a^2[C_1xj_2(x)-C_2zi_2(z)]/3 \quad , \tag{1.3.24}$$

where

$$x=ka \quad , \tag{1.3.25}$$

and

$$z=pa \quad . \tag{1.3.26}$$

Inserting Eq.(1.3.21) into the Poisson equation yields the following expressions for C_1 and C_2:

$$C_1=4\pi e(1-Q_1)A_+/k^2 \quad , \tag{1.3.27}$$

and

$$C_2=-4\pi e(1-Q_2)B_+/p^2 \quad . \tag{1.3.28}$$

Next, we focus our attention on the ion displacement field $\vec{u}$, which obeys Eq.(1.2.24). We let

$$\vec{r}\cdot\vec{u}=F(r)\cos\theta \ . \tag{1.3.29}$$

We make use of the identity

$$\vec{r}\cdot\nabla^2\vec{u}=\nabla^2(\vec{r}\cdot\vec{u})-2\nabla\cdot\vec{u} \quad , \tag{1.3.30}$$

and Eqs.(1.2.21), (1.2.24), (1.3.1), (1.3.18) and (1.3.21), to obtain

$$\begin{aligned}&(\nabla^2+q^2)F(r)\cos\theta\\ &=\{n_oe\alpha^{-1}[C_or+C_1krj_1'(kr)+C_2pri_1'(pr)]\\ &\quad+\beta(\alpha n_o)^{-1}[A_+krj_1'(kr)+B_+pri_1'(pr)]\\ &\quad-2n_o^{-1}[A_+j_1(kr)+B_+i_1(pr)]\}\cos\theta \ ,\end{aligned} \tag{1.3.31}$$

where we have defined

$$q^2 = \omega(\omega + i\gamma)/c_t^2 \quad . \tag{1.3.32}$$

The solution to Eq.(1.3.31) which is finite at the origin is

$$F(r) = Dj_1(qr) + n_o e C_0 r/\alpha q^2 + rA_+ j_1'(kr)/n_o k - rB_+ i_1'(pr)/n_o p \tag{1.3.33}$$

where D is an integration constant.

The displacement vector may be expressed as

$$\vec{u} = \hat{r}(F(r)/r)\cos\theta + \hat{\theta} G(r)\sin\theta \quad , \tag{1.3.34}$$

where $\hat{\theta}$ is a unit vector in the polar-angle direction. Eq.(1.2.21) gives us an equation from which we can determine G(r):

$$r^{-2}d(rF)/dr + 2Gr^{-1} = -n_o^{-1}[A_+ j_1(kr) + B_+ i_1(pr)] \tag{1.3.35}$$

and thus

$$G(r) = r[-(D/2r^2)[j_1(qr) + qrj_1'(qr)] - n_o e C_o/\alpha q^2 r - A_+ j_1(kr)/n_o(kr)^2 + B_+ i_1(pr)/n_o(pr)^2] \quad . \tag{1.3.36}$$

We must impose boundary conditions on the system. Three constants need to be determined, A_+, B_+, and D. In terms of these, the other constants may be obtained. Hence, three boundary conditions are called for.

Two boundary conditions result from the fact that the

stress must vanish on the surface of the sphere. An expression for the stress tensor may be derived from Eqs.(1.2.7) and (1.2.8). It will be necessary to neglect damping to obtain this expression, however. The resulting expression will therefore be approximate. However since we are ultimately interested in the absorption of the sphere, and this is linearly proportional to the damping, the accuracy is still maintained to first order in the damping. The net force on the system (ions and electrons) is

$$\vec{F} = \int (\rho_i \ddot{\vec{u}} + n_o m_e \ddot{\vec{v}}) d\vec{r} \quad . \tag{1.3.37}$$

This may be written as

$$\vec{F} = \int (-n_o \nabla \mu + \alpha \nabla^2 \vec{u} + \beta \nabla \nabla \cdot \vec{u}) d\vec{r} \quad . \tag{1.3.38}$$

Making use of standard vector identities allows us to rewrite this as a surface integral,

$$\vec{F} = \int \hat{r} \cdot \overleftrightarrow{\sigma} \, dS \quad , \tag{1.3.39}$$

where the stress tensor is given by

$$\overleftrightarrow{\sigma} = -\mu n_o \overleftrightarrow{I} + 2\alpha \overleftrightarrow{u} + (\beta - \alpha) \overleftrightarrow{I} \nabla \cdot \vec{u} \quad . \tag{1.3.40}$$

Here, $\overleftrightarrow{u}$ is the strain dyadic whose elements are given by

$$u_{ij} = 0.5[\partial_j u_i + \partial_i u_j] \quad , \tag{1.3.41}$$

and $\overleftrightarrow{I}$ is the unit dyadic. The vanishing of the surface stress implies

$$\hat{r} \cdot \overleftrightarrow{\sigma} \cdot \hat{r} = 0 = -\mu n_o + 2\alpha u_{rr} + (\beta - \alpha) \nabla \cdot \vec{u} \quad , \tag{1.3.42}$$

and

$$\hat{r} \cdot \overleftrightarrow{\sigma} \cdot \hat{\theta} = 0 = 2\alpha u_{r\theta} \quad . \tag{1.3.43}$$

Using the formulas

$$u_{rr} = \partial_r u_r \ , \tag{1.3.44}$$

and

$$u_{r\theta} = 0.5[\partial_r u_\theta - r^{-1} u_\theta + r^{-1} \partial_\theta u_r] \ , \tag{1.3.45}$$

we obtain the boundary conditions(at r=a)

$$2\alpha r^{-1} \partial_r F - 2\alpha r^{-2} F - \mu n_o/\cos\theta + (\beta - \alpha) \nabla \cdot \vec{u}/\cos\theta = 0 \tag{1.3.46}$$

and

$$\partial_r G - r^{-1} G - r^{-2} F = 0 \ . \tag{1.3.47}$$

A third boundary condition is obtained by assuming that the electrons do not penetrate the surface, i.e.,

$$v_r = 0, \text{ at } r=a \ . \tag{1.3.48}$$

From Eq.(1.3.3), this is equivalent to

$$e \partial_r \phi = \chi_o \partial_r \nu_- \ , \quad \text{at } r=a \ . \tag{1.3.49}$$

The three boundary conditions may be written as

$$\begin{aligned} &-2n_o D y a^{-2} j_2(y) \\ &= A_+[(\tfrac{\Lambda}{\lambda})^2(1+\tfrac{\beta}{\alpha})Q_1 j_1(x) + (\tfrac{\beta}{\alpha} - 1) j_1(x) \\ &\qquad -2j_1''(x)] \\ &\quad +B_+[(\tfrac{\Lambda}{\lambda})^2(1+\tfrac{\beta}{\alpha})Q_2 i_1(z) + (\tfrac{\beta}{\alpha} - 1) i_1(z) \\ &\qquad +2i_1''(z)] \end{aligned} \tag{1.3.50}$$

$$\begin{aligned} &0.5 n_o D q^3 j_1''(y)/y \\ &= 2k j_2(x) A_+/x^2 + 2p i_2(z) B_+/z^2 \end{aligned} \tag{1.3.51}$$

$$\begin{aligned} -\Xi_o/4\pi e &= A_+[2(1-Q_1) j_2(x)/3k + Q_1 k j_1'(x)/\lambda^2] \\ &\quad +B_+[2(1-Q_2) i_2(z)/3p + Q_2 p i_1'(z)/\lambda^2] \ , \end{aligned} \tag{1.3.52}$$

where

$$y=qa \quad . \tag{1.3.53}$$

Eqs. (1.3.50)-(1.3.52) may be solved simutaneously for A_+, B_+, and D in terms of E_o and the other parameters of the problem. Thus, in particular,

$$A_+=-[E_o/4\pi ea][D_+/(C_+D_+-E_+N_+)] \tag{1.3.54}$$

and

$$B_+=-N_+A_+/D_+ \quad , \tag{1.3.55}$$

where

$$N_+=[-2j_1''(x)+(\frac{\Delta}{\lambda})^2(1+\frac{\beta}{\alpha})Q_1 j_1(x) +(\frac{\beta}{\alpha}-1)j_1(x)]j_1''(y) +8j_2(x)j_2(y)/xy \quad , \tag{1.3.56}$$

$$D_+=[2i_1''(z)+(\frac{\Delta}{\lambda})^2(1+\frac{\beta}{\alpha})Q_2 i_1(z) +(\frac{\beta}{\alpha}-1)i_1(z)]j_1''(y) +8i_2(z)j_2(y)/zy \quad , \tag{1.3.57}$$

$$C_+=x^{-1}[2(1-Q_1)j_2(x)/3+Q_1(\frac{\kappa}{\lambda})^2 j_1'(x)] \tag{1.3.58}$$

and

$$E_+=z^{-1}[2(1-Q_2)i_2(z)/3+Q_2(\frac{\rho}{\lambda})^2 i_1'(z)] \tag{1.3.59}$$

The electric polarizability for the sphere is given by

$$\alpha_E=\mu_s/E_o \quad , \tag{1.3.60}$$

where μ_s is given by Eqs. (1.3.24), (1.3.27), and (1.3.28).

Let us now return to Eqs. (1.3.13) and (1.3.14) and study the "trivial" solution $A_+=0=A_-$. In this case

$$\nu_{\pm} = 0 \quad . \tag{1.3.61}$$

From Eq.(1.2.21) we obtain

$$\nabla \cdot \vec{u} = 0 \quad , \tag{1.3.62}$$

and from Eq.(1.3.2),

$$\nabla^2 \phi = 0 \quad . \tag{1.3.63}$$

The potential inside the sphere may be written as

$$\phi = C_1' r\cos\theta \quad , \tag{1.3.64}$$

while outside the sphere it is still given by (1.3.22). Matching boundary conditions at r=a yields

$$C_1 a = -E_o a + \mu_s/a^2 \quad , \tag{1.3.65}$$

and

$$C_1 = -E_o - 2\,\mu_s/a^3 \quad . \tag{1.3.66}$$

Hence,

$$\mu_s = 0 \quad . \tag{1.3.67}$$

Since the electric dipole moment vanishes for this solution, it does not contribute to the electric polarizability.

It is worth comparing the theoretical formula obtained with the corresponding case, in which the ions are held frozen in place. We shall refer to this as the " frozen jellium " model. In this limit $\vec{u} \to 0$, and so from Eq.(1.2.21) it also follows that $\nu_+ = 0$. The remaining equations, (1.2.17), (1.2.22), (1.2.23), and (1.3.1), may be solved for the electric response. In place of

Eq.(1.3.4), we have

$$[\nabla^2 + \lambda^2 \epsilon/(1-\epsilon)]\,\nu_- = 0, \tag{1.3.68}$$

whose solution is now simply

$$\nu_- = Ai_1(pr)\cos\theta \quad , \tag{1.3.69}$$

where p is given by

$$p = \lambda[\epsilon/(1-\epsilon)]^{1/2} \quad , \tag{1.3.70}$$

For frequencies far below the plasma frequency, p, and hence z, will become approximately real numbers. This is in contrast to the general case where phonon effects cause z to be imaginary in the low frequency domain, as will be seen later (see Fig.1.3). The dipolar solution to the Poisson equation now becomes

$$\Phi = [C_0 r + 4\pi e Ai_1(pr)/p^2]\cos\theta \quad , \quad r < a \tag{1.3.71}$$

and Eq.(1.3.22) when $r > a$. Application of the electrical boundary conditions yields

$$\mu_s = -4\pi e A a^3 i_2(z)/3p \quad , \tag{1.3.72}$$

and

$$C_0 = -E_o - 4\pi e Ai_0(z)/3p \quad . \tag{1.3.73}$$

The radial velocity at the boundary is

$$\begin{aligned} v_r(a) &= 0 \\ &= im_e^{-1}(\omega + i/\tau)^{-1}[eC_0 + 4\pi e^2 Ai_1'(z)/p \\ &\qquad - \chi_o p Ai_1'(z)] \end{aligned} \tag{1.3.74}$$

Solving Eqs. (1.3.72)-(1.3.74) simultaneously, and making use of Eq.(1.3.72), yields

$$\alpha_E = a^3 i_2(z)/[i_o(z)+3i_1'(z)/(\epsilon -1)] \ , \qquad (1.3.75)$$

where ϵ is the Drude dielectric constant,

$$\epsilon = 1-\omega_p^2/\omega(\omega+i/\tau) \ . \qquad (1.3.76)$$

In the limit where shielding is strong, i.e., $|z| = |pa| >> 1$, Eq.(1.3.75) reduces to the familiar formula for a dielectric sphere,

$$\alpha_E \rightarrow a^3(\epsilon -1)/(\epsilon +2). \qquad (1.3.77)$$

For finite shielding, however, Eq.(1.3.75) must be used. In the most general case, where the ionic motion is taken into account, Eq.(1.3.6) must be used along with its associated equations.

1.4. Magnetic Polarizability

Let us now choose the z axis along the magnetic field vector $\vec{B}_0$ and disregard the external field $\vec{E}_0$. In place of Eq.(1.2.18), we introduce the vector potential $\vec{A}$ and write

$$\vec{B} = \nabla \times \vec{A} \ . \qquad (1.4.1)$$

Faraday's law yields the following expression for the

induced electric field:

$$\vec{E} = i\frac{\omega}{c}\vec{A} \quad . \tag{1.4.2}$$

We look for a solution with no scalar potential. Thus,

$$v_+ = v_- \quad . \tag{1.4.3}$$

From Eqs.(1.2.21)-(1.2.24), we obtain

$$m_e(-i\omega+1/\tau)i\omega v_-/n_o = -\chi_o \nabla^2 v_- , \tag{1.4.4}$$

and

$$\rho_i(-\omega^2 - i\omega\gamma) v_+/n_o = (\alpha+\beta)\nabla^2 v_+/n_o , \tag{1.4.5}$$

In general, Eqs.(1.4.3)-(1.4.5) will be incompatible with each other unless

$$v_+ = 0 = v_- \quad . \tag{1.4.6}$$

It then follows from (1.2.21) and (1.2.22) that both $\vec{u}$ and $\vec{v}$ are divergenceless. Working in the Coulomb gauge

$$\nabla\cdot\vec{A} = 0 \quad , \tag{1.4.7}$$

we obtain two equations coupling $\vec{A}$ and $\vec{u}$,

$$\nabla^2\vec{A} = (\omega_p/c)^2\omega\vec{A}/(\omega+i/\tau) + i4\pi n_o e\omega\vec{u}/c \tag{1.4.8}$$

and

$$\nabla^2\vec{u} = -q^2\vec{u} - in_0 e\omega\vec{A}/c\alpha \quad . \tag{1.4.9}$$

In addition, $\vec{v}$ is simply related to $\vec{A}$,

$$\vec{v} = (\omega e/m_e c)\vec{A}/(\omega+i/\tau) \quad . \tag{1.4.10}$$

As in our study of Eqs.(1.3.4) and (1.3.5), we again look for solutions which satisfy

$$(\nabla^2 + k^2)\vec{A} = 0 \quad , \tag{1.4.11}$$

and

$$(\nabla^2+k^2)\vec{u} = 0 \quad . \tag{1.4.12}$$

Then

$$(k^2-q^2)\vec{u} = in_o e\omega\vec{A}/c\alpha \quad , \tag{1.4.13}$$

and

$$-k^2\vec{A} = (\omega/c)^2(1-\epsilon)\vec{A} + i4\pi en_o\omega\vec{u}/c \quad . \tag{1.4.14}$$

A nontrivial solution results when

$$(k^2-q^2)[k^2+(\omega/c)^2(1-\epsilon)]=[\omega L/c]^2 \quad , \tag{1.4.15}$$

where

$$L=\Omega_p/c_t \quad . \tag{1.4.16}$$

Again, it is convevient to denote the two roots as $k_+^2=k^2$ and $k_-^2=-p^2$:

$$k^2=0.5\left\{q^2-(\omega/c)^2(1-\epsilon) + \sqrt{[q^2+(\omega/c)^2(1-\epsilon)]^2+(2\omega L/c)^2}\right\} \tag{1.4.17}$$

and

$$-p^2=0.5\left\{q^2-(\omega/c)^2(1-\epsilon) - \sqrt{[q^2+(\omega/c)^2(1-\epsilon)]^2+(2\omega L/c)^2}\right\} \tag{1.4.18}$$

The vector potential may be expressed as

$$\vec{A} = [L_+ j_1(kr)+M_+ i_1(pr)]\sin\theta\,\hat{\phi} \quad , \tag{1.4.19}$$

and the ion displacement field as

$$\vec{u} = [L_- j_1(kr)+M_- i_1(pr)]\sin\theta\,\hat{\phi} \quad , \tag{1.4.20}$$

where $\hat{\phi}$ is a unit vector in the azimuthal direction. Defining

$$Q_1' = c(4\pi e n_o i\omega)^{-1}[-k^2-(\omega/c)^2(1-\epsilon)] \quad , \tag{1.4.21}$$

$$Q_2' = c(4\pi e n_o i\omega)^{-1}[p^2-(\omega/c)^2(1-\epsilon)], \tag{1.4.22}$$

we find

$$L_- = Q_1' L_+ \tag{1.4.23}$$

$$M_- = Q_2' M_+ \quad . \tag{1.4.24}$$

Note that Eqs. (1.4.19) and (1.4.20) satisfy Eq.(1.4.7) and $\nabla \cdot \vec{u}=0$.

The vector potential outside the sphere corresponds to a uniform magnetic field plus a magnetic dipole potential,

$$\vec{A} = [0.5B_o r+Mr^{-2}]\sin\theta\,\hat{\phi} \quad , \tag{1.4.25}$$

where M is the magnetic dipole. The boundary conditions are that A_ϕ and B_θ be continuous at r=a, so that

$$0.5B_o a+Ma^{-2} = L_+ j_1(x)+M_+ i_1(z) \tag{1.4.26}$$

and

$$B_o a-Ma^{-2} = L_+[xj_1(x)]'+M_+[zi_1(z)]' \quad . \tag{1.4.27}$$

The boundary condition of vanishing surface stress gives

$$\hat{r}\cdot\overleftrightarrow{\sigma}\cdot\hat{\phi} = 0 \quad , \tag{1.4.28}$$

where $\overleftrightarrow{\sigma}$ is now given simply by

$$\overleftrightarrow{\sigma} = 2\alpha\overleftrightarrow{u} \quad . \tag{1.4.29}$$

Hence,

$$u_{r\phi} = 0 = 0.5[(r\sin\theta)^{-1}\partial_\phi u_r + \partial_r u_\phi - u_\phi r^{-1}] \tag{1.4.30}$$

which yields the relation

$$k^2 L_-[j_1(x)/x]'+p^2 M_-[i_1(z)/z]' = 0 \quad . \tag{1.4.31}$$

Eqs. (1.4.26), (1.4.27), and (1.4.31), along with (1.4.23) and (1.4.24), may be solved for L_+, M_+, L_-, M_- and

M in terms of B_o. In particular, we find

$$M=0.5B_o a^3(Q_2'-Q_1')[Q_2'(j_o(x)/j_2(x)) + Q_1'(i_o(z)/i_2(z)]^{-1}, \tag{1.4.32}$$

and the magnetic polarizability is

$$\alpha_M=M/B_o \quad . \tag{1.4.33}$$

Let us now examine the magnetic polarizability in the frozen jellium limit. We shall let $c_t \to \infty$, and thus Eq.(1.4.16) implies $L \to 0$. Then

$$p^2 \to (\omega/c)^2(1-\epsilon) \tag{1.4.34}$$

and

$$k^2 \to q^2 \quad . \tag{1.4.35}$$

From Eq.(1.4.22), we have $Q_2' \to 0$, so that

$$\alpha_M \to -0.5a^3 i_2(z)/i_o(z) \quad . \tag{1.4.36}$$

This formula has been obtained in the literature. In the particular case where $z \ll 1$,

$$\alpha_M \to -(a^5/30)(\omega/c)^2(1-\epsilon) \quad . \tag{1.4.37}$$

Thus Eq.(1.4.32) represents the general formula, while eqs.(1.4.36) and (1.4.37) are successively severer approximations.

In sections 1.3 and 1.4 we have obtained the solutions of the linear dipole response of a small sphere which are based on the long wavelength approximation. The full electrodynamic solution is obtained in appendix B and it has been proved that under long wavelength approximation these two solutions are consistent.

1.5. Electromagnetic Absorption

Let us assume that the particle is isolated in free space and an electromagnetic wave of electric field strength E_0 impinges upon it. The magnetic field strength B_0 is, of course, just equal to E_0. The power absorbed by the particle will be the sum of the powers absorbed by the electric and magnetic dipoles,

$$p = 0.5\omega \, \mathrm{Im}(E_0^* \alpha_E E_0 + B_0^* \alpha_M B_0) \quad . \tag{1.5.1}$$

The cross section for electromagnetic absorption is obtained by dividing this by the incident intensity, so

$$\sigma = 4\pi \frac{\omega}{c} \, \mathrm{Im}(\alpha_E + \alpha_M) \quad . \tag{1.5.2}$$

If we had a dilute nonclustered assembly of such particles of concentration n per unit volume, the attenuation constant for the electromagnetic indensity would be

$$\alpha_\gamma = n\sigma = 4\pi n \frac{\omega}{c} \, \mathrm{Im}(\alpha_E + \alpha_M) \quad . \tag{1.5.3}$$

Expressing this in terms of the filling factor f,

$$f = 4\pi n a^3/3 \quad , \tag{1.5.4}$$

we obtain the familiar result

$$\alpha_\gamma = (3\omega f/ca^3) \, \mathrm{Im}(\alpha_E + \alpha_M) \quad . \tag{1.5.5}$$

It should be emphasized, however, that the experiments are often done for situations where clustering does occur, and so Eq. (1.5.5) may not be directly applicable to currently available experimental data.

We have applied our theory to the case of a 200 Å-radius sphere of aluminum. The electron concentration

was taken to be $n_o=1.81\times10^{23}$ cm^{-3} and the mass density is $\rho_i=2.692$ g/cm^3. The longitudinal speed of sound is $v_\ell=6.42\times10^5$ cm/s and the transverse speed of sound is $c_t=3.04\times10^5$ cm/s. The electron collision time was taken as $\tau=10^{-14}$ s (because the particle size is small) and the phonon damping rate was taken as $\gamma=\gamma'\omega$, where $\gamma'=0.01$, in line with the estimates of Glick and York[35]. The filling factor f was taken to be 0.041.

In order to determine the constant c appearing in Eqs.(1.3.9) and (1.3.10), we fit the low frequency part of the dispersion curve of Eq.(1.3.17) to the straight line that characterizes the longitudinal-acoustic mode. Thus we obtained

$$c_\ell = \Omega_p [v_\ell^2(\Omega_p^{-2}+\omega_p^{-2})-\lambda^{-2}]^{1/2} \quad . \tag{1.5.6}$$

For Al, we have $\Omega_p=1.9\times10^{14}$ rad/s, $\omega_p=2.4\times10^{16}$ rad/s, and $\lambda=2.6\times10^8$ cm^{-1}. Thus $c_\ell=i(3.63\times10^5)$, and the bare elastic constant β appearing in Eq.(1.3.10) is thus negative. The actual longitudinal sound velocity is thus seen to arise from the combination of Coulombic and elastic effects.

It was found that throughout the frequency range scanned, the real part of the electric polarizability was accurately given by the Drude formula. Thus,

$$\mathrm{Re}\,\alpha_E \approx a^3 \quad , \tag{1.5.7}$$

and for a=200 Å this number was 8×10^{-18} cm^{-3}. The imaginary part of the polarizability, however, exhibited

wide variations as either the frequency or size of the particle was changed. This is illustrated in Fig. 1.1 and 1.2 in plots of the attenuation constant, which, by Eq.(1.5.5), is proportional to the imaginary part of the polarizability. In Fig.1.1 the attenuation constant is plotted as a function of frequency. In Fig. 1.1(a) the low frequency part is studied, while in Fig. 1.1(b) the high frequency part is studied. Series of sharp peaks occurs at both low and high frequencies. At frequencies above 400 cm^{-1}, the electric dipole absorption is seen to fall off rather quickly. In Fig.1.2 the frequency is held fixed at 40 cm^{-1} and the size of the sphere is allowed to vary. One notices that there exists a set of closely spaced resonances which are swept through if the particle changes by only 0.7 Å. In crossing such a resonance the electric dipole absorption can vary by almost 4 orders of magnitude. It should also be noted that the magnitude of the absorption is considerably larger than that predicted by the Drude theory even off resonance ($\alpha_{Drude} = 1.2 \times 10^{-4}$ cm^{-1} at $\tilde{\nu} = 40$ cm^{-1}).

In Fig.1.3 we present the dispersion curves corresponding to the electric dipole absorption. These curves show the frequency (in wave numbers) plotted against the variables x,y, and z defined by Eqs.(1.3.25), (1.3.26), and (1.3.53). The variables x and z (or k and p) are determined from Eqs. (1.3.16) and (1.3.17), while

the variable y (or q) is obtained from Eq.(1.3.32). For frequencies greater than 500 cm^{-1}, x developes a large imaginary part and z developes a large real part. Let us analyze some interesting features of this figure. At low frequencies and low wave numbers we have two acoustic branches, corresponding to the longitudinal (x) and transverse (y) modes. The longitudinal mode, however, is strongly coupled to plasmon modes through the Coulomb field and is therefore repelled by them. For large wave vectors it becomes the z mode and its frequency drops. This is probably a reminder that the ions would prefer to organize themselves into a crystalline array. In our jellium model, however, the ions are treated somewhat unrealistically, so numerically trustworthy predictions of lattice constants cannot be obtained. The fact that Rex and Imz appear as one continuous curve is expected, since Eq.(1.3.16) and (1.3.17), from which the variables x=ka and z=pa are defined, are both solutions to Eq.(1.3.15).

It is interesting, however, that z is largely imaginary at low frequencies. Since the variable z appears mainly as the argument of a modified spherical Bessel function [see, e.g., Eqs. (1.3.19) to (1.3.21)], this implies that shielding is not occuring in the usual manner. The fields inside the crystal are all oscillatory and not exponentially damped at low frequencies. This is presumably related to the fact that the phonons can

penetrate the particle. This is quite different from the true shielding that one finds when the ions are held frozen in place[see Eq.(1.3.69) and (1.3.71)]. In that case, z is determined from Eq.(1.3.70) and is found to be real at low frequencies. Consequently, the fields are exponentially damped inside the crystal. In the case where the ions are dynamic, however, we see that charge-density waves may be set up which penetrate the small particle. Since the shielding is incomplete, this can account for the increased electric dipole absorption seen in Fig. 1.1 and 1.2.

The strong resonance seen in Fig. 1.1 and 1.2 occur because of the near vanishing of the denominator in Eq.(1.3.54). Physically, they correspond to the exitation of a vibronic mode of the coupled electron-phonon system. The spacing of the resonances can be understood by examining Fig. 1.3 again and noting that Imz is a rapidly changing function of frequency. For large values of Imz, the function $i_1(z)$ can be approximated by a sinusoidally varying function. Whenever Imz changes by π, the possibility of sweeping through a resonance occurs. As may be seen from Fig. 1.3, Imz ≈ 900 at low frequencies and becomes smaller at high frequencies. At high frequencies, Imz changes more rapidly as $\tilde{\nu}$ is varied, and thus the resonances become more closely packed together. At low frequencies, Imz changes very slowly with $\tilde{\nu}$, and thus

there is a lack of this kind of resonance.

In addition to the strong resonances, we also see a set of weak resonances occuring at low frequencies (i.e., $\tilde{\nu} \lesssim 40$ cm^{-1}). These are due to the Rex variable sweeping through multiples of π, and correspond to the acoustic oscillations of the sphere; they have been seen in Raman scattring from small particles and surface protrusions[54].

In order to detect the resonances it is important to work with a single particle or a dilute concentration of spheres of precisely the same size. Fig. 1.2 shows that a size distribution that varies by only half of a percent would be sufficient to wash out the oscillatory structure.

We now turn our attention to the magnetic polarizability. The magnetic polarizability discussed here arises from the eddy currents induced in the sphere. The intrinsic permeability of the system is ignored. In Fig. 1.4 a plot is made of the real and imaginary parts of the magnetic polarizability of the same 200-Å-radius sphere considered before. In Fig. 1.5(a) and 1.5(b) we plot the dispersion curve for z=pa and x=ka given by Eqs.(1.4.17) and (1.4.18), respectively. We notice that the x dispersion curve is practically identical to the y dispersion curve in Fig. 1.3. The z dispersion curve, however, is radically different from the previously considered curves. Now, Rez and Imz are of comparable

magnitude, and are both of the order of unity in the domain of interest.

In Fig. 1.6 the magnetic absorption constant is plotted as a function of frequency. Several curves are shown. In curves a and b the absorption constant is computed from the exact theoretical expressions[Eqs.(1.4.32), (1.4.33), and (1.5.5)] for Al spheres of radii 200 and 500 Å, respectively. In curve c and d, the same quantity is calculated using the expression derived in the literature which neglects phonon effects[46],

$$\alpha_M = (3f\omega/2c)\mathrm{Im}[j_2(pa)/j_0(pa)] \quad , \qquad (1.5.8)$$

where $p=(\omega_p/c)(\omega\tau/2)^{1/2}(1+i)$. One notices a significant deviation of these curves at the high frequencies. This indicates the importance of phonons in modifying the magnetic response of the particle. Also shown are a set of curves, e and f, corresponding to the approximation in which pa is assumed to be small; thus Eq.(1.5.8) is replaced by

$$\alpha_M = (3f\omega/15c)\mathrm{Im}[(pa)^2] \quad . \qquad (1.5.9)$$

For a=200 Å there is not much difference between curves c and e. However, for a=500 Å one notices a significant disagreement. As a becomes larger, the disagreement becomes more pronounced.

The need for averaging over the size distribution has been pointed out in the literature[46,47]. Since the

magnetic absorption increaces strongly with increasing a, those radii in the size distribution which are large tend to dominate the magnetic absorption. We adopt the size distributior that has been proposed[46,47] and average α_M over this distribution:

$$n(a) = Aa^{\alpha} \exp(-\alpha a/a_m) \quad , \tag{1.5.10}$$

where a_m is a characteristic radius and α is a constant characterizing the standard deviation. We will take $\alpha = 0.5$, as in the literature. The constant A is determined from the normalization condition that

$$\int n(a) f da = 4\pi n a_m^3/3 \quad . \tag{1.5.11}$$

The results of the averaging are presented in Fig. 1.7. We first remark that the approximate formula of Eq.(1.5.9) disagrees strongly with the exact formula of Eq.(1.5.8). Thus the conclusions reached in the literature[46,47] which were based on the approximate formula are called into question. Eq.(1.5.9) would have α_M growing as a^5 for large a, while Eq.(1.5.8) has it ultimately saturating to an a^3 behaviour. This comes about because $j_2(pa)/j_0(pa)$ approaches unity as pa develops a large imaginary part. In curve a we present the results based on the exact formula, including phonon effects. Curve b gives the prediction based on Eq.(1.5.8), while curve c gives the prediction based on Eq.(1.5.9). Curve d represents the electric dipole absorption contribution to the total attenuation constant. It is seen

to be more than 2 orders of magnetude smaller than the magnetic dipole absorption. The oscillations appearing in Figs. 1.1 and 1.2 are washed out when integrating over the distribution of the radii of Eq.(1.5.10). Several experimental points[3] are also graphed for the sake of comparison. We see that the present theory is still about a factor of 4 too small to account for the observations.

References

1. C. G. Granqvist and R. A. Buhrman, J. Appl. Phys. 47, 2200(1976)
2. L. P. Gor'kov and G. M. Eliashberg, Sov. Phys. JETP 21, 940(1965)
3. D. B. Tanner, A. J. Sievers and R. A. Buhrman, Phys. Rev. B 11, 1330(1975)
4. C. G. Granqvist, R. A. Buhrman, J. Wynes and A. J. Sievers, Phys. Rev. Lett. 37, 625(1976)
5. N. E. Russell, J. C. Garland and D. B. Tanner, Phys.Rev. B 23, 632(1981)
6. G. L. Carr, R. L. Henry, N. E. Russell, J. C. Garland and D. B. Tanner, Phys. Rev. B 24, 777(1981)
7. R. P. Devaty and A. J. Sievers, Phys. Rev. Lett. 52, 1344(1984)
8. W. A. Curtin, R. C. Spitzer, N. W. Ashcroft and A. J. Sievers, Phys. Rev. Lett. 54, 1071(1985)
9. L. P. Kadanoff, Phys. Today 39, No. 2, 6(1986)
10. J. W. Gibbs, Collected Works, ed. by W. R. Longley and R. G. Van Name, (Longmans, Green and Co., New York, 1931)
11. G. Wulff, Z. Kristall, (Leipzig) 34, 449(1901)
12. R. Kubo, J. Phys. Soc. Jpn. 17, 975(1962)
13. H. Fröhlich, Physica (Utr.) 6, 406(1937)
14. E. P. Wigner, Ann. Math. 53, 36(1951); 62, 548(1955)

15. F. J. Dyson, J. Math. Phys. 3, 140, 157, 166(1962)

16. M. L. Mehta and F. J. Dyson, J. Math. Phys. 4, 713(1963)

17. A. A. Lushnikov, V. V. Maksimenko and A. Ya. Simonov, Sov. Phys. Solid State 20, 292(1978)

18. B. I. Shklovskii, JETP Lett. 36, 352(1983)

19. D. M. Wood and N. W. Ashcroft, Phys. Rev. B 25, 6255(1981)

20. R. Devaty and A. J. Sievers, Phys. Rev. B 22, 2123(1980)

21. S. Strassler, M. J. Rice and P. Wyder, Phys. Rev. B 6, 2575(1972)

22. A. Kawabata and R. Kubo, J. Phys. Soc. Jpn. 21, 1765 (1966)

23. M. J. Rice, W. R. Schneider and S. Strassler, Phys. Rev. B 8, 474(1973)

24. A. A. Lushnikov and A. J. Simononv, Phys. Lett. 44A, 45(1973)

25. M. Cini and P. Ascarelli, J. Phys. F 4, 1998(1974)

26. A. A. Lushnikov and A. J. Simonov, Z. Phys. 270, 17(1974)

27. L. Genzel, T. P. Martin and U. Kreibig, Z. Phys. B 21, 339(1975)

28. R. Fuchs and S. H. Lin, Phys. Rev. B 14, 5521(1976)

29. R. Ruppin and H. Yatom, Phys. Status Solidi B 74, 647(1976)

30. L. Genzel and U. Kreibig, Z. Phys. B 37, 93(1980)

31. E. Simanek, Phys. Rev. Lett. 38, 1161(1977)

32. R. Ruppin, Phys. Rev. B 19, 1318(1979)

33. P. N. Sen and D. B. Tanner, Phys. Rev. B 26, 3582(1982)

34. D. Stroud and F. P. Pan, Phys. Rev. B 17, 1602(1978)

35. A. J. Glick and E. D. Yorke, Phys. Rev. B 18, 2490(1978)

36. R. Monreal, J. Giraldo, F. Flores and P. Apell, Solid State Comm. 54, 661(1985)

37. P. Sheng, Phys. Rev. B 31, 4906(1985)

38. X. M. Hua and J. I. Gersten, Phys. Rev. B 31, 855(1985)

39. U. Kreibig, A. Althiff and H. Pressmann, Surf. Sci. 106, 308(1981)

40. J. M. Gerardy and M. Ausloos, Phys. Rev. B 22, 4950(1980); 25, 4204(1982); 26, 4703(1982); 27, 6446(1983)

41. R. Landauer, in Electrical Transport and Optical Properties of Inhomogeneous Media, ed. by J. C. Garland and D. B. Tanner (AIP, New York, 1978) p.2.

42. J. C. Maxwell Garnett, Philos. Trans. R. Soc. London 203, 385(1904)

43. D. A. G. Bruggeman, Ann. Phys. (Leipzig) 24, 636(1935)

44. R. Landauer, J. Appl. Phys. 23, 779(1952)

45. D. Stroud, Phys. Rev. B 12, 3368(1975); 19, 1783(1979)

46. P. Chy'lek and V. Srivastava, Phys. Rev. B 27, 5098(1983)

47. P. Chy'lek, D. Boice and R. G. Pinnick, Phys. Rev. B 27, 5107(1983)

48. P. Chy'lek and V. Srivastava, Phys. Rev. B 30, 1008(1984)

49. D. B. Tanner, Phys. Rev. B 30, 1042(1984)

50. A. Leibsch and B. N. J. Persson, J. Phys. C 16, 5375(1983)

51. W. A. Curtin and N. W. Ashcroft, Phys. Rev. B 31, 3287(1985)

52. S. John, Phys. Rev Lett. 53, 2169(1984)

53. K. Arya, Z. B. Su and J. L Birman, " Anderson Localization of Electromagnetic Wave in a Dielectric Medium of Randomly Distributed Metal Particles ", preprint.

54. J. I. Gersten, D. A. Weitz, T. J. Gramila, and A. Z. Genack, Phys. Rev. B 22, 456(1980); D. A. Weitz, A. Z. Genack, T. J. Gramila and J. I. Gersten, Phys. Rev Lett. 45, 355(1980)

55. W. P Halperin, Rev. Mod. Phys. 58, 533(1986).

Appendix A

In this appendix the classical hydrodynamic equation of motion of an electron in the metal is derived from the Boltzmann equation. The E. M. fields are treated as external perturbations.

In a phase space $(\vec{r},\vec{k},t)$, where $\vec{r}$, $\vec{k}$, and t are independent variabales, the $\vec{r}$ and $\vec{k}$ coordinates of every electron would evolve, if no collisions occured, according to the semiclassical equations of motion:

$$\dot{\vec{r}} = \vec{v}(\vec{k}) \quad , \tag{A.1a}$$

$$\hbar \dot{\vec{k}} = -e(\vec{E} + \vec{v} \times \vec{B}/c) = \vec{F}(\vec{r},\vec{k}) \quad , \tag{A.1b}$$

where $\vec{v}(\vec{k})$ is the velocity of the electron and $\vec{F}(\vec{r},\vec{k},t)$ is Lorentz force.

By considering the collision correction, the dynamic motion of an electron in phase space should obey the Boltzmann equation:

$$\partial_t f + \vec{v} \cdot \nabla_r f + (\vec{F}/\hbar) \cdot \nabla_k f = (\partial_t f)_c \quad . \tag{A.2}$$

Here, the terms on the left side are often refered to as the drift terms, and the term on the right side as the collision term. The nonequilibrium distribution function $f(\vec{r},\vec{k},t)$ in (A.2) is defined so that

$$dn(\vec{r},\vec{k},t) = f(\vec{r},\vec{k},t)\, d\vec{r}\, d\vec{k}/4\pi^3 \quad . \tag{A.3}$$

By definition

$$n(\vec{r}) = \int \frac{d\vec{k}}{4\pi^3} \; f(\vec{r},\vec{k},t) \quad , \tag{A.4a}$$

and

$$n(\vec{r})\langle A\rangle = \int \frac{d\vec{k}}{4\pi^3} f(\vec{r},\vec{k},t)A(\vec{r},\vec{k},t), \quad (A.4b)$$

where $n(\vec{r})$ is the density of electrons at point $\vec{r}$ in real space $(\vec{r},t)$, and $A(\vec{r},\vec{k},t)$ is any kind of physical quantity in phase space $(\vec{r},\vec{k},t)$; and the bracket $\langle\ \rangle$ means averaged over $\vec{k}$.

We multiply both sides of the Boltzmann equation (A.2) by $A(\vec{r},\vec{k},t)$ and then integrate over $\vec{k}$. Thus we get

$$\partial_t n(\vec{r})\langle A\rangle + \partial_i n(\vec{r})\langle v_i A\rangle - n(\vec{r})\langle DA\rangle = \int \frac{d\vec{k}}{4\pi^3} (\partial_t f)_c A \ , \quad (A.5)$$

where i=x,y,z and D is a differential operator defined as

$$D = \partial_t + \vec{v}\cdot\nabla_r + (\vec{F}/\hbar)\cdot\nabla_k \ . \quad (A.6)$$

The classical equation of motion in real space $(\vec{r},t)$ should be recovered from (A.5) when we specialize A. As is well-known, for A=1, (A.5) is the continuity eqution; and for $A=\vec{v}(\vec{r},\vec{k},t)$, Newton's equation is obtained. Indeed, for A=1, (A.5 jives

$$\partial_t n(\vec{r}) + \partial_i n(\vec{r}) v_i(\vec{r}) = 0 \ . \quad (A.7)$$

The right side is zero because the number of electrons is conserved during collisions in a classical process. For $A=\vec{v}$, (A.5) becomes

$$\partial_t n(\vec{r})\langle v_j\rangle + \partial_i n(\vec{r})\langle v_i v_j\rangle - n(\vec{r})\langle Dv_j\rangle = \int \frac{d\vec{k}}{4\pi^3} (\partial_t f)_c v_j \ . \quad (A.8)$$

Keeping in mind that $\vec{r}$, $\vec{k}$, and t are independent in phase

space, and $\vec{v}=\hbar\vec{k}/m$ in the free electron approximation, we could write

$$Dv_j=F_i\,\partial_{k_i}k_j/m=F_i\,\delta_{ij}/m=F_j/m. \qquad (A.9)$$

The second term in (A.5) is usually expressed in terms of $\langle\vec{v}\rangle$ and the peculiar velocity $\vec{U}$ with

$$\vec{U}=\vec{v}-\langle\vec{v}\rangle\ . \qquad (A.10)$$

Thus,

$$\langle v_iv_j\rangle=\langle v_i\rangle\langle v_j\rangle+\langle U_iU_j\rangle\ , \qquad (A.11)$$

since

$$\langle U_i\rangle=\langle U_j\rangle=0\ .$$

The term $n(\vec{r})\langle U_iU_j\rangle$ is usually refered to as the "presure" term in textbooks of statistical mechanics.

Under the relaxation time approximation

$$(\partial_t f)_c=-(f-f^{(o)})/\tau\ , \qquad (A.12)$$

where $f^{(o)}$ is the equilibrium distribution function,

$$f^{(o)}=[\exp(\beta(\epsilon-\mu))+1]^{-1}\ , \qquad (A.13)$$

with $\beta=1/k_BT$, $\epsilon=\epsilon(\vec{k})$, and $\mu=\mu(r)$. We assume that the relaxation time τ in (A.12) depends on $\vec{k}$ only through $|\vec{k}|$, or, in other words, τ does not depend on the orientation of $\vec{k}$. Then

$$\int\frac{d\vec{k}}{4\pi^3}(\partial_t f)_c v_j=-\int\frac{d\vec{k}}{4\pi^3}(f-f^{(o)})v_j/\tau$$

$$=-n(\vec{r})\langle v_j\rangle/\tau\ , \qquad (A.14)$$

since

$$\int \frac{d\vec{k}}{4\pi^3} f^{(o)} \vec{v} = 0 \quad . \tag{A.14'}$$

Using (A.9) through (A.14), (A.8) becomes

$$\begin{aligned} & v_j(\vec{r})\partial_t n(\vec{r}) + n(\vec{r})\partial_t v_j(\vec{r}) + v_j(\vec{r})\partial_i n(\vec{r}) v_i(\vec{r}) \\ & + n(\vec{r}) v_i(\vec{r}) \partial_i v_j(\vec{r}) \quad - n(\vec{r}) F_j(\vec{r})/m + \partial_i n(\vec{r}) \langle U_i U_j \rangle \\ & = -n(\vec{r}) v_j(\vec{r})/\tau \quad . \end{aligned} \tag{A.15}$$

Here the first term and the third term cancel each other because of the continuity equation. Furthermore, we define a substantial derivative as

$$\frac{d}{dt} = \partial_t + v_i \partial_i \quad , \tag{A.16}$$

and rearrange (A.15), and we get

$$\begin{aligned} & n(\vec{r}) \left[\frac{d}{dt} v_j(\vec{r}) + v_j(\vec{r})/\tau \right] \\ & = n(\vec{r}) F_j(\vec{r})/m - \partial_i n(\vec{r}) \langle U_i U_j \rangle \quad . \end{aligned} \tag{A.17}$$

The pressure term could be evaluated as follows.

$$\begin{aligned} \partial_i n(\vec{r}) \langle U_i U_j \rangle &= \partial_i \int \frac{d\vec{k}}{4\pi^3} f U_i U_j \\ &= \partial_i \int \frac{d\vec{k}}{4\pi^3} f [v_i v_j - v_i \langle v_j \rangle - v_j \langle v_i \rangle \\ &\qquad + \langle v_i \rangle \langle v_j \rangle] \\ &= \partial_i \int \frac{d\vec{k}}{4\pi^3} f v_i (v_j - \langle v_j \rangle) \quad , \end{aligned} \tag{A.18}$$

since

$$\int \frac{d\vec{k}}{4\pi^3} f[-v_j\langle v_i\rangle + \langle v_i\rangle\langle v_j\rangle] = 0 \quad .$$

As we observed that $(v_j - \langle v_j\rangle)$ is the fluctuation of velocity, it is a small quantity so that we could replace f by $f^{(0)}$ in (A.18) without losing too much. By using (A.14'), (A.18) thus approximately becomes

$$\partial_i n(\vec{r})\langle U_i U_j\rangle \cong \partial_i \int \frac{d\vec{k}}{4\pi^3} f^{(0)} v_i v_j$$

$$= \int \frac{d\vec{k}}{4\pi^3} (\partial_i f^{(0)}) v_i v_j. \qquad (A.19)$$

Assuming that the temprature has a uniform distribution over the system, we could write

$$\partial_i f^{(0)} = \frac{\partial f^{(0)}}{\partial \mu} \partial_i \mu(\vec{r}) = -\frac{\partial f^{(0)}}{\partial \epsilon} \partial_i \mu(\vec{r}). \qquad (A.20)$$

We evaluate $f^{(0)}$ at T=0, so

$$f^{(0)} = \theta(\mu - \epsilon) = 1 - \theta(\epsilon - \mu)$$

and

$$\frac{\partial f^{(0)}}{\partial \epsilon} = -\delta(\epsilon - \mu) = -(2m/\hbar^2)\,\delta(k^2 - k_f^2)$$

$$= -(m/\hbar^2 k_f)[\,\delta(k - k_f) + \delta(k + k_f)\,].$$

As we know that the term $\delta(k+k_F)$ is out of the picture so (A.19) becomes

$$\int \frac{d\vec{k}}{4\pi^3} (mk_f)^{-1}\, \delta(k - k_f)[\,\partial_i \mu(\vec{r})]k_i k_j. \qquad (A.21)$$

We know

$$\int d\Omega\, \hat{k}\,\hat{k} = \frac{4\pi}{3}\,\overleftrightarrow{I}\ ,$$

and

$$k_f = (3\pi^2 n)^{1/3}\ .$$

Finishing integral (A.21), then we obtain

$$\partial_i n(\vec{r})\langle U_i U_j\rangle \cong (n(\vec{r})/m)\,\partial_j \mu(\vec{r}) \quad . \tag{A.22}$$

Combine (A.17) and (A.22), cancel $n(\vec{r})$ on both sides, and we finally get the hydrodynamic equation of motion of an electron as

$$m(\frac{d}{dt} + 1/\tau\ )v_j(\vec{r}) = F_j(\vec{r}) - \partial_j \mu(\vec{r})\ , \tag{A.23}$$

or, writing this in vector form as

$$m(\frac{d}{dt} + 1/\tau\ )\vec{v}(\vec{r}) = \vec{F}(\vec{r}) - \nabla\mu\ (\vec{r})\ . \tag{A.24}$$

This is the equation we use in Chapter I and II.

Appendix B

In this appendix a full electrodynamic solution of the linear equations is presented. (see section 1.2 for a definition of the symbols.)

We want to solve the following linear equations of motion:

$$\nabla \cdot \vec{E} = 4\pi e(\nu_+ - \nu_-), \tag{B.1a}$$

$$\nabla \cdot \vec{B} = 0 , \tag{B.1b}$$

$$\nabla \times \vec{E} = i\frac{\omega}{c}\vec{B}, \tag{B.1c}$$

$$\nabla \times \vec{B} = -\frac{1}{c}[4\pi e n_o(i\omega\vec{u} + \vec{v}) - i\omega\vec{E}] , \tag{B.1d}$$

$$\nabla \cdot \vec{u} = -\nu_+/n_o , \tag{B.1e}$$

$$\nabla \cdot \vec{v} = i\omega\nu_-/n_o , \tag{B.1f}$$

$$\vec{v} = -i(e\vec{E} + \chi_o\nabla\nu_-)/m_e(\omega + i/\tau) , \tag{B.1g}$$

$$\vec{u} = -(n_o e\vec{E} + \alpha\nabla^2\vec{u} + \beta\nabla\nabla\cdot\vec{u})/\rho_i\omega(\omega + i\gamma) , \tag{B.1h}$$

where the continuity equations (B.1e) and (B.1f) are not independent from (B.1d), so we have six independent equations and therefore we have six independent coefficients.

The divergence of $\vec{v}$ and $\vec{u}$ give the wave equations of ν_+ and ν_- by using (B.1a), (B.1e) and (B.1f). Substituting (B.1c) into (B.1h) gives the wave equation for $\vec{u}$. Double curl of (B.1g) gives the wave equation for $\vec{v}$. These wave equations are

$$(\nabla^2 + k_\lambda^2)\nu_- = -\lambda^2\nu_+, \tag{B.2a}$$

$$(\nabla \quad k_\Lambda^2)\,\mathcal{V}_+ = -\Lambda^2\,\mathcal{V}_-, \tag{B.2b}$$

$$(\nabla^2 + p_\lambda^2)\vec{v} = i\frac{\omega}{n_o}\left[1 - \frac{q^2}{\lambda^2}(1-\epsilon)\right]\nabla\mathcal{V}_- + i\omega q^2(1-\epsilon)\vec{u}\ , \tag{B.2c}$$

$$(\nabla^2 + p_\Lambda^2)\vec{u} = \left(\frac{1}{\alpha}\right)\left[\frac{\beta}{n_o}\nabla\mathcal{V}_+ + n_o\chi_o\nabla\mathcal{V}_- - in_o m_e(\omega + i/\tau)\vec{v}\ \right], \tag{B.2d}$$

where

$$k_\lambda^2 = \lambda^2\frac{\epsilon}{1-\epsilon}\ , \qquad k_\Lambda^2 = \Lambda^2\frac{\epsilon_i}{1-\epsilon_i}\ ,$$

$$p_\lambda^2 = q^2\epsilon\ , \qquad p_\Lambda^2 = \omega(\omega + i\gamma)/c_t^2\ ,$$

$$\lambda^2 = 4\pi e^2/\chi_o\ , \qquad \Lambda^2 = \Omega_p^2/c_l^2\ ,$$

$$\epsilon = 1 - \omega_p^2/\omega(\omega + i/\tau), \qquad \epsilon_i = 1 - \Omega_p^2/\omega(\omega + i\gamma)\ ,$$

$$\omega_p^2 = 4\pi n_o e^2/m_e\ , \qquad \Omega_p^2 = 4\pi n_o^2 e^2/\rho_i\ ,$$

$$c_t^2 = \alpha/\rho_i\ , \qquad c_l^2 = (\alpha + \beta)/\rho_i\ ,$$

$$q = \omega/c\ .$$

The physical intepretation of the above symbols were presented in section 2 already.

Equations (B.2a) and (B.2b) are the same as (1.3.4) and (1.3.5), using the same technique we can get the solutions for $\mathcal{V}_\pm$ as

$$\mathcal{V}_-(\vec{r}) = \sum_{lm}\ [\ A_{lm}j_l(k_+r) + B_{lm}j_l(k_-r)\ ]Y_{lm} \tag{B.3a}$$

$$\mathcal{V}_+(\vec{r}) = \sum_{lm}\ [\alpha_+A_{lm}j_l(k_+r) + \alpha_-B_{lm}j_l(k_-r)\ ]Y_{lm} \tag{B.3b}$$

where

$$k_\pm^2 = \tfrac{1}{2}\left[\ k_\lambda^2 + k_\Lambda^2 \pm \sqrt{(k_\lambda^2 - k_\Lambda^2)^2 + 4\lambda^2\Lambda^2}\ \right],$$

$$\alpha_\pm = (\ k_\pm^2 - k_\lambda^2\ )/\lambda^2 = \Lambda^2/(\ k_\pm^2 - k_\Lambda^2\ )$$

Making use of the identity

$$\vec{r}\cdot\nabla^2\vec{A} = \nabla^2(\vec{r}\cdot\vec{A}) - 2\nabla\cdot\vec{A},$$

the radial components of $\vec{v}$ and $\vec{u}$ obey the equations:

$$(\nabla^2 + p_\lambda^2)\,\vec{r}\cdot\vec{v} = i\omega q^2(1-\epsilon)\vec{r}\cdot\vec{u} + i\frac{\omega}{n_o}\left[1 - \frac{q^2}{\lambda^2}(1-\epsilon)\right]r\partial_r\mathcal{V}_- + 2i\frac{\omega}{n_o}\mathcal{V}_-\ ,$$

$$(\nabla^2 + p_\lambda^2)\,\vec{r}\cdot\vec{u} = -i\frac{n_e m_e(\omega + i/\tau)}{\alpha}\,\vec{r}\cdot\vec{v} + \frac{\beta}{\alpha n_e} r\partial_r \nu_+ + \frac{n_e \chi_e}{\alpha} r\partial_r \nu_- - 2\frac{\nu_z}{n_e} \quad .$$

Substituting (B.3) into above equations we found

$$\vec{r}\cdot\vec{v} = \sum_{\ell m} [\, E_{\ell m} j_\ell(p_+ r) + F_{\ell m} j_\ell(p_- r) + c_+ A_{\ell m} j_\ell(k_+ r) + c_- B_{\ell m} j_\ell(k_- r) + e_+ A_{\ell m} k_+ r\, j_\ell'(k_+ r) + e_- B_{\ell m} k_- r\, j_\ell'(k_- r)\,] Y_{\ell m} \quad , \tag{B.4a}$$

and

$$\vec{r}\cdot\vec{u} = \sum_{\ell m} [\, \beta_+ E_{\ell m} j_\ell(p_+ r) + \beta_- F_{\ell m} j_\ell(p_- r) + f_+ A_{\ell m} j_\ell(k_+ r) + f_- B_{\ell m} j_\ell(k_- r) + d_+ A_{\ell m} k_+ r\, j_\ell'(k_+ r) + d_- B_{\ell m} k_- r\, j_\ell'(k_- r)\,] Y_{\ell m} \quad , \tag{B.4b}$$

where

$$c_\pm = \frac{2i\omega}{n_e}\,\frac{p_\lambda^2 - g^2\lambda^{-2}(1-\epsilon)k_\pm^2}{(p_\lambda^2 - k_\pm^2)^2} \quad ,$$

$$e_\pm = \frac{i\omega}{n_e}\,\frac{1 - g^2\lambda^{-2}(1-\epsilon)}{p_\lambda^2 - k_\pm^2} \quad ,$$

$$d_\pm = \frac{1}{n_e c_s^2}\,\frac{(c_s^2 - c_z^2)\alpha_\pm + \Omega_p^2/\lambda^2}{p_\Lambda^2 - k_\pm^2} \quad ,$$

$$f_\pm = \frac{2\Omega_p^2}{n_e c_s^2}\,\frac{(\lambda^{-2} + \Lambda^{-2}\alpha_\pm)k_\pm^2 - \alpha_\pm(1-\epsilon_i)^{-1}}{(p_\Lambda^2 - k_\pm^2)^2} \quad .$$

$$\beta_\pm = \frac{p_\lambda^2 - p_\pm^2}{i\omega g^2(1-\epsilon)} = -i\,\frac{n_e m_e(\omega + i/\tau)}{\alpha(p_\Lambda^2 - p_\pm^2)} \quad ,$$

$$p_\pm^2 = \tfrac{1}{2}\left[\, p_\lambda^2 + p_\Lambda^2 \pm \sqrt{(p_\lambda^2 - p_\Lambda^2)^2 + 4g^2\Omega_p^2/c_s^2}\,\right] .$$

In general we can write

$$\vec{v}(\vec{r}) = \sum_{\ell m} \vec{v}_{\ell m}(\vec{r}) \quad , \tag{B.5a}$$

and

$$\vec{u}(\vec{r}) = \sum_{\ell m} \vec{u}_{\ell m}(\vec{r}) \quad , \tag{B.5b}$$

where

$$\vec{v}_{\ell m}(\vec{r}) = \hat{r}\, v_0(r) Y_{\ell m} + v_1(r)\vec{X}_{\ell m} + v_2(r)\hat{r}\times\vec{X}_{\ell m} \quad , \tag{B.6a}$$

and

$$\vec{u}_{\ell m}(\vec{r}) = \hat{r}\, u_0(r) Y_{\ell m} + u_1(r)\vec{X}_{\ell m} + u_2(r)\hat{r}\times\vec{X}_{\ell m} \quad , \tag{B.6b}$$

and, $\vec{X}_{\ell m} = [\ell(\ell+1)]^{-1/2}\,\vec{L}Y_{\ell m}$ is the vector spherical harmonic function while $\vec{L} = -i\,\vec{r}\times\nabla$ is the angular momentum operator.

In general for an arbitrary vector function $\vec{A}(\vec{r})$, which could be expressed in spherical coordinates as

$$\vec{A}(\vec{r}) = \hat{r}\, A_0(r) Y_{\ell m} + A_1(r)\vec{X}_{\ell m} + A_2(r)\hat{r}\times\vec{X}_{\ell m} \quad , \tag{B.7}$$

the differential operation would give

$$\nabla\cdot\vec{A}(\vec{r}) = \frac{1}{r}\left[2A_0(r) + r\partial_r A_0(r) - i\sqrt{\ell(\ell+1)}\, A_2(r)\right] Y_{\ell m}, \tag{B.8}$$

$$\begin{aligned} r\nabla\times\vec{A}(\vec{r}) = {} & i\hat{r}\, A_1(r)\sqrt{\ell(\ell+1)}\, Y_{\ell m} \\ & - \left[A_2(r) + r\partial_r A_2(r) + i\sqrt{\ell(\ell+1)}\, A_0(r) \right]\vec{X}_{\ell m} \\ & + \left[A_1(r) + r\partial_r A_1(r) \right]\hat{r}\times\vec{X}_{\ell m} \, . \end{aligned} \tag{B.9}$$

We could get v_2 and u_2 by simply using the continuity equations (B.1e) and (B.1f) in combination with (B.8), they are

$$\begin{aligned} v_\ell(r) = {} & -i\left[r\sqrt{\ell(\ell+1)}\right]^{-1}\Big\{ E_{\ell m}[p_+ r j_\ell(p_+ r)]' + F_{\ell m}[p_- r j_\ell(p_- r)]' \\ & + A_{\ell m}\left[\left(c_+ - i\tfrac{\omega}{n_0} r^2\right) j_\ell(k_+ r) + (c_+ + 2e_+) k_+ r j_\ell'(k_+ r) \right. \\ & \qquad \left. + e_+ (k_+ r)^2 j_\ell''(k_+ r)\right] \\ & + B_{\ell m}\left[\left(c_- - i\tfrac{\omega}{n_0} r^2\right) j_\ell(k_- r) + (c_- + 2e_-) k_- r j_\ell'(k_- r) \right. \\ & \qquad \left. + e_- (k_- r)^2 j_\ell''(k_- r)\right] \Big\} \quad , \end{aligned} \tag{B.10a}$$

$$u_\ell(r) = -i\left[r\sqrt{\ell(\ell+1)}\right]^{-1}\Big\{E_{\ell m}\beta_+[p_+ r j_\ell(p_+ r)]' + \beta_- F_{\ell m}[p_- r j_\ell(p_- r)]' + \sqrt{\ell(\ell+1)}\Big[A_{\ell m}\big((f_+ + \tfrac{\alpha_+}{n_o}r^2)j_\ell(k_+ r) + (f_+ + 2d_+)k_+ r j_\ell'(k_+ r) + d_+(k_+ r)^2 j_\ell''(k_+ r)\big) + B_{\ell m}\big((f_- + \tfrac{\alpha_-}{n_o}r^2)j_\ell(k_- r) + (f_- + 2d_-)k_- r j_\ell'(k_- r) + d_-(k_- r)^2 j_\ell''(k_- r)\big)\Big]\Big\} \quad . \tag{B.10b}$$

To get the solutions for v_1 and u_1, we note from (B.9) that the r components of $\nabla \times \vec{v}$ and $\nabla \times \vec{u}$ are proportional to v_1 and u_1, hence we should construct the wave equations for $\nabla \times \vec{v}$ and $\nabla \times \vec{u}$. To do so we note that (B.1g) gives the relations between the e.m. fields and the density of electrons as well as the velocity of electrons, they are

$$e\vec{E} = im_e(\omega + i/\tau)\vec{v} - \chi_o \nabla \nu_- \quad , \tag{B.11a}$$

$$eq\vec{B} = m_e(\omega + i/\tau)\nabla \times \vec{v} \quad . \tag{B.11b}$$

The curl of (B.1h) gives the wave equation for $\nabla \times \vec{u}$, and the curl of (B.1d) gives the wave equation for $\vec{B}$, substituting (B.11) into these wave equations and taking their r components we get the wave equations for v_1 and u_1 as follows:

$$(\nabla^2 + p_\lambda^2)v_1(r)Y_{\ell m} = iq^2\omega(1-\epsilon)u_1(r)Y_{\ell m} \tag{B.12a}$$

$$(\nabla^2 + p_\Lambda^2)u_1(r)Y_{\ell m} = -i[\, n_o m_e(\omega + i/\tau)/\alpha\,]v_1(r)Y_{\ell m} \tag{B.12b}$$

The solutions are

$$v_1(r) = C_{\ell m} j_\ell(p_+ r) + D_{\ell m} j_\ell(p_- r) \quad , \tag{B.13a}$$

$$u_1(r) = \beta_+ C_{\ell m} j_\ell(p_+ r) + \beta_- D_{\ell m} j_\ell(p_- r) \quad . \tag{B.13b}$$

Solutions (B.3), (B.4), (B.10), (B.13) and (B.5), (B.6)

are the full solution of wave equations (B.2), and by using (B.11) we can get the solutions for the e.m. fields.

The fields outside the sphere are well-known. Assume that the incident wave is a circular polarized plane wave

$$\vec{E}^i(\vec{r}) = \mathcal{E}\,(\,\hat{x} + i\hat{y}\,)\,e^{iqz-i\omega t}\quad , \tag{B.14a}$$

$$\vec{B}^i(\vec{r}) = \hat{z}\times\vec{E}^i(\vec{r}) = \mp\, i\vec{E}^i(\vec{r})\quad , \tag{B.14b}$$

where $\mathcal{E}$ is the amplitude of the incident fields. The spherical expansion of the fields outside the sphere, including the incident wave and the scattering wave, is given in (2.2.17) where the coefficients β_{lm} and α_{lm} correspond to the electric and magnetic response, respectively.

The boundary conditions are the follows: at r=a, both $\vec{E}$ and $\vec{B}$ are continuous. This gives 6 equations of which only 5 are independent. The surface force and the stress tensor are given in section 3 already. The vanishing of the surface stress implies

$$\hat{r}\cdot\overleftrightarrow{\sigma}\cdot\hat{r} = 0\ ,$$

$$\hat{r}\cdot\overleftrightarrow{\sigma}\cdot\hat{\theta} = 0\ ,$$

$$\hat{r}\cdot\overleftrightarrow{\sigma}\cdot\hat{\phi} = 0\ .$$

or, in a explicit form

$$-n_0\chi_0 v_0(a) + 2\alpha\,\partial_r u_0(r)\Big|_{r=a} - (\beta-\alpha)\frac{v_1(a)}{n_0} = 0\ , \tag{B.15a}$$

$$\alpha\,\partial_r u_1(r)\Big|_{r=a} - u_1(a) = 0\quad , \tag{B.15b}$$

$$\frac{i}{\sqrt{l(l+1)}}\,(a\,\partial_r u_2(r)\Big|_{r=a} - u_2(a)\,) + u_0(a) = 0\ . \tag{B.15c}$$

Thus we have total 8 independent conditions to determine 8 coefficients. These 8 conditions are separated into two groups, one is related to β_{lm} , the electric response, another is related to α_{lm} , the magnetic response.

They are

$$C_{lm} j_l(y_+) + D_{lm} j_l(y_-) = G_1 [\, j_l(z) + \frac{\alpha_{lm}}{2} h_l^{(1)}(z) \,], \quad \text{(B.16a)}$$

$$C_{lm} y_+ j_l'(y_+) + D_{lm} y_- j_l'(y_-) = G_1 z [j_l'(z) + \frac{\alpha_{lm}}{2} h_l^{(1)\prime}(z)] \,, \quad \text{(B.16b)}$$

$$C_{lm} \beta_+ [y_+ j_l'(y_+) - j_l(y_+)] + D_{lm} \beta_- [y_- j_l'(y_-) - j_l(y_-)] = 0, \quad \text{(B.16c)}$$

and

$$E_{lm} j_l(y_+) + F_{lm} j_l(y_-) + A_{lm}[2L_+ j_l(x_+) + W_+ x_+ j_l'(x_+)]$$
$$+ B_{lm}[2L_- j_l(x_-) + W_- x_- j_l'(x_-)] = G_2 [j_l(z) + \frac{\beta_{lm}}{2} h_l^{(1)}(z)] \,, \quad \text{(B.17a)}$$

$$E_{lm}[y_+ j_l(y_+)]' + F_{lm}[y_- j_l(y_-)]'$$
$$+ A_{lm}\{[L_+(2-p_\lambda^2 a^2 + x_+^2) + l(l+1)W_+] j_l(x_+) + 2L_+ x_+ j_l'(x_+)\}$$
$$+ B_{lm}\{[L_-(2-p_\lambda^2 a^2 + x_-^2) + l(l+1)W_-] j_l(x_-) + 2L_- x_- j_l'(x_-)\}$$
$$= G_2 [(z j_l(z))' + \frac{\beta_{lm}}{2} (z h_l^{(1)}(z))'] \,, \quad \text{(B.17b)}$$

$$E_{lm} y_+^2 j_l(y_+) + F_{lm} y_-^2 j_l(y_-)$$
$$+ A_{lm}[2p_\lambda^2 a^2 L_+ j_l(x_+) + (p_\lambda^2 a^2 - x_+^2) L_+ x_+ j_l'(x_+)]$$
$$+ B_{lm}[2p_\lambda^2 a^2 L_- j_l(x_-) + (p_\lambda^2 a^2 - x_-^2) L_- x_- j_l'(x_-)]$$
$$= G_2 z^2 [j_l(z) + \frac{\beta_{lm}}{2} h_l^{(1)}(z)] \,, \quad \text{(B.17c)}$$

$$E_{lm} \beta_+ [y_+ j_l'(y_+) - j_l(y_+)] + F_{lm} \beta_- [y_- j_l'(y_-) - j_l(y_-)]$$
$$+ A_{lm}[D_+ j_l(x_+) + (f_+ - 2d_+) x_+ j_l'(x_+)]$$
$$+ B_{lm}[D_- j_l(x_-) + (f_- - 2d_-) x_- j_l'(x_-)] = 0 \,, \quad \text{(B.17d)}$$

$$E_{\ell m}\beta_+[(\ell(\ell+1)-1-0.5y_+^2)j_\ell(y_+) - y_+ j'_\ell(y_+)]$$
$$+ F_{\ell m}\beta_-[(\ell(\ell+1)-1-0.5y_-^2)j_\ell(y_-) - y_- j'_\ell(y_-)]$$
$$+ A_{\ell m}[E_+ j_\ell(x_+) + F_+ x_+ j'_\ell(x_+)]$$
$$+ B_{\ell m}[E_- j_\ell(x_-) + F_- x_- j'_\ell(x_-)] = 0 , \qquad \text{(B.17e)}$$

where $x_\pm = k_\pm a$, $y_\pm = p_\pm a$, $z = qa$,

$$G_1 = -i^{\ell+1}\,\delta_{m,\pm1}[4\pi(2\ell+1)]^{1/2} e/m_e(\omega+i/\tau) ,$$

$$G_2 = +i^{\ell+1}\,\delta_{m,\pm1}[4\pi(2\ell+1)\ell(\ell+1)]^{1/2} e\omega/n_o q m_e(\omega+i/\tau),$$

and

$$D_\pm = d_\pm \ell(\ell+1) - x_\pm^2) - f_\pm + \frac{a^2}{2\alpha}\left(\frac{\alpha-\beta}{n_o}\alpha_\pm - n_o\chi_o\right) ,$$
$$E_\pm = \ell(\ell+1)(f_\pm - d_\pm) - f_\pm (1+0.5x_\pm^2) ,$$
$$F_\pm = d_\pm \ell(\ell+1) - f_\pm + \frac{a^2}{2n_o}\alpha_\pm - 0.5 d_\pm x_\pm^2 ,$$

$$L_\pm = \frac{i\omega}{n_o}\,\frac{P_\lambda^2 - g^2\lambda^{-2}(1-\epsilon)K_\pm^2}{(P_\lambda^2 - K_\pm^2)^2} ,$$

$$W_\pm = \frac{i\omega}{n_o}\,\frac{1+\lambda^{-2}(1-\epsilon)(P_\lambda^2 - g^2 - K_\pm^2)}{P_\lambda^2 - K_\pm^2} ,$$

From (B.16) the magnetic response coefficient $\alpha_{\ell m}$ is

$$\alpha_{\ell m} = -2\,\frac{\Delta_\alpha}{\Delta} \qquad \text{(B.18)}$$

where

$$\Delta_\alpha = \beta_+[j_\ell(y_+) - y_+ j'_\ell(y_+)][y_- j_\ell(z) j'_\ell(y_-) - z j_\ell(y_-) j'_\ell(z)]$$
$$- \beta_-[j_\ell(y_-) - y_- j'_\ell(y_-)][y_+ j_\ell(z) j'_\ell(y_+) - z j_\ell(y_+) j'_\ell(z)] , \qquad \text{(B.19a)}$$

$$\Delta = \beta_+[j_\ell(y_+) - y_+ j'_\ell(y_+)][y_- h^{(1)}_\ell(z) j'_\ell(y_-) - z j_\ell(y_-) h^{(1)\prime}_\ell(z)]$$
$$- \beta_-[j_\ell(y_-) - y_- j'_\ell(y_-)][y_+ h^{(1)}_\ell(z) j'_\ell(y_+) - z j_\ell(y_+) h^{(1)\prime}_\ell(z)], \qquad \text{(B.19b)}$$

Th electric response coefficient $\beta_{\ell m}$ has a more complicated form, and it is better to solve for them on a computer.

In long wavelength approximation, $z \ll 1$,

$$j_1(z) \approx z/3, \qquad h_1^{(1)}(z) \approx -i/z ,$$

the magnetic dipole response goes to

$$\alpha_1 \cong i\frac{2}{3} z^3 \frac{p_-^2 - p_+^2}{-(p_\lambda^2 - p_-^2)\frac{2 j_1(y_+) + y_+ j_1'(y_+)}{j_1(y_+) - y_+ j_0(y_+)} + (p_\lambda^2 - p_+^2)\frac{2 j_1(y_-) + y_- j_1'(y_-)}{j_1(y_-) - y_- j_0(y_-)}} \qquad (B.20)$$

since

$$x j_0(x) = 2 j_1(x) + x j_1'(x) ,$$

$$x j_2(x) = j_1(x) - x j_1'(x) ,$$

and

$$i_0(ix) = j_0(x), \qquad i_2(ix) = -j_2(x) ,$$

it becomes

$$\alpha_1 \cong i\frac{2}{3} z^3 \frac{-p_-^2 + p_+^2}{(p_\lambda^2 - p_+^2)\frac{i_0(iy_-)}{i_2(iy_-)} + (p_\lambda^2 - p^2)\frac{j_0(y_+)}{j_2(y_+)}} \qquad (B.21)$$

This is exactly the (1.4.32).

In the frozen jellium limit, $\rho_i \sim \infty$ and $\alpha \sim \infty$, $\beta \sim \infty$, the magnetic response becomes

$$\alpha_{\ell m} \cong -2 \frac{y j_\ell(z) j_\ell'(y) - z j_\ell(y) j_\ell'(z)}{y h_\ell^{(1)}(z) j_\ell'(y) - z j_\ell(y) h_\ell^{(1)\prime}(z)} \qquad (B.22)$$

where $y = p_\lambda a = \frac{\omega}{c} a\sqrt{\epsilon}$. (B.22) is consistent with (2.2.18) in Chapter II. In this limit $L_+=0$, $y_-=0$, $x_-=0$, $y_+=y=p_\lambda a$, $x_+=x=k_\lambda a$, and equations (B.17) become

$$E_{\ell m} j_\ell(y) + A_{\ell m} W_+ x j_\ell'(x) = G_\ell [j_\ell(z) + \frac{\beta_{\ell m}}{2} h_\ell^{(1)}(z)] , \qquad (B.23a)$$

$$E_{\ell m}[yj_\ell(y)]'+A_{\ell m}\,\ell(\ell+1)W_+ j_\ell(x) = G_2[(zj_\ell(z))' + \frac{\beta_{\ell m}}{2}(zh_\ell^{(1)}(z))'], \tag{B.23b}$$

$$E_{\ell m}y^2 j_\ell(y) = G_2 z^2[j_\ell(z) + \frac{\beta_{\ell m}}{2} h_\ell^{(1)}(z)] \ . \tag{B.23c}$$

The solution for the electric response in the frozen jellium limit is the same as (2.2.19) in Chapter II.

The full electrodynamic solution is then checked under two approximations: the long wavelength and the frozen jellium approximations.

The scattering cross section σ_s, the absorption cross section σ_a, and the exinction cross section σ_e are then given by

$$\sigma_s = (\pi/2q^2)\sum_\ell (2\ell+1)[\,|\alpha_\ell|^2 + |\beta_\ell|^2\,] \tag{B.24a}$$

$$\sigma_a = (\pi/2q^2)\sum_\ell (2\ell+1)[2-|\alpha_\ell+1|^2-|\beta_\ell+1|^2], \tag{B.24b}$$

$$\sigma_e = -(\pi/q^2)\sum_\ell (2\ell+1)\mathrm{Re}[\alpha_\ell + \beta_\ell] \ . \tag{B.24c}$$

Figure Captions

Fig.1.1 (a). Electric-dipole-absorption contribution to the attenuation constant vs frequency for a 200 Å-radius Al sphere. The frequency range is seen from 0 to 100 cm^{-1}.
(b). Same as (a), but with a frequency range extending to 500 cm^{-1}. Series of sharp peaks occurs at both (a) and (b). At frequencies above 400 cm^{-1}, the electrical dipole absorption is seen to fall off rather quickly.

Fig.1.2 Electric-dipole-absorption attenuation constant vs sphere radius for frequency $\tilde{\nu}$ =40cm^{-1}. There exists a set of closely spaced resonances which are swept through if the particle size changes by only 0.7 Å.

Fig.1.3 Mode frequency vs scaled wave vector for the longitudinal (x and z) and transverse (y) modes. The abscissa is in dimensionless units. The real and imaginary parts of x and z are shown along with the real part of y. The imaginary part of y is small.

Fig.1.4 Real and imaginary parts of the magnetic polarizability for a 200 Å-radius sphere plotted as a function of frequency.

Fig.1.5 (a). Real and imaginary parts of the scaled wave vector z=pa plotted as a function of the frequency for the magnetic mode.
(b). Real part of the scaled wave vector x=ka plotted as a function of frequency for the magnetic mode.

Fig.1.6 Magnetic contribution to the attenuation constant plotted as a function of the frequency. Curves a, c, and e are for a 200 Å-radius Al sphere, and curves b, d, and f are for a 500 Å-radius Al sphere. Curve a and b include phonon effects, curve c and d exclude phonons, and curve e and f involve further approximation.

Fig.1. Magnetic contribution to the attenuation constant averaged over the size distribution plotted as a function of frequency. Curve a includes phonon effects, curve b neglets phonons, and curve c involves a further approximation. Curve d represents only the electric-dipole-absorption contribution to the attenuation constant. Several experimental points are also shown as X's. The electric-dipole-absorption is two more orders smaller than the magnetic dipole absorption. The present theory is still about a factor of 4 too small to account for the observation even in small filling factor case.

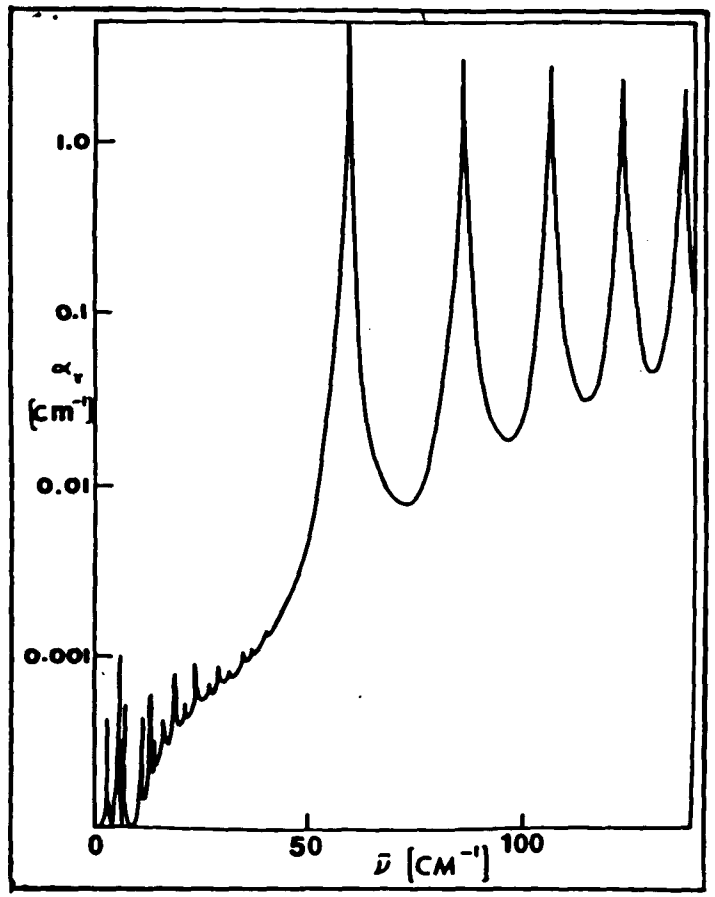
1.0
0.1
α_ν [cm^{-1}]
0.01
0.001
0
50
100
$\bar{\nu}$ [CM^{-1}]

(a)

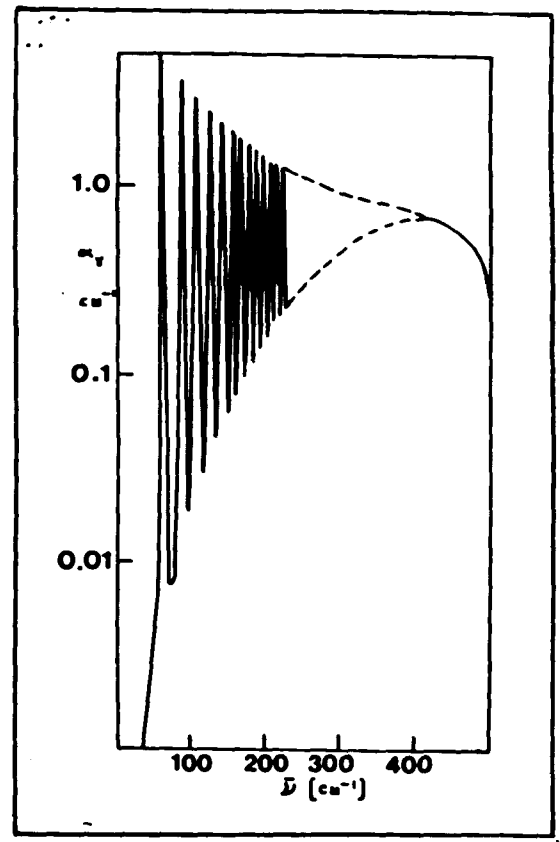
1.0
0.1
0.01
100
200
300
400
$\bar{\nu}$ [cm^{-1}]

(b)

Fig.1.1

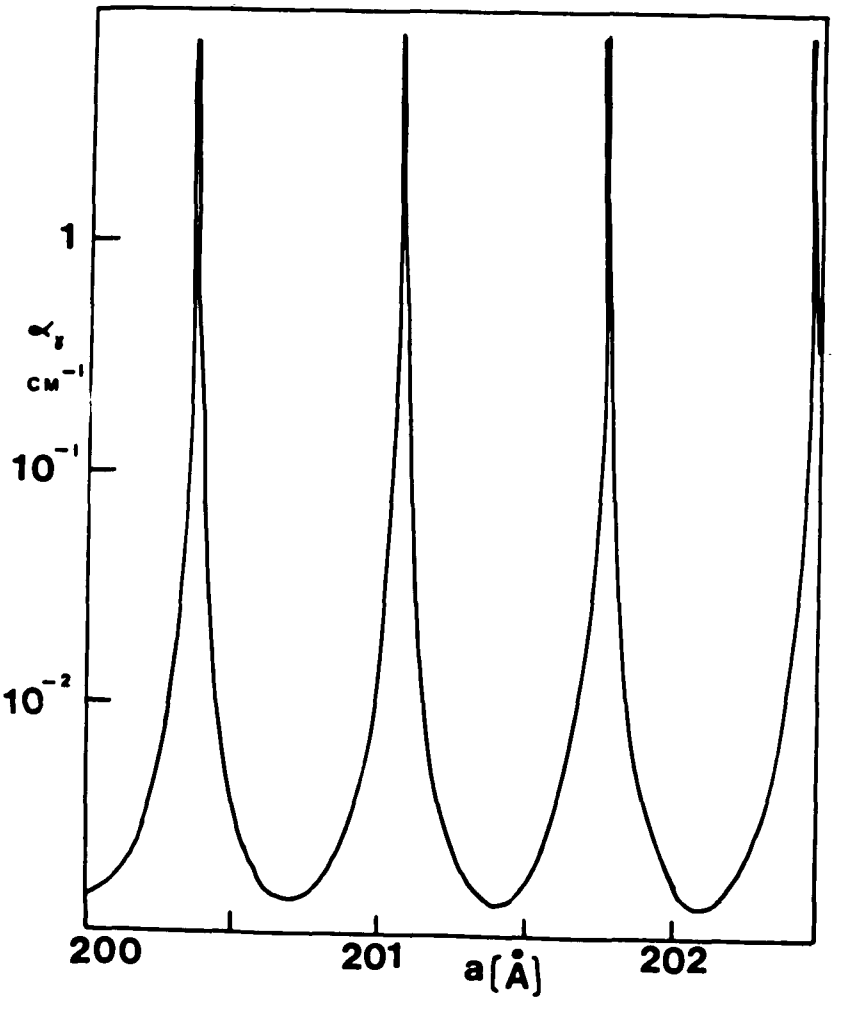

Fig.1.2

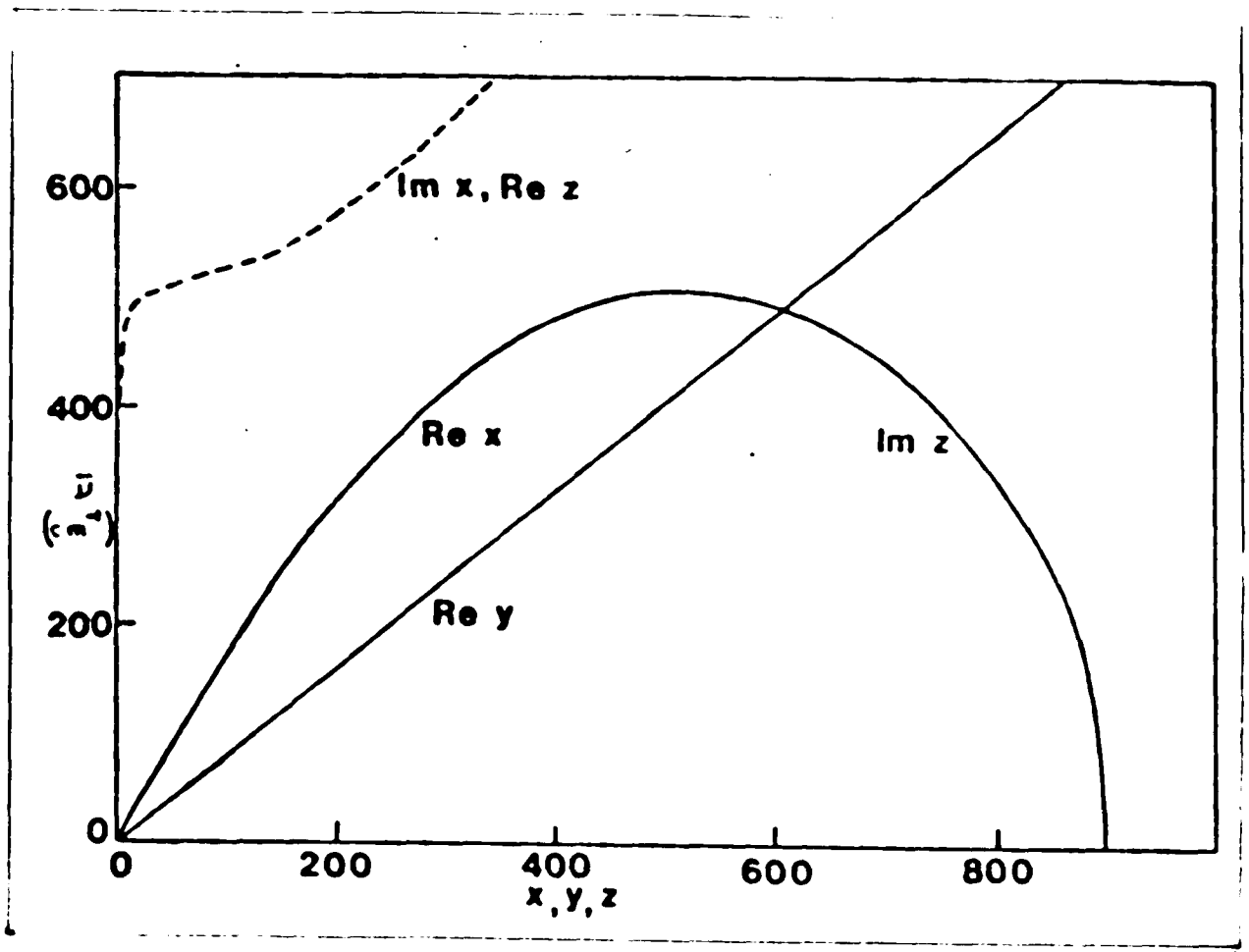

Fig.1.3

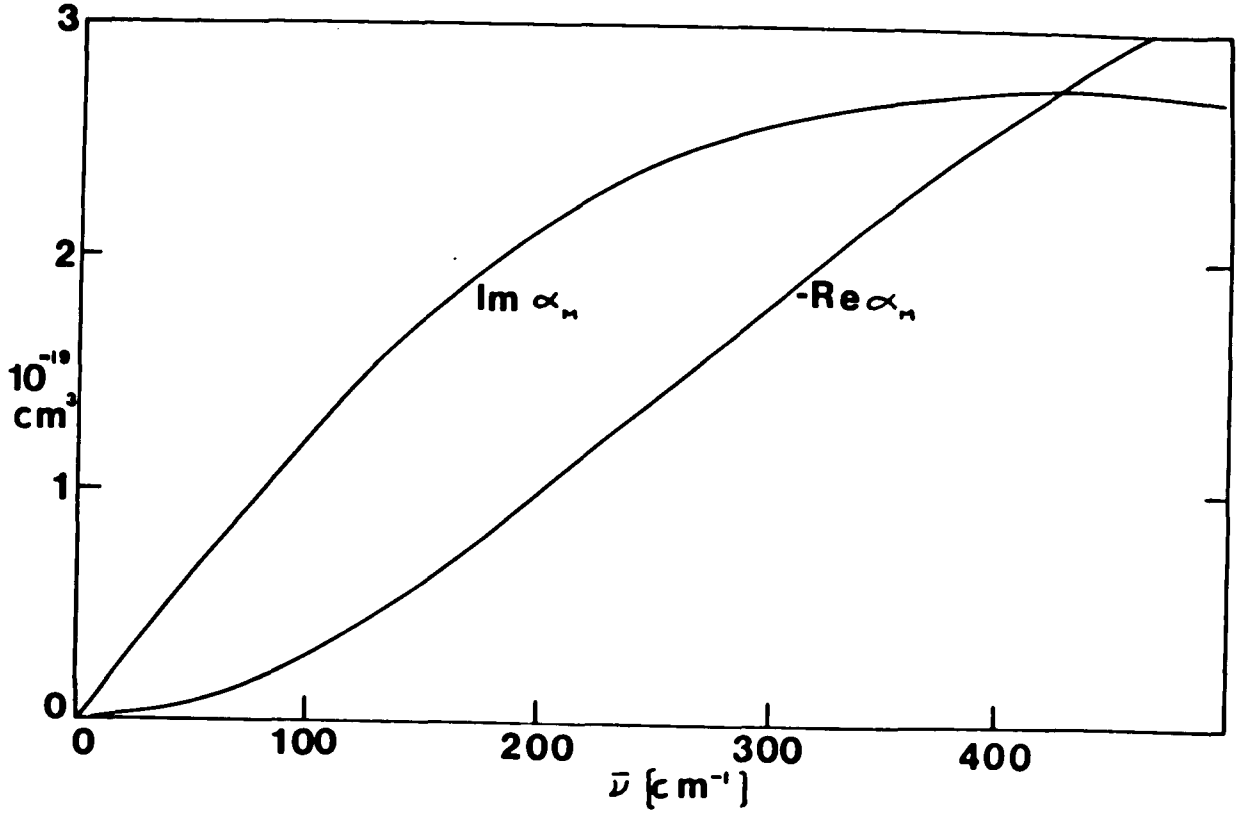

Fig.1.4

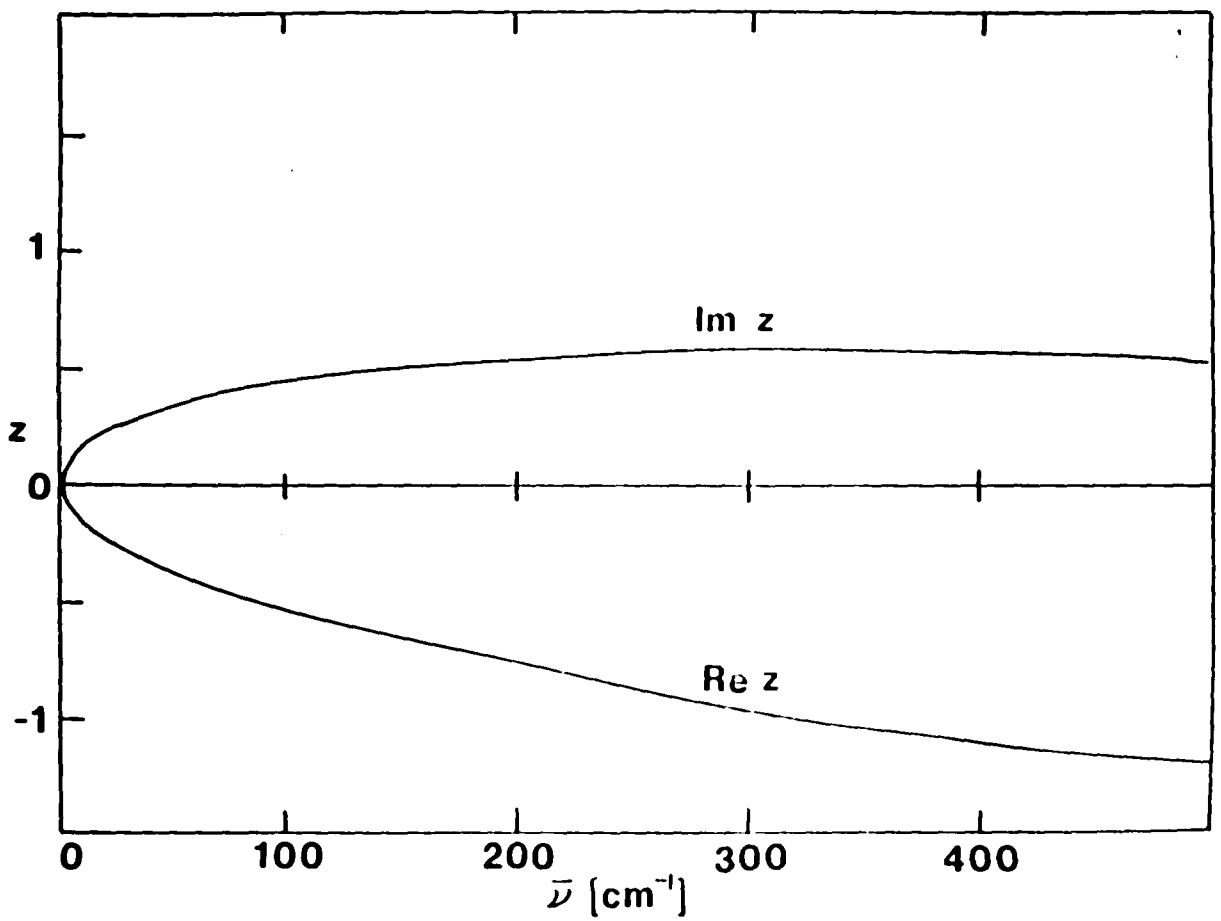

Fig.1.5 (a)

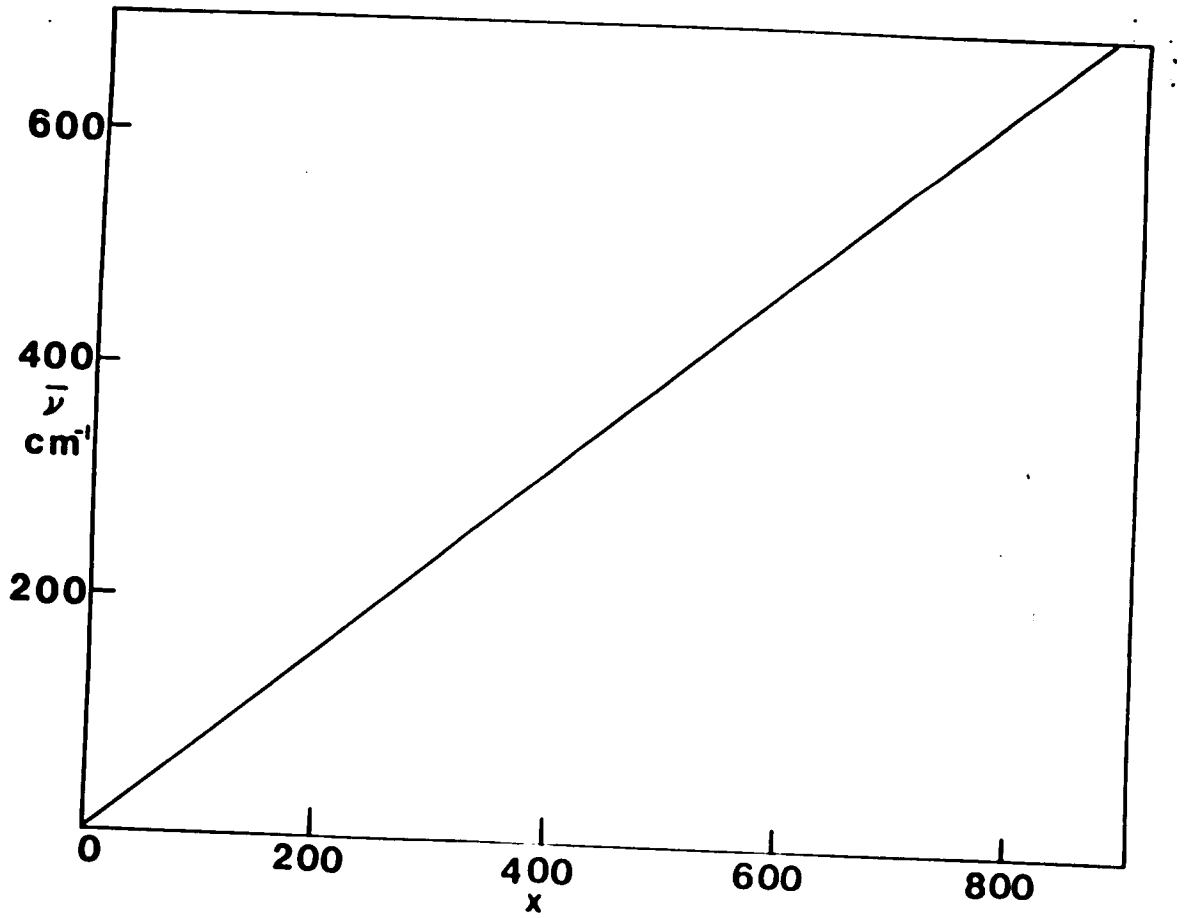

Fig.1.5 (b)

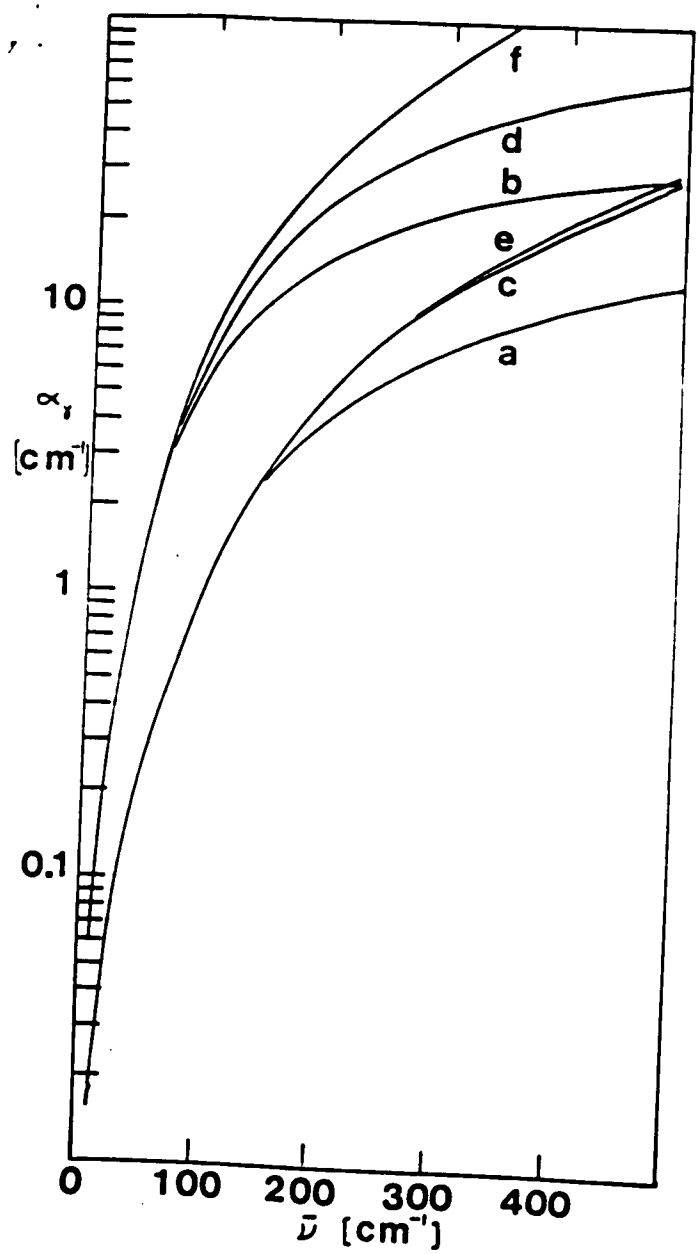

Fig.1.6

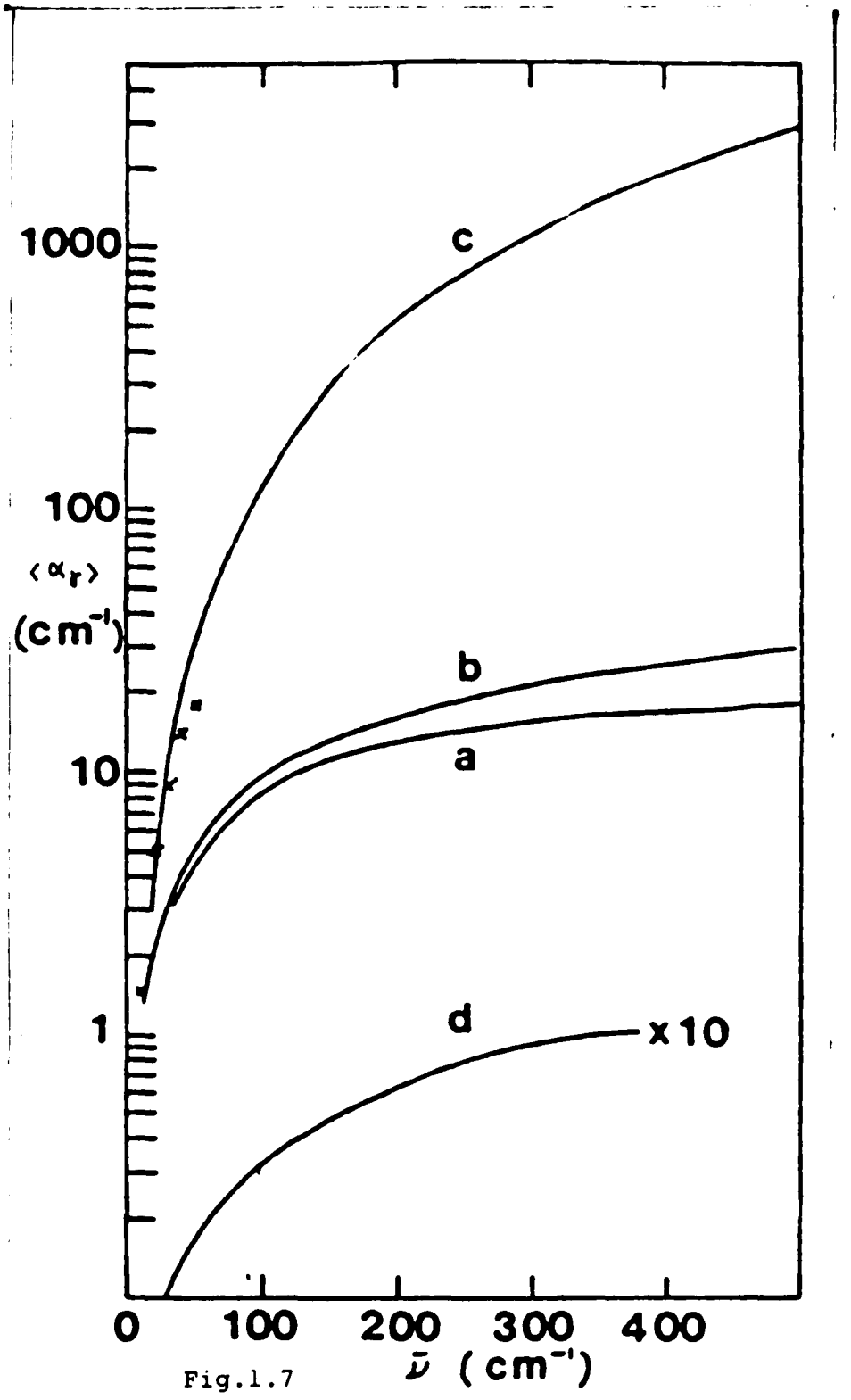

Fig.1.7

Chapter II. Second Harmonic Generation by Small Metallic Particles

2.1. Introduction

Ever since intense sources of electromagnetic radiation have become available, interest in the nonliear optical properties of matter has persisted[1]. One of the most elementary manifestations of such a nonlinear property is second harmonic generation (SHG). First-priciples calculations of the effect in bulk matter have been carried out by numerous researchers. Adler[2] discussed the general symmetry properties of nonlinear media and outlined a formalism to compute the nonlinear polarization currents in polarization theory. Early theoretical studies of the nonlinear optical behavior of metallic surfaces were conducted by Jha and co-workers[3-4]. Experiments on media with inversion symmetry confirmed[5],to within an order of magnitude, these theoretical models. In more recent years attention has turned to rough surfaces primarily because of the observation of surface-enhanced Raman scattering[6]. Agarwal and Jha[7] have studied the surface enhancement of SHG at a metal grating using a perturbation expansion based on an expansion in terms of the surface roughnees parameter. Chen et al.[8] have

studied the interconnection between SHG and Raman scattering. Arya[9] has developed a Green's-function formalism for treating SHG from rough metal surface. Chen et al.[10] measured SHG at a silver-air interface and found that SHG was enhanced by a factor of 10^4 by surface roughnees. Since SHG is electric dipole forbidden within the bulk of centrosymmetric media it is very strongly affected by the surface layer in such a material. Therefore the SHG technique has recently attracted considerable attention as an optical probe with intrinsic surface sensitivity. It is useful at the interface between two condensed matter phases where the conventional tools of surface science are not generally applicable. Boyd et al.[11] made a detailed study of the local field enhancement of various solids using SHG as a probe. Heinz et al.[12] applied the SHG technique to study the surface reconstruction and surface phase transition on Si(111). Akhmanov et al.[13] reported the determination of the degree of disorder of the surface of a noncentrosymmetric semiconductor by using SHG and sum-frequency mixing with a high time and spatial resolution. The recent theoretical remark pertaining to SHG by Keller[14] emphasized the need for including nonlocal electronic transport effects in describing SHG.

In a somewhat unrelated development there has also developed in recent years an interest in the properties of

small particles. An extensive body of work has been devoted to the study of the linear optical response of such particles[15]. Recently the interest in nonlinear optical response of small particles is increasing. Agarwal et al[6] studied SHG of spherical particles in the context of a dielectric model for the limiting case of the particle size being much smaller than the wavelength of light. Hua and Gersten[16] extended their work in two directions. On one hand, instead of employing a dielectric theory a more microscopic theory was applied to include screening effects; on the other hand, a full Mie theory was used to avoid the limitations arising from the long wavelength approximation in dealing with particle sizes more commonly found in nature. Heilweil et al.[17] reported the first measurement of the nonlinear dispersion of $\chi^{(3)}$ of aqueous colloidal gold at the frequency of the surface plasmon resonance.

As is well-known that the harmonic expansion of the polarization P of matter could be written as

$$\vec{P} = \chi^{(\omega)} \cdot \vec{E} + \chi^{(2\omega)} : \vec{E}\,\vec{E} + \ldots \quad . \qquad (2.1.1)$$

The susceptibility tensor $\chi^{(2\omega)}$ is vanishing for the dipole response in centrosymmetric crystals, but nonvanishing for the quadrupole response. As the particle grows in size, higher multipolar responses become more and more important. Thus we may envisage a range of particle size for which quadrupolar and higher multipolar harmonic

generation becomes significant.

Bloembergen et al.[5] have discussed the contribution of the conduction electrons in media with inversion symmetry to SHG. The equation of motion for the averaged velocity $\vec{v}$ of an electron in the hydrodynamic approximation is given by

$$\partial_t \vec{v} + \vec{v}\cdot\nabla\vec{v} = -(e/m_e)(\vec{E} + \vec{v}\times\vec{B}/c) \qquad (2.1.2)$$

Expanding the fields and the source quantities (currents and charge density) in an harmonic expansion series, the SHG polarization could be written as

$$\begin{aligned}\vec{P}(2\omega) = &(n_o e^3/4m_e^2\omega^4)[\vec{E}(\omega)\cdot\nabla]\vec{E}(\omega)\\ &+(e/8\pi m_e\omega^2)\vec{E}(\omega)\nabla\cdot\vec{E}(\omega)\\ &+i(n_o e^3/4m_e^2 c\omega^3)\vec{E}(\omega)\times\vec{B}(\omega),\end{aligned} \qquad (2.1.3)$$

where n_o is the number of conduction electrons per unit volume. Based on simple symmetry considerations and Maxwell's equations, it is possible to extend this formula and develop simple formulas for the multipolar moments of a small particle in terms of the incident fields. We restrict our attention to SHG and let $\vec{\mu}$, $\vec{m}$, $\overleftrightarrow{Q}$, and $\overleftrightarrow{\chi}$ denote the electric dipole moment, the magnetic dipole moment, the electric quadrupole moment and the magnetic quadrupole moment, respectively. Note that $\vec{\mu}$ and $\overleftrightarrow{\chi}$ are odd under parity reversals, while $\vec{m}$ and $\overleftrightarrow{Q}$ are even. Also note that $\vec{\mu}$ and $\overleftrightarrow{Q}$ are even under time reversal, while $\vec{m}$ and $\overleftrightarrow{\chi}$ are odd. Thus, in a truncated hierarchy,

$$\vec{\mu}(2\omega) = \beta_E \nabla E^2 + \gamma_E \vec{E}\cdot\nabla\vec{E} + \delta_E \nabla B^2 + \epsilon_E \vec{B}\cdot\nabla\vec{B} \quad ,$$

$$\vec{m}(2\omega) = \beta_M \vec{E}\times(\nabla\times\vec{B}) + \gamma_M \vec{B}\times(\nabla\times\vec{E}) + \delta_M E_i \nabla B_i$$

$$+ \epsilon_M B_i \nabla E_i + \nu_M \vec{E}\cdot\nabla\vec{B} + \sigma_M \vec{B}\cdot\nabla\vec{E} \quad ,$$

$$\overleftrightarrow{Q}(2\omega) = \alpha_Q (E^2 \overleftrightarrow{I} - 3\vec{E}\vec{E}) + \beta_Q (B^2 \overleftrightarrow{I} - 3\vec{B}\vec{B}) \quad ,$$

$$\overleftrightarrow{\chi}(2\omega) = \gamma \overleftrightarrow{I}\, \vec{E}\cdot\vec{B} + \delta \vec{E}\vec{B} + \delta' \vec{B}\vec{E} \quad ,$$

where α, β, γ, δ,... are coefficients which depend on the nature of the particle's composition.

This chapter is based on the work [16] and arranged as follows. In section II a classical model is presented, the linear solution is obtained in analytic form and the nonlinear solution is obtained by using the Green's function method. In section III numerical results are obtained for small Al and Ag particles and the discussion of the results is presented.

2.2 Theory

a. The Model

Consider a metallic sphere of radius a interacting with an incident plane electromagnetic wave. In our previous work[18] we introduced a model in which both the electrons and ions were modeled as interacting hydrodynamic and elastic systems. For the case of SHG, however, we are likely to be concerned with photon frequencies sufficiently high that the ionic contribution will not be of significant size to warrant its inclusion in the model. Thus we consider an electronic fluid moving in the presence of a uniform ionic jellium background. Our goal is to solve Maxwell's equations.

$$\nabla \cdot \vec{E}=4\pi\rho \ , \tag{2.2.1a}$$

$$\nabla \cdot \vec{B}=0 \ , \tag{2.2.1b}$$

$$\nabla \times \vec{E}+(1/c)\partial_t \vec{B}=0 \ , \tag{2.2.1c}$$

$$\nabla \times B-(1/c)\partial_t \vec{E}=(4\pi/c)\vec{J} \ , \tag{2.2.1d}$$

together with the hydrodynamical equation for the electrons

$$m_e \left[d\vec{v}/dt+\vec{v}/\tau\right]=-e[\vec{E}+\vec{v}\times\vec{B}/c]-\nabla\mu \ . \tag{2.2.2}$$

Here ρ and $\vec{J}$ are the charge and current densities, e and m_e are the charge and mass of the electron, τ is the electron relaxation time, $\vec{v}$ is the electron velocity and μ is the chemical potential. Thus

$$\rho=-e(n-n_o), \tag{2.2.3a}$$

$$\vec{J}=-ne\vec{v} \ , \tag{2.2.3b}$$

where n is the electron density and n_o is the ion density. At the level of Thomas-Fermi-Dirac theory

$$\mu = (\hbar k_f)^2/2m_e - e^2(3n/\pi)^{1/3} \quad , \tag{2.2.4}$$

where $k_f=(3\pi^2 n)^{1/3}$ is the Fermi wave vector.

We shall derive our description of SHG from perturbation theory. The first order response will be at the incident frequency, ω, while the second order response includes, in principle, contributions from both 2ω and D.C. effects. The latter are of no interest here so will be neglected. Thus let

$$n-n_o=n_L+n_S+\ldots \quad , \tag{2.2.5a}$$

$$\vec{v}=\vec{v}_L+\vec{v}_S+\ldots \quad , \tag{2.2.5b}$$

$$\vec{E}=\vec{E}_L+\vec{E}_S+\ldots \quad , \tag{2.2.5c}$$

$$\vec{B}=\vec{B}_L+\vec{B}_S+\ldots \quad , \tag{2.2.5d}$$

where the subscripts denote the particular harmonic in question (L = linear, S = second harmonic,...). By assumption, $|n_S| << |n_L| << n_o$ etc. Noting that the chemical potential is nonlinear in the electron density we obtain

$$\mu = \mu_o + \chi_o n_L + \chi_o n_S + \chi_1 n_L^2 + \ldots \quad , \tag{2.2.6}$$

where the expansion constants are

$$\mu_o = (\hbar k_f^o)^2/2m_e - e^2 k_f^o/\pi \quad , \tag{2.2.7a}$$

$$\chi_o = (\hbar k_f^o)^2/3n_o m_e - e^2 k_f^o/3\pi n_o \quad , \tag{2.2.7b}$$

$$\chi_1 = -\mu_o/9n_o^2 \quad , \tag{2.2.7c}$$

and $k_f^o = (3\pi^2 n_o)^{1/3}$. Carrying out similar

expansions for ρ and J and the various terms of Eq.(2.2.2) leads to a revised set of equations which may be separated into first and second order equations:

$$\nabla \cdot \vec{E}_L = -4\pi e n_L \quad , \tag{2.2.8a}$$

$$\nabla \cdot \vec{B}_L = 0 \quad , \tag{2.2.8b}$$

$$\nabla \times \vec{E}_L = i\frac{\omega}{c}\vec{B}_L \quad , \tag{2.2.8c}$$

$$\nabla \times \vec{B}_L = -i\frac{\omega}{c}\vec{E}_L - 4\pi e n_o \vec{v}_L/c \quad , \tag{2.2.8d}$$

$$m_e(-i\omega + 1/\tau)\vec{v}_L = -e\vec{E}_L - \chi_o \nabla n_L \quad , \tag{2.2.8e}$$

and

$$\nabla \cdot \vec{E}_S = -4\pi e n_S \quad , \tag{2.2.9a}$$

$$\nabla \cdot \vec{B}_S = 0 \quad , \tag{2.2.9b}$$

$$\nabla \times \vec{E}_S = 2i\frac{\omega}{c}\vec{B}_S \quad , \tag{2.2.9c}$$

$$\nabla \times \vec{B}_S = -2i\frac{\omega}{c}\vec{E}_S - 4\pi e(n_o \vec{v}_S + n_L \vec{v}_L)/c \quad , \tag{2.2.9d}$$

$$m_e(-2i\omega + 1/\tau)\vec{v}_S + m_e \vec{v}_L \cdot \nabla \vec{v}_L = -e(\vec{E}_S + \vec{v}_L \times \vec{B}_L/c) - \chi_o \nabla n_S - \chi_1 \nabla n_L^2 \quad , \tag{2.2.9e}$$

Note that the first order equations are homogeneous equations whereas the second order equations are inhomogeneous with the first order variables acting as source terms. The incident field for the linear equations enters through the boundary conditions.

To compare with (2.1.3), we could define the second order polarization $\vec{P}(2\omega)$ by setting the Maxwell's equation as

$$\nabla \times \vec{B}_S = -i(2\omega/c)\epsilon_2 \vec{E}_S + (4\pi/c)\partial_t \vec{P}(2\omega) \quad .$$

Identify the above equation to Eq.(2.2.9d), $\vec{P}(2\omega)$ could

be derived as

$$\vec{P}(2\omega)=e(1-\epsilon_2)[4\pi m_e(\omega+i/\tau)]^{-1}\vec{E}_L\cdot\nabla\vec{E}_L$$
$$+e(1-\epsilon_2)[4\pi m_e\omega(\omega+i/\tau)]^{-1}\vec{E}_L\times(\nabla\times\vec{E}_L)$$
$$+e[8\pi m_e\omega(\omega+i/\tau)]^{-1}\vec{E}_L\nabla\cdot\vec{E}_L$$
$$+\vec{P}^c(2\omega) \quad ,$$

where $\vec{P}^c(2\omega)$ is correction to the second order polarization from the screening and is given by

$$\vec{P}^c(2\omega)=-(\chi_e/4\pi e)\{(1-\epsilon_2)[4\pi m_e(\omega+i/\tau)^2]^{-1}[$$
$$\vec{E}_L\cdot\nabla\nabla(\nabla\cdot\vec{E}_L)+\nabla(\nabla\cdot\vec{E}_L)\cdot\nabla\vec{E}_L$$
$$-(\chi_e/4\pi e^2)\nabla(\nabla\cdot\vec{E}_L)\cdot\nabla\nabla(\nabla\cdot\vec{E}_L)]$$
$$-(1-\epsilon_2)[4\pi m_e\omega(\omega+i/\tau)]^{-1}\nabla(\nabla\cdot\vec{E}_L)\times(\nabla\times\vec{E}_L)$$
$$-[8\pi m_e\omega(\omega+i/\tau)]^{-1}(\nabla\cdot\vec{E}_L)\nabla(\nabla\cdot\vec{E}_L)$$
$$-(1-\epsilon_2)[(\chi_1/\chi_e)(4\pi e)^{-2}\nabla(\nabla\cdot\vec{E}_L)^2-(1/4\pi e)\nabla\nabla\cdot\vec{E}_S]$$

If the correction $\vec{P}^c(2\omega)$ is very small, and we are interested in the case that $\omega >> 1/\tau$, then the above equation for $\vec{P}(2\omega)$ coincides with Eq.(2.1.3).

b. Solution of the first order equations

Wave equations for $n_L, \vec{E}_L$, and $\vec{B}_L$ follow directly from Eqs. (2.2.8):

$$(\nabla^2+k^2)n_L=0 \quad , \qquad (2.2.10a)$$

$$(\nabla^2 + p^2)\vec{E}_L = (4\pi e/k^2)(p^2 - k^2)\nabla n_L \quad , \tag{2.2.10b}$$

$$(\nabla^2 + p^2)\vec{B}_L = 0 \quad , \tag{2.2.10c}$$

where we have introduced the plasma frequency,

$$\omega_p = (4\pi n_o e^2/m_e)^{1/2} \quad , \tag{2.2.11a}$$

the Thomas-Fermi screening constant,

$$\lambda = \omega_p (m_e/\chi_o n_o)^{1/2} \quad , \tag{2.2.11b}$$

and

$$p = q\sqrt{\epsilon} \quad , \tag{2.2.11c}$$

where q is the wave vector of the photon in free space $q = \omega/c$, and

$$k = \lambda[\epsilon/(1-\epsilon)]^{1/2} \quad , \tag{2.2.11d}$$

and ϵ is the Drude dielectric constant

$$\epsilon = 1 - \omega_p^2/[\omega(\omega + i/\tau)] \quad . \tag{2.2.11e}$$

Boundary conditions for the above equations will be introduced late. The continuity equation follows directly from Maxwell's equations:

$$\nabla \cdot \vec{v}_L = i\omega n_L/n_o \quad . \tag{2.2.12}$$

The solutions to (2.2.10) which apply inside the sphere (r<a) are:

$$n_L = \sum_{\ell m} C_{\ell m} j_\ell(kr) Y_{\ell m}(\hat{r}) \quad , \tag{2.2.13a}$$

$$E_{Lr}(\vec{r}) = (1/r) \sum_{\ell m} [F_{\ell m} j_\ell(pr) + C_{\ell m}(4\pi e/k) j_\ell'(kr)] Y_{\ell m}(r) \quad , \tag{2.2.13b}$$

$$\vec{E}_{Lt}(\vec{r}) = \sum_{\ell m} \Big\{ R_{\ell m}(\ell(\ell+1))^{-1/2} j_\ell(pr) \vec{X}_{\ell m} - (\ell(\ell+1)^{1/2} [(\ell(\ell+1)r)^{-1} F_{\ell m} \partial_r(r j_\ell(pr)) + (4\pi e/k^2 r) C_{\ell m} j_\ell(kr)] \hat{r} \times \vec{X}_{\ell m} \Big\} \quad . \tag{2.2.13c}$$

$$B_{Lr}(\vec{r})=(qr)^{-1}\sum_{\ell m} R_{\ell m} j_\ell(pr) Y_{\ell m}(r) \quad , \tag{2.2.13d}$$

$$\vec{B}_{Lt}(\vec{r})=-q^{-1}\sum_{\ell m} [p^2 F_{\ell m} j_\ell(pr)\vec{}_{\ell m} + iR_{\ell m} r^{-1}\partial_r(r j_\ell(pr))\hat{r}\times\vec{X}_{\ell m}](\ell(\ell+1))^{-1/2} \tag{2.2.13e}$$

where the fields are expressed as radial and tangential fields

$$\vec{E}_L(\vec{r})=\hat{r}\, E_{Lr}(\vec{r})+\vec{E}_{Lt}(\vec{r}) \quad , \tag{2.2.14a}$$

$$\vec{B}_L(\vec{r})=\hat{r}\, B_{Lr}(\vec{r})+\vec{B}_{Lt}(r) \quad , \tag{2.2.14b}$$

and $\vec{X}_{\ell m}$ are the vector spherical harmonics defined by

$$\vec{X}_{\ell m}=(\ell(\ell+1))^{-1/2}\,\vec{L}Y_{\ell m}(\hat{r}) \quad , \tag{2.2.15a}$$

where

$$\vec{L}=-i\vec{r}\times\nabla \quad . \tag{2.2.15b}$$

The coefficients $C_{\ell m}$, $F_{\ell m}$ and $R_{\ell m}$ are to be determined by matching boundary conditions on the surface of the sphere.

Let us focus our attention on an incident circularly polarized plane wave:

$$\vec{E}=E_o(\hat{i}\pm\hat{j})e^{iqz} \quad , \tag{2.2.16a}$$

$$\vec{B}=\mp i\vec{E} \quad , \tag{2.2.16b}$$

where E_o is the amplitude of the electric field. For the linear fields the general solution for elliptically polarized light may be obtained by superposition, but for the nonlinear fields simple superposition does not apply and a more extensive analysis will be needed.

The fields outside the sphere ($r > a$) are[19].

$$\vec{E}_L = E_o \sum_{\ell m} G_{\ell m} \left\{ [j_\ell(qr) + 0.5\,\alpha_{\ell m} h_\ell^{(1)}(qr)]\vec{X}_{\ell m} \right.$$
$$\pm q^{-1}[\nabla \times (j_\ell(qr)\vec{X}_{\ell m})$$
$$\left. + 0.5\,\beta_{\ell m} \nabla \times (h_\ell^{(1)}(qr)\vec{X}_{\ell m})] \right\} , \quad (2.2.17a)$$

and

$$\vec{B}_L = -E_o \sum_{\ell m} iG_{\ell m} \left\{ q^{-1} \nabla \times [j_\ell(qr)\vec{X}_{\ell m}] \right.$$
$$+ (2q)^{-1} \alpha_{\ell m} \nabla \times [h_\ell^{(1)}(qr)\vec{X}_{\ell m}]$$
$$\left. \pm [j_\ell(qr) + 0.5\,\beta_{\ell m} h_\ell^{(1)}(qr)]\vec{X}_{\ell m} \right\} \quad (2.2.17b)$$

with

$$G_{\ell m} = \delta_{m,\pm 1} i^\ell [4\pi(2\ell+1)]^{1/2} .$$

Again the coefficients $\alpha_{\ell m}$ and $\beta_{\ell m}$ are to be determined by matching boundary conditions.

In the present model we have explicitly taken into account all dielectric effects in the charge and current densities, so the boundary conditions are that E_{Lr}, $\vec{E}_{Lt}$, B_{Lr}, and $\vec{B}_{Lt}$ be continuous at r=a. This leads to

$$\alpha_{\ell m} = 2D_\ell^{-1}[z j_\ell(x) j_\ell'(z) - x j_\ell(z) j_\ell'(x)] , \quad (2.2.18a)$$

$$R_{\ell m} = E_o \delta_{m,\pm 1} i^{\ell+1} (xD_\ell)^{-1} [4\pi(2\ell+1)\ell(\ell+1)]^{1/2} , \quad (2.2.18b)$$

where

$$D_\ell = x j_\ell(z) h_\ell^{(1)}(x) - z h_\ell^{(1)}(x) j_\ell'(z) , \quad (2.2.18c)$$

and

$$\beta_{\ell m} = -(2/\Delta_\ell) \left\{ (x j_\ell(x))' - j_\ell(x)[(x/z)^2 (z j_\ell(z))'/j_\ell(z) \right.$$
$$\left. + (1-(x/z)^2)\ell(\ell+1) j_\ell(y)/y j_\ell'(y)] \right\} , \quad (2.2.19a)$$

$$C_{\ell m} = \pm(1/\Delta_\ell) H_{\ell m} [kE_o/4\pi e x^2 j'_\ell(y)][1-(x/z)^2] \quad , \tag{2.2.19b}$$

$$F_{\ell m} = \pm(1/\Delta_\ell) H_{\ell m} [qE_o/p^2 x j_\ell(z)] \quad , \tag{2.2.19c}$$

with

$$H_{\ell m} = \delta_{m,\pm 1} i^{\ell+2} [4\pi(2\ell+1)\ell(\ell+1)]^{1/2} \quad ,$$

where

$$\Delta_\ell = (x h_\ell^{(1)}(x))' - h_\ell^{(1)}(x)[(x/z)^2 (z j_\ell(z))'/j_\ell(z) + (1-(x/z)^2)\ell(\ell+1) j_\ell(y)/y j'_\ell(y)] \quad , \tag{2.2.19d}$$

and $x = qa$, $y = ka$, and $z = pa$. Note that the coefficients $\beta_{\ell m}$ and $\alpha_{\ell m}$ refer to the electric and magnetic multipoles of the sphere, respectively. The coefficients $C_{\ell m}$ are related to the charge density fluctuations. In the present model the boundary condition $v_{Lr}(a) = 0$ is automatically satisfied, as would be expected for a problem in which the electrons are confined to the interior of the sphere.

In summary, Eqs. (2.2.13) and (2.2.17), in combination with Eqs. (2.2.18) and (2.2.19) provide an analytic solution to the linear problem.

c. Second Harmonic Generation

In order to solve Eq. (2.2.9) let us introduce two auxiliary vectors

$$\vec{\mathfrak{J}} = n_L \vec{v}_L \quad , \tag{2.2.20a}$$

$$\vec{\eta} = -m_e \vec{v}_L \cdot \nabla \vec{v}_L - (e/c)\vec{v}_L \times \vec{B}_L - \chi_1 \nabla n_L^2 \quad . \tag{2.2.20b}$$

Then the wave equations for the second harmonic fields become

$$(\nabla^2 + k_2^2) n_S(\vec{r}) = S(\vec{r}) \quad , \tag{2.2.21a}$$

$$(\nabla^2 + p_2^2) \vec{B}_S(\vec{r}) = \vec{T}(\vec{r}) \quad , \tag{2.2.21b}$$

and

$$(\nabla^2 + p_2^2) \vec{E}_s(\vec{r}) = 4\pi e[(p_2/k_2)^2 - 1] \nabla n_S + \vec{U}(\vec{r}), \tag{2.2.21c}$$

where we have introduced a second harmonic Drude dielectric constant

$$\epsilon_2 = 1 - \omega_p^2 / 2\omega(2\omega + i/\tau) \quad , \tag{2.2.22a}$$

and let

$$k_2 = \lambda [\epsilon_2/(1-\epsilon_2)]^{1/2} \quad , \tag{2.2.22b}$$

and

$$p_2 = 2q\sqrt{\epsilon_2} \quad . \tag{2.2.22c}$$

The source terms appearing in Eq. (2.2.21) are

$$\vec{T} = (4\pi e/c)\nabla \times \vec{\xi} + i(\omega_p^2/ce)\nabla \times \vec{\eta}/(2\omega + i/\tau) \quad , \tag{2.2.23a}$$

$$\vec{U} = i(8\pi\omega e/c^2)\vec{\xi} + (2q)^2(\epsilon_2 - 1)\vec{\eta}/e \quad , \tag{2.2.23b}$$

$$S = -i(\lambda^2/2\omega)\nabla \cdot \vec{\xi}/(1-\epsilon_2) + \chi_e^{-1} \nabla \cdot \vec{\eta} \quad . \tag{2.2.23c}$$

The radial components of $\vec{E}_2$ and $\vec{B}_2$ obey

$$(\nabla^2 + p_2^2) r B_{Sr} = \vec{r} \cdot \vec{T} \quad , \tag{2.2.24a}$$

and

$$(\nabla^2 + p_2^2) r E_{Sr} = -8\pi e n_S + \vec{r} \cdot \vec{U} + 4\pi e[(p_2/k_2)^2 - 1] r \partial_r n_S . \tag{2.2.24b}$$

Equations (2.2.21a) and (2.2.24) may be solved by using the Green function $G_\mu(\vec{r},\vec{r}')$ which satisfies

$$(\nabla^2+\mu^2)G_\mu(\vec{r},\vec{r}')=-\delta(\vec{r}-\vec{r}') \quad . \tag{2.2.25}$$

In free space we have

$$G_\mu(\vec{r},\vec{r}')=e^{i\mu|\vec{r}-\vec{r}'|}/4\pi|\vec{r}-\vec{r}'|$$
$$=i\mu\sum_\ell j_\ell(\mu r_<)h_\ell^{(1)}(\mu r_>)\sum_m Y^*_{\ell m}(\hat{r}')Y_{\ell m}(\hat{r}) \quad . \tag{2.2.26}$$

In order to obtain solutions that are not overly involved let us simplify matters by making two assumptions now: a).the incident plane wave has positive helicity, i.e. m=+1 and b).the linear dipole response is assumed to be much more important than higher order multipole responses, i.e. the wavelength is not too short. In this case the subscripts ℓ,m may be restricted to take the value 1,1 when considering the linear fields. Let

$$n_L=n_1(r)Y_{11} \quad , \tag{2.2.27a}$$
$$B_{Lr}=B_1(r)Y_{11} \quad , \tag{2.2.27b}$$
$$B_{L\theta}=B_2(r)Y_{11}/\sin\theta + B_3(r)\partial_\theta Y_{11} \quad , \tag{2.2.27c}$$
$$B_{L\phi}=i[B_2(r)\partial_\theta Y_{11}+B_3(r)Y_{11}/\sin\theta \,] \quad , \tag{2.2.27d}$$
$$v_{Lr}=-iv_1(r)Y_{11} \quad , \tag{2.2.27e}$$
$$v_{L\theta}=-i[v_2(r)Y_{11}/\sin\theta + v_3(r)\partial_\theta Y_{11}] \tag{2.2.27f}$$
$$v_{L\phi}=v_2(r)\partial_\theta Y_{11}+v_3(r)Y_{11}/\sin\theta \quad . \tag{2.2.27g}$$

Here

$$n_1(r)=C_{11}j_1(kr) \quad , \tag{2.2.28a}$$
$$B_1(r)=R_{11}(qr)^{-1}j_1(pr) \quad , \tag{2.2.28b}$$
$$B_2(r)=p^2(2q)^{-1}F_{11}j_1(pr) \quad , \tag{2.2.28c}$$

$$B_3(r)=R_{11}(2qr)^{-1}\partial_r[rj_1(pr)]\ , \tag{2.2.28d}$$

$$v_1(r)=(\omega C_{11}/n_o k)j_1'(kr) + (eF_{11}/m_e(\omega+i/\tau))j_1(pr)/r, \tag{2.2.28e}$$

$$v_2(r)=-[eR_{11}/2m_e(\omega+i/\tau)]j_1(pr)\ , \tag{2.2.28f}$$

$$v_3(r)=(\omega C_{11}/n_o k^2)j_1(kr)/r + [eF_{11}/2m_e(\omega+i/\tau)]r^{-1}\partial_r[rj_1(pr)]\ . \tag{2.2.28g}$$

Also we write

$$\vec{r}\cdot\vec{U}=\Pi(r)Y_{22}\ , \tag{2.2.29a}$$

$$\vec{r}\cdot\vec{T}=\Theta(r)Y_{22}\ , \tag{2.2.29b}$$

$$S=\Sigma(r)Y_{22}\ , \tag{2.2.29c}$$

where

$$\Pi(r)=(3/10\pi)^{1/2}\{(8\pi\omega e/c^2)rn_1v_1 - (2q)^2(\epsilon_s-1)e^{-1}[m_e(-rv_1\partial_r v_1+v_1v_3+v_2^2-v_3^2) +erc^{-1}(v_2B_3-v_3B_2)+2\chi_i rn_1\partial_r n_1]\} \tag{2.2.30a}$$

$$\Theta(r)=(3/10\pi)^{1/2}\{-12\pi ec^{-1}n_1v_2 +[3\omega_p^2/ce(2\omega+i/\tau)][m_e(v_1\partial_r v_2 +v_1v_2/r-2v_2v_3/r) +ec^{-1}(v_1B_3-v_3B_1)]\}, \tag{2.2.30b}$$

and

$$\sigma(r)=(3/10\pi)^{1/2}(\lambda^2/2\omega)(1-\epsilon_2)^{-1}[n_1 v_3/r-v_1\partial_r n_1 + \frac{\omega_i}{n_e}n_1^2]$$
$$-(1/\chi_e)(3/10\pi)^{1/2} m_e[-v_1\frac{\partial^2}{\partial r^2}v_1-(\partial_r v_1)^2 -2v_1 r^{-1}\partial_r v_1+4r^{-2}v_1 v_3-2(v_2/r)^2 -4(v_3/r)^2+4v_1 r^{-1}\partial_r v_3+v_3 r^{-1}\partial_r v_1 +2v_2 r^{-1}\partial_r v_2-2v_3 r^{-1}\partial_r v_3]$$
$$+(e/c)[2r^{-1}(v_2 B_3-v_3 B_2)+B_3\partial_r v_2+v_2\partial_r B_3 -B_2\partial_r v_3-v_3\partial_r B_2+3r^{-1}(v_1 B_2-v_2 B_1)]$$
$$+2\chi_1[n_1\frac{\partial^2}{\partial r^2}n_1+(\partial_r n_1)^2+2n_1 r^{-1}\partial_r n_1 -3(n_1/r)^2] \qquad (2.2.30c)$$

Expressed in terms of $\pi(r)$, $\rho(r)$ and $\sigma(r)$, the solutions for n_S, $\vec{r}\cdot\vec{B}_S$ and $\vec{r}\cdot\vec{E}_S$ are:

$$n_S=[C_{22}j_2(k_2r)+\nu(r)]Y_{22}\ , \qquad (2.2.31a)$$
$$\vec{r}\cdot\vec{B}_S=[(2q)^{-1}r_{22}j_2(p_2r)+Z(r)]Y_{22}\ , \qquad (2.2.31b)$$
$$\vec{r}\cdot\vec{E}_S=[f_{22}j_2(p_2r)+k(r)+C_{22}I(r)]Y_{22} \qquad (2.2.31c)$$

where

$$\nu(r)=-ik_2\int dr' r'^2 j_2(k_2 r_<)h_2^{(1)}(k_2 r_>)\sigma(r'), \qquad (2.2.32a)$$
$$Z(r)=-ip_2\int dr' r'^2 j_2(p_2 r_<)h_2^{(1)}(p_2 r_>)\rho(r'), \qquad (2.2.32b)$$
$$k(r)=-ip_2\int dr' r'^2 j_2(p_2 r_<)h_2^{(1)}(p_2 r_>)[-8\pi e\,\nu(r')+4\pi e((p_2/k_2)^2-1)r'\partial_{r'}\nu(r')+\pi(r')] \qquad (2.2.32c)$$
$$I(r)=-ip_2\int dr' r'^2 j_2(p_2 r_<)h_2^{(1)}(p_2 r_>)[-8\pi e j_2(k_2 r')+4\pi e((p_2/k_2)^2-1)k_2 r' j'(k_2 r')]. \qquad (2.2.32d)$$

To obtain the tangential components of $\vec{E}_S$ and $\vec{B}_S$ let us write

$$\vec{E}_S=\hat{r}\,E_{Sr}Y_{22}+\phi(r)\vec{X}_{22}+\psi(r)\hat{r}\times\vec{X}_{22}$$

$$\vec{B}_S=\hat{r}\,B_{Sr}Y_{22}+u(r)\vec{X}_{22}+v(r)\hat{r}\times\vec{X}_{22}$$

$$\vec{E}_S=\hat{r}\,E_{Sr}Y_{22}+\phi(r)\vec{X}_{22}+\psi(r)\hat{r}\times\vec{X}_{22}\ , \qquad (2.2.33a)$$

$$\vec{B}_S=\hat{r}\,B_{Sr}Y_{22}+u(r)\vec{X}_{22}+v(r)\hat{r}\times\vec{X}_{22}\ , \qquad (2.2.33b)$$

and

$$\phi(r)=(2q/\sqrt{6}\,)\vec{r}\cdot\vec{B}_S\ , \qquad (2.2.34a)$$

$$\psi(r)=(-i/\sqrt{6}\,)[4\pi er\nu(r)+4\pi eC_{22}rj_2(k_2r)+2E_{Sr}+r\partial_rE_{Sr}], \qquad (2.2.34b)$$

$$u(r)=(i/2q)[i\sqrt{6}r^{-1}E_{Sr}+r^{-1}\partial_r[r\psi(r)]\ , \qquad (2.2.34c)$$

$$v(r)=(-i/\sqrt{6}\,)[2B_{Sr}+r\partial_rB_{Sr}]\ . \qquad (2.2.34d)$$

There are three coefficients, r_{22}, C_{22}, and f_{22}, to be determined by matching boundary conditions. The fields outside the sphere are given by formulas analogous to those of Eq. (2.2.17) but without an incident field at frequency 2ω being present. Thus, for r>a:

$$\vec{E}_S(\vec{r})=-(5\pi)^{1/2}\{a_{22}h_2^{(1)}(2qr)\vec{X}_{22}+(b_{22}/2q)[(i\sqrt{6}/r)\hat{r}n_2^{(1)}(2qr)Y_{22}+r^{-1}\partial_r(rh_2^{(1)}(2qr))\hat{r}\times\vec{X}_{22}], \qquad (2.2.35a)$$

$$\vec{B}_S(\vec{r})=-(i/2q)\nabla\times\vec{E}_S(\vec{r})\ . \qquad (2.2.35b)$$

Again $\hat{r}\cdot\vec{E}_S$, $\hat{r}\cdot\vec{B}_S$, $\vec{E}_{St}$ and $\vec{B}_{St}$ must be continuous at r=a. We find, after some lengthy algebra, that

$$a_{22}=-(2q/p_2^2a\sqrt{30\pi}\,)I_1(a)/\Delta\ , \qquad (2.2.36)$$

where

$$I_1(a)=\int_0^a dr(p_2r)^2j_2(p_2r)\rho(r)\ , \qquad (2.2.37a)$$

$$\Delta=2qaj_2(p_2a)h_2^{(1)\prime}(2qa)-p_2ah_2^{(1)}(2qa)j_2'(p_2a) \qquad (2.2.37b)$$

and

$$b_{22}=(2iq/\sqrt{30\pi})\Delta_b'/\Delta_2' \quad , \tag{2.2.38}$$

where

$$\begin{aligned}\Delta_b' =&[1+p_2aj_2'(p_2a)/j_2(p_2a)\\ &-(6/k_2a)j_2(k_2a)/j_2'(k_2a)]\\ &+4\pi eaI_3(a)/(k_2a)^2j_2(p_2a)\\ &+I_4(a)/aj_2(p_2a)\\ &-24\pi eaI_2(a)/(k_2a)^3 \quad ,\end{aligned} \tag{2.2.39a}$$

$$\begin{aligned}\Delta_2' =&p_2^2\,[2qah_2^{(1)}(2qa)]'\\ &-h_2^{(1)}(2qa)[(2q/p_2)^2(p_2aj_2(p_2a))'/j_2(p_2a)\\ &+(1-(2q/p_2)^2)6j_2(k_2a)/k_2aj_2'(k_2a)] \quad ,\end{aligned} \tag{2.2.39b}$$

and

$$I_2(a)=\int_0^a dr(p_2r)^2[j_2(k_2r)/j_2'(k_2r)]\sigma(r) \quad , \tag{2.2.39c}$$

$$I_3(a)=\int_0^a dr(p_2r)^2[p_2rj_2'(p_2r)+j_2(p_2r)]\sigma(r) \tag{2.2.39d}$$

$$I_4(a)=\int_0^a dr(p_2r)^2j_2(p_2r)\pi(r) \quad . \tag{2.2.39e}$$

The integrals I_1 to I_4 are evaluated numerically.

2.3. Results and Discussion

In the previous section we have derived expressions for the linear and nonlinear electric and magnetic fields both inside and outside a small metallic spherical

particle illuminated by an incident electromagnetic wave. The sources of the nonlinearity included the Lorentz force, the convection of electron velocity, nonlinear contributions to the electron current and nonlinear chemical potential terms. In order to be able to compare these expressions with laboratory measurements let us compute the cross section for SHG and compare it with the corresponding linear cross section. We define the SHG cross section as the ratio between the radiated SHG power at frequency 2 and the incident intensity at frequency ω.

Thus, putting in the atomic units explicitly,

$$\sigma_{SHG}=(5\pi/8q^2)(|a_{22}|^2+|b_{22}|^2)\,[E_o a_o^2/e]^2 a_o^2, \tag{2.3.1}$$

where e is the electron charge and a_o is the Bohr radius. The cross section is proportional to the square of the incident electric field. It includes contributions form both the electric and magnetic quadrupole terms. The corresponding linear cross section may be written as a multipole series

$$\sigma_L=(\pi/2q^2)\sum_{\ell}(2\ell+1)(|\alpha_{\ell 1}|^2+|\beta_{\ell 1}|^2), \tag{2.3.2}$$

where, in the dipole approximation, only the terms with $\ell = 1$ are retained. This cross section will be denoted

by σ_1.

In order to compare our results with those of Agarwal and Jha[7] let us start by writing expressions for the general solution for the linear internal electric fields given by Eqs. (2.2.13b,c) in the limit in which the wave length is much larger than the particle size both inside and outside the particle ($pa \ll 1$ and $qa \ll 1$) and the screening length is much less than the particle size ($ka \gg 1$). Then our formulas reduce to that given by dielectric theory and we get the formula quoted in Ref. 7 for the internal field

$$\vec{E}=3\vec{E}_o/(\epsilon+2) - (i/2)\hat{r}\times(\vec{q}\times\vec{E}_o) \quad . \qquad (2.3.3)$$

However, for the cases of interest in this paper the above limits are not satisfied. Thus at the resonance frequency for Al, for example, $qa = 0.43$ for $a = 100$ Å and $qa = 0.74$ for $a = 200$ Å. Typical values of pa for a 100 Å sphere are in the range 0.6 to 0.8 and typical values of ka are around 200. The fact that the values of qa and pa are not that small points to the need for using the full Mie theory in evaluating the cross sections.

Another point of comparison between our theory and the standard Mie theory involves evaluating Eq. (2.2.19a) explicitly. We do this for the linear theory because it is simpler to write analytic expressions than for the nonlinear theory. Analogous considerations hold, of course, for the nonlinear coefficient given by

Eq.(2.2.38). The general expression for β_ℓ is

$$\beta_\ell = -2\frac{[x j_\ell(x)]' - j_\ell(x)\left\{\left(\frac{x}{z}\right)^2\frac{[z j_\ell(z)]'}{j_\ell(z)} + \left[1-\left(\frac{x}{z}\right)^2\right]\frac{\ell(\ell+1)j_\ell(y)}{y j_\ell'(y)}\right\}}{[x h_\ell^{(1)}(x)]' - h_\ell^{(1)}(x)\left\{\left(\frac{x}{z}\right)^2\frac{[z j_\ell(z)]'}{j_\ell(z)} + \left[1-\left(\frac{x}{z}\right)^2\right]\frac{\ell(\ell+1)j_\ell(y)}{y j_\ell'(y)}\right\}} \quad (2.3.4)$$

In the strong screening limit ($y \to \infty$) this result reduces to the Mie formula

$$\beta_\ell^{Mie} = -2\frac{[x j_\ell(x)]' - j_\ell(x)\left(\frac{x}{z}\right)^2\frac{[z j_\ell(z)]'}{j_\ell(z)}}{[x h_\ell^{(1)}(x)]' - h_\ell^{(1)}(x)\left(\frac{x}{z}\right)^2\frac{[z j_\ell(z)]'}{j_\ell(z)}} \quad . \quad (2.3.5)$$

In Fig.2.1 we plot the quantity $\sigma_{SHG}/(\pi a^2 E_o^2)$ for aluminum as a function of the dimensionless parameter $x = qa = \omega a/c$. Graphs are presented for several values of the sphere radius varying from 50 Å to 200 Å. Several features are worthy of note. At low values of x, corresponding to low frequencies, the cross sections rise rapidly with frequency, as would be expected for a sphere of finite conductivity. The bulk plasma frequency for Al corresponds to $\omega_p = 2.4\times10^{16}$ rad/sec. In each case we see two resonance peaks. The low frequency peak corresponds to the quadrupolar plasmon resonance frequency while the higher frequency peak occurs at the dipole plasmon resonance. In Mie theory these occur at frequencies given by the condition[7]

$$\ell\epsilon(\omega) + \ell + 1 + 2\left(\frac{\omega}{c}a\right)^2\frac{(\ell+1)(2\ell+1)}{\ell(2\ell-1)(2\ell+3)} = 0 \quad .$$

The dipole plasmon is excited for $\ell = 1$ and the quadrupole plasmon for $\ell = 2$. Since we are concerned with values for a which are reasonably large, the approximation $\ell\epsilon(\omega)+\ell+1 = 0$ is not appropriate for determining the position of the resonances.

In Fig.2.2 we plot, for comparison purposes, the linear dipole and linear quadrupole cross sections as a function of $x = qa$ for spheres of the same size as in Fig.2.1 (100 Å). We note that the linear quadrupole cross section is several orders of magnitude smaller than the linear dipole cross section. These results including the screening effects are in good agreement with the Mie scattering formulas.

In Fig.2.3 curves similar to those of Fig.2.1 are presented, but this time for Ag spheres ranging in size from 50 to 200 Å. Again the nonlinear cross section displays the pronounced dipolar and quadrupolar resonances. One would naturally expect these linear resonances to play a role in the nonlinear quadrupolar resonance because the nonlinear quadrupole is generated by the mixing of two dipole excitations in the incoming field and the production of a quadrupole outgoing field.

We have not shown the differential cross sections for SHG explicitly, but these may be obtained from the total cross sections by noting that the fields have an angular dependence associated with $Y_{22}(\hat{r})$. Thus a standard

quadrupolar pattern is to be expected.

In Fig.2.4 we compare our calculations with the calculations of Agarwal and Jha[7] for Al spheres of two sizes: a = 50 Å and 100 Å. We see that for small spheres the agreement is good, whereas for large spheres there is considerable disagreement. For larger spheres the need for a full Mie theory accounts for a considerable amount of the disagreement. Then the wave length of the light inside the sphere becomes smaller than the radius and different parts of the sphere begin to destructively interfere in the production of both a dipole in the in-field and a quadrupole in the out-field. This leads to a diminished cross section.

In Fig.2.5 we plot the dimensionless linear dipolar cross section $\sigma_1/\pi a^2$ and the cross section for second harmonic generation $\sigma_{SHG}/\pi a^2$ as a function of radius a for two fixed values of the frequency $\omega = 5.0\times10^{15}$ rad/sec and $\omega = 1.0\times10^{16}$ rad/sec. The curves are plotted for aluminum particles. The SHG cross section is plotted for an incident electric field strength corresponding to one atomic unit (e/a_o^2). Values for other field strengths may be obtained by multiplying by $(E_o a_o^2/e)^2$. For low values of a the cross section rises rapidly with size but tends to saturate when the dimensionless parameter becomes of the order of unity. For values of x larger than one we know that higher order

linear multipoles begin playing a more important role in scattering. Presumably the same thing will occur in the nonlinear scattering, but we have not computed higher multipoles as of yet.

Let us estimate the rate of generation of SHG photons for a hypothetical experimental arrangement. Suppose we prepare a smoke of 100 Å Al particles with a concentration of 10^{12} cm^{-3}. For an incident intensity of 10^{12} W/cm^2 we have a field strength E_0^2 = 8.4×10^9 $esu^2 cm^{-4}$ = 2.9×10^{-5} atomic units. For the quadrupolar resonance frequency in Fig.2.1, ω = 1.3×10^{16} rad/sec the flux of incident photons is 7.4×10^{29} $cm^{-2} sec^{-1}$. The cross section for second harmonic generation is $6.4 \times 10^{-15} cm^2$ as compared with the cross section for linear dipole scattering which 6.3×10^{-11} cm^2. Thus 4.7×10^{15} photons per second will be produced at frequency 2ω, per sphere. Taking an illuminated volume of $10^{-5} cm^3$ we would have 10^7 spheres contributing, for a net rate of 4.7×10^{22} photons per second. This large number may be increased even further by increasing the illumination volume, the concentration of the spheres, or the intensity of the radiation.

References

1. For a general review of classical and quantum theory of nonlinear optics see N. Bloembergen, " Nonlinear Optics ", (Benjamin, New York, 1965). For the elementary applications of nonlinear optics and, in particular, early literature relating to SHG see A. Yariv, "Quantum Electronics", 2nd edition, (Wiley, New York, 1975) . For recent developments of nonlinear optics see Y. R. Shen, " The Priciples of Nonlinear Optics ", (Wiley, New York, 1984).

2 E. Adler, Phys. Rev. 134, A728(1964)

3. S. S. Jha, Phys. Rev. Lett. 15, 412(1965); Phys. Rev. 140, A2020(1965); 145, 500(1966)

4. S. S. Jha and C. S. Warke, Phys. Rev. 153, 751(1967)

5. N. Bloembergen, R. K. Chang, S. S. Jha and C. H. Lee, Phys. Rev. 174, 813(1968)

6. For a recent review of surface effects see A. Wokaun, Surface Enhanced Electromagnetic Processes, " Solid State Physics Advances in Research and Application ", ed. by H. Ehrenreich and D. Turnbull, (Acadamic Press, Orlando, 1984)

7. G. S. Agarwal and S. S. Jha, Solid State Commun. 41, 499(1982)

8. C. K. Chen, T. F. Heinz, D. Richard and Y. R. Shen, Phys. Rev B 27, 1965(1983)

9. K. Arya, Phys. Rev B 29, 4451(1984)

10. C. K. Chen, A. B. de Castro and Y. R. Shen, Phys. Rev. Lett. 46, 145(1981)

11. G. T. Boyd, Th. Rasing, J. R. R. Leite and Y. R. Shen, Phys. Rev. B 30, 519(1984)

12. T. F. Heinz, M. M. T. Loy amd W. A. Thompson, Phys. Rev. Lett. 54, 63(1985)

13. S. A. Akhmanov, M. F. Galyautdinov, N. I. Koroteev, G. A. Paityan, A. A. Sumbatov, I. B. Kraibullin, E. I. Shtyrkov and I. L. Shumai, Sov. Tech. Phys. Lett. 10, 473(1984)

14. O. Keller, Phys. Rev. B 31, 5028(1985)

15. See the references in chapter I.

16. X. M. Hua and J. I. Gersten, Phys. Rev. B 33, 3756(1986)

17. E. J. Heilweil and R. M. Hochstrasser, J. Chem. Phys. 82, 4762(1985)

18. X. M. Hua and J. I. Gersten, Phys. Rev. B 31, 855(1984)

19. J. D. Jackson, Classical Electrodynamics, 2nd ed. (Wiley, New York, 1975).

Figure Captions

Fig.2.1 Cross sections for scattering of electromagnetic radiation by aluminum spheres in units of the geometric cross section for spheres of radii 50, 100, 150 and 200Å radii. Abscissa denotes the dimensionless parameter $x = \omega a/c$, where ω is the radian frequency, a is the sphere radius and c is the speed of light. The set of curves give second harmonic generation cross sections corresponding to an incident electric field of strength one atomic unit ($E_o = e/a_o^2$).

Fig.2.2 Linear cross sections for dipole (electric and magnetic) and quadrupole interaction for spheres of various radii (50, 100, 150 and 200 Å).

Fig.2.3 Same as Fig.2.1 but for silver spheres.

Fig.2.4 Comparison of the second harmonic cross sections as computed in this paper (solid curves) with those given by Ref. 7 (broken curves). Curves are given for a = 50 Å and 100 Å.

Fig.2.5 Linear dipolar cross section (broken curves) and second harmonic cross section (solid curves) as a function of sphere radius for Al spheres. Graphs for two frequencies are given, $\omega = 5 \times 10^{15}$ rad/s and 1.0×10^{16} rad/s.

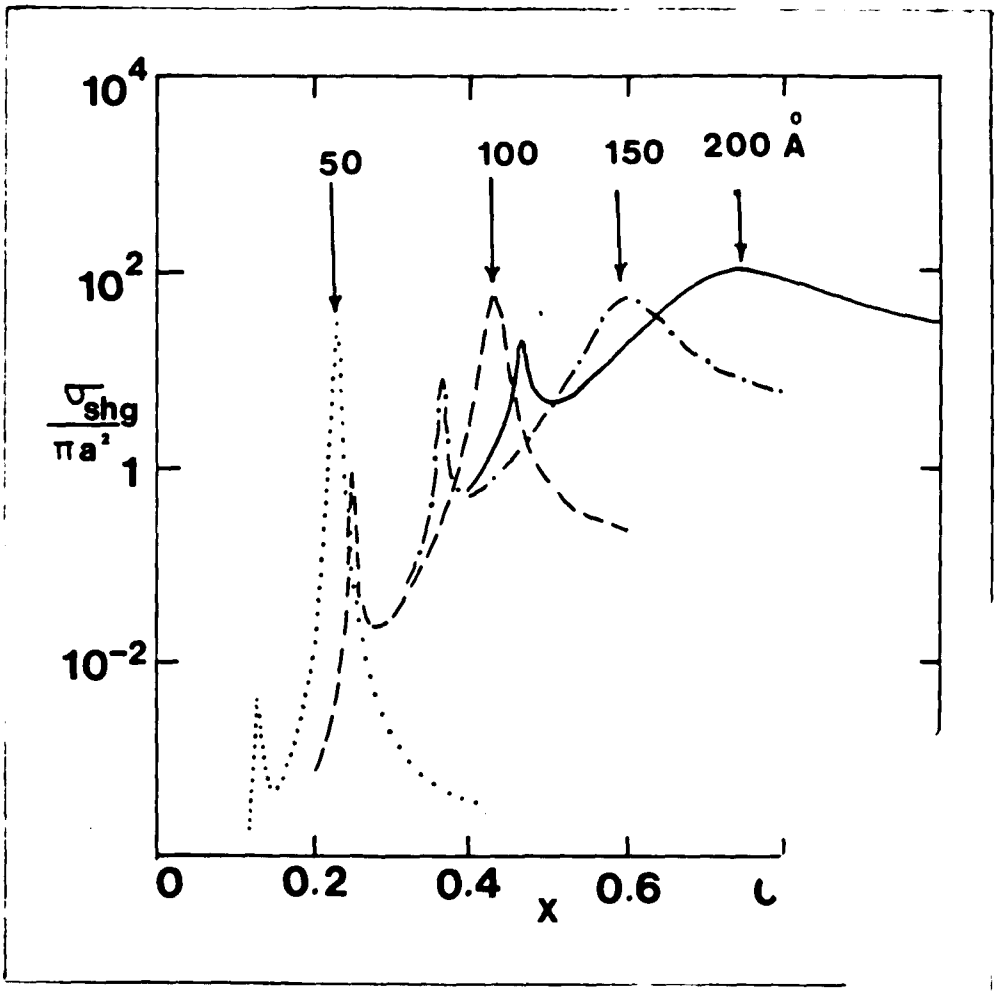

Fig.2.1

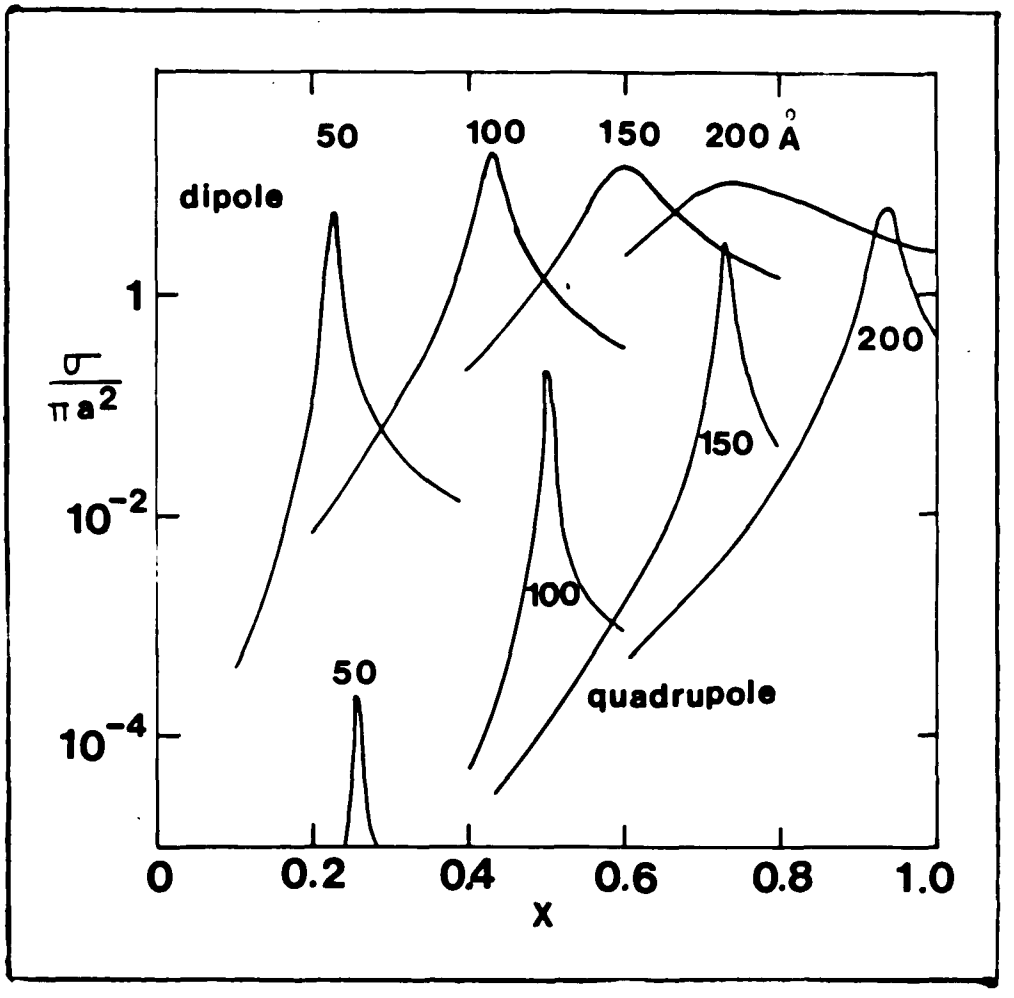
50
100
150
200 Å
dipole
1
$\frac{\sigma}{\pi a^2}$
10^{-2}
10^{-4}
200
150
100
50
quadrupole
0
0.2
0.4
0.6
0.8
1.0
X

Fig.2.2

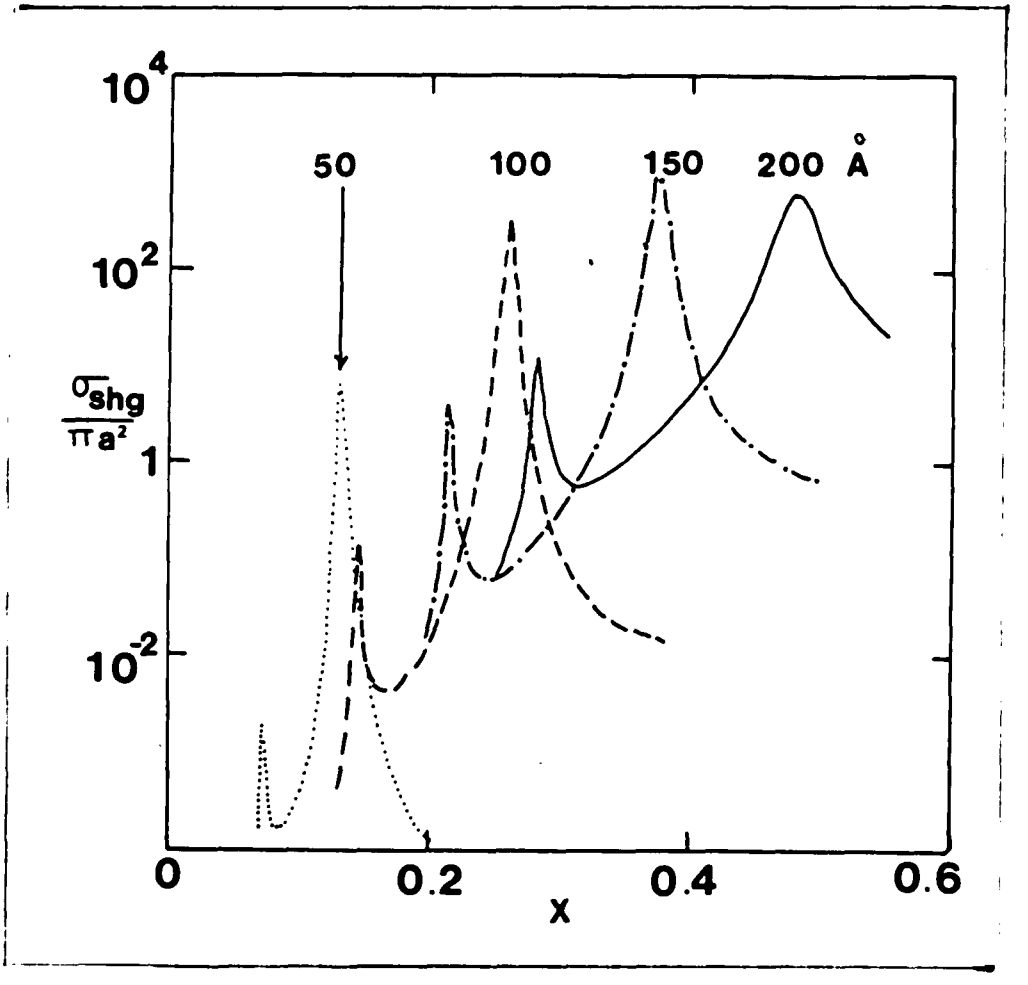

Fig.2.3

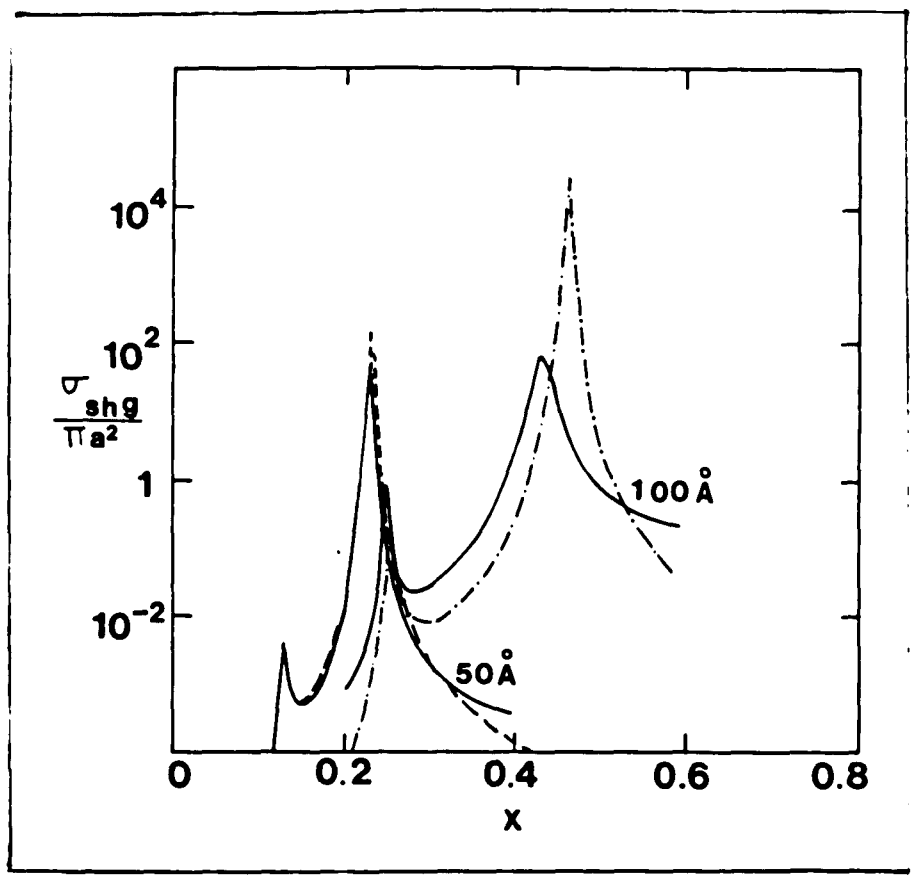

Fig.2.4

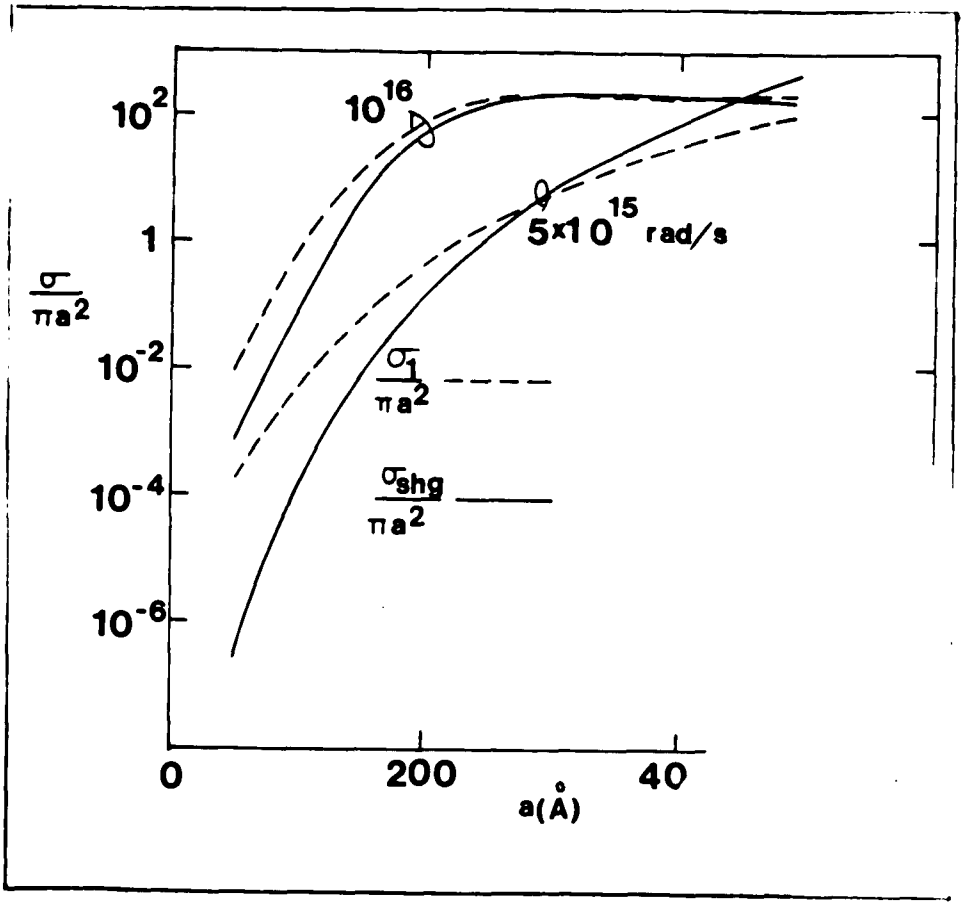
10^2
1
10^{-2}
10^{-4}
10^{-6}
$\frac{\sigma}{\pi a^2}$
10^{16}
5×10^{15} rad/s
$\frac{\sigma_1}{\pi a^2}$
$\frac{\sigma_{shg}}{\pi a^2}$
0
200
40
a(Å)

Fig.2.5

Chapter III. Enhanced Energy Transfer between Donor and Acceptor Molecules near a Spheroidal Small Particle

3.1. Introduction

Currently energy transfer is a wide open subject in physics, chemistry and biology. Research on energy transfer either as a basic process or a perturbation has attracted a considerable amount of attention both from theoretical and experimental physicists. The mechanisms of energy transfer which have been discussed in detail are mainly for transfer in position coordinate space. The transfer in momentum space and wave vector space have also been noted. The dominant processes which compete with energy transfer are radiative and nonradiative decay[1]. It has been realized for a long time that energy transfer plays a fundamental role in such optical processes related to molecular spectroscopy as quenching of luminescence, sensitizing of luminescence, and photosynthesis. Concrete measurements on energy transfer rates have also been performed by fluorescence measurements[2].

A well-known mechanism for the transfer of energy from one site to another in crystals, amorphous materials, solutions and biological systems is resonant energy

transfer. This mechanism was explained quantum mechanically by Förster[3], in the dipole approximation, for transfer between organic molecules. Dexter[4,5] generalized the theory to higher order interactions, including the exchange interaction, and applied the theory to energy transfer between dopant ions in inorganic solids. The earlier work based on the long range electromagnetic interaction was due originally to Vavilov[6], Perrin[7] and Perrin[8]. The basic point of Förster-Dexter theory is that the donor molecule couples to the acceptor molecule through a dipole-dipole interaction. The quantum transition probability of deexciting the donor and exciting the acceptor simultaneously could be simply formulated by using the Fermi Golden Rule and expressed in terms of the emissivity of the donor and the absorptivity of the acceptor. The theory is successful in explaining the energy transfer between donor and acceptor molecules. Of course, when dealing with different processes other mechanisms and theories may apply.

In recent years active research has been performed on a variety of optical processes when they occur near a solid state particle as well as a rough surface. The motivation is due to the anomalous enhancement effects. For example, in Raman scattering the cross section can be enhanced by 6 orders of magnitude near a rough surface[9]. Detailed

calculation of Raman scattering by molecules adsorbed on spherical particles[10] were also performed. Gersten et al.[11,12] studied the energy transfer process when it occurs near a solid spheroidal particle by using a long wavelength approximation. The frequency dependence of the energy transfer enhancement ratio showed explicitly the importance of the surface plasmon excitation. They also found that there exist zones of activity (around the tip of the spheroid) in which the molecules display significantly enhanced energy transfer. In contrast, the orientation of the molecules is less sensitive. The competition between the energy transfer and the radiative and nonradiative decay are also obvious. The enhanced ratio of energy transfer would be as high as 5 orders of magnitude if the frequency approached the surface plasmon frequency and the molecules were inside the active zones. Folan et al.[13] reported the first measuremant of enhanced energy transfer. The overall transfer within a particle 10 microns in diameter was found to exceed conventional dipole-dipole transfer by more than a factor of 10^2.

It is clear today that a large part of the enhancement mechanism is of purely electrodynamic origin. It is also clear that the existence of a solid state particle would modify the local electric field in the region near the surface. The modification would be very strong if the

surface modes were excited, or if the morphology of the particle allowed the concentration of the electric field lines[10-14]. Electromagnetic theory has also been applied to explaining enhanced fluorescence[15], photochemistry[16], and second harmonic generation[17].

This chapter is based on the work [12] and arranged as follows. In section II we develop the theory for energy transfer and define the enhanced ratio of energy transfer. In section III we develop the theory of nonradiative decay and establish its connection to the energy transfer. In section IV we focus our attention on radiative decay. Finally, in section V we present the results of our computations and discuss them.

3.2. Theory of energy transfer

We shall study the transfer of energy between a donor molecule (d) and an acceptor molecule (a) in the vicinity of a solid state particle. The particle will be taken to have a spheroidal shape with semi-major axis a and semi-minor axis b. It will be assumed to possess a frequency-dependent dielectric function, $\epsilon(\omega)$. The donor and acceptor molecules will be represented by point electric dipoles $\vec{\mu}_d$ and $\vec{\mu}_a$ at locations $\vec{r}_d$ and $\vec{r}_a$, respectively. It will be assumed that all distances of relevance (a,b,r_d, and r_a) are small compared with the wave length of light whose frequency corresponds to molecular electronic transitions of interest, so that retardation effects may be neglected. On the other hand, it will be assumed that the distance scales are sufficiently large that nonlocal dielectric effects are not of significant importance.

Let us take the z-axis parallel to the symmetry axis (the major axis) and introduce prolate spheroidal coordinates ξ, η and ϕ. The surface of the particle will be denoted by $\xi = \xi_0$, where $\xi_0 = a/f$ and $f=(a^2-b^2)^{1/2}$. While this description more naturally applies to prolate shaped particles, the generalization to oblate structures may readily be obtained by analytic continuation. The coordinates of the donor and acceptor

molecules will be denoted by (ξ_d, η_d, ϕ_d and (ξ_a, η_a, ϕ_a). The Cartesian coordinates are related to the spheroidal coordinates by

$$x=f[(\xi^2-1)(1-\eta^2)]^{1/2}\cos\phi \,, \qquad (3.2.1a)$$

$$y=f[(\xi^2-1)(1-\eta^2)]^{1/2}\sin\phi \,, \qquad (3.2.1b)$$

$$z=f\xi\eta \,, \qquad (3.2.1c)$$

Before developing the theory for the general case, consider first the situation in the absence of the particle. Förster and Dexter have described the energy transfer rate from the donor to the acceptor molecule in terms of Fermi's golden rule, taking the dipole-dipole interaction as the perturbation responsible for driving the transition. The donor molecule is initially in an excited state $|f_d)$ with energy ϵ_{f_d} and falls to a lower state $|i_d)$ with energy ϵ_{i_d}. At the same time the acceptor molecule is promoted from an initial state $|i_a)$ to some excited state $|f_a)$, with corresponding energies ϵ_{i_a} and ϵ_{f_a}, respectively. Because of the presence of a high density of vibrational levels associated with the electronic states we expect some distribution of initial donor and acceptor levels. These will be described by the distribution function $F_d(f_d)$ and $F_a(i_a)$. The average transition rate is given by

$$K_o=(2\pi/\hbar)\sum_{i_a}\sum_{f_d}F_d(f_d)F_a(i_a) \times |(i_d f_a|U_o|f_d i_a)|^2 \times \delta(\epsilon_{f_d}+\epsilon_{i_a}-\epsilon_{i_d}-\epsilon_{f_a}), \qquad (3.2.2)$$

where U_o is the dipole-dipole interaction

$$U_o = \frac{\vec{\mu}_d \cdot \vec{\mu}_a - 3\vec{\mu}_d \cdot \hat{r}\, \vec{\mu}_a \cdot \hat{r}}{r^3} , \qquad (3.2.3)$$

and $\vec{r} = \vec{r}_d - \vec{r}_a$ is the intermolecular displacement vector.

Let

$$(i_d|\vec{\mu}_d|f_d) = \chi_d(i_d, f_d)\vec{m}_d \qquad (3.2.4a)$$

and

$$(f_a|\vec{\mu}_a|i_a) = \chi_a(f_a, i_a)\vec{m}_a , \qquad (3.2.4b)$$

where $\vec{m}_d$ and $\vec{m}_a$ are transition moments and $\chi_d(i_d, f_d)$ and $\chi_a(f_a, i_a)$ are Franck-Condon factors. Then U_o may be written as

$$(i_d f_a|U_o|f_d i_a) = m_a m_d \chi_d \chi_a A_o \qquad (3.2.5)$$

where A_o is an angular-dependent factor

$$A_o = \frac{\hat{m}_d \cdot \hat{m}_a - 3\hat{m}_d \cdot \hat{r}\, \hat{m}_a \cdot \hat{r}}{r^3} . \qquad (3.2.6)$$

Then, introducing an auxiliary integration, we obtain

$$K_o = 2\pi A_o^2 \int_{-\infty}^{\infty} d\omega \Big\{ \sum_{i_a} [F_a |\chi_a|^2 |\vec{m}_a|^2 \delta(\epsilon_{i_a} - \epsilon_{f_a} + \hbar\omega)] \times \sum_{f_d} [F_d |\chi_d|^2 |\vec{m}_d|^2 \delta(\epsilon_{f_d} - \epsilon_{i_d} - \hbar\omega)] \Big\} , \qquad (3.2.7)$$

which may be rewritten as

$$K_o=(9A_o^2c^4/8\pi)\int_{-\infty}^{\infty}d\omega\ \frac{\sigma_a(\omega)\,\Gamma_d(\omega)}{\omega^4}\ , \qquad (3.2.8)$$

where $\sigma_a(\omega)$ is the electromagnetic absorption cross section for the acceptor molecule

$$\sigma_a=(4\pi^2\omega/3c)\sum_{i_a} F_a\,|\chi_a|^2|\vec{m}_a|^2\,\delta(\epsilon_{i_a}-\epsilon_{f_a}+\hbar\omega)\ . \qquad (3.2.9)$$

and $\Gamma_d(\omega)$ is the emission rate per unit frequency of the donor

$$\Gamma_d=(4\omega^3/3c^3)\sum_{f_d} F_d\,|\chi_d|^2|\vec{m}_d|^2\,\delta(\epsilon_{f_d}-\epsilon_{i_d}-\hbar\omega)\ . \qquad (3.2.10)$$

Let us now introduce the particle. Since Eq. (3.2.8) involves an integration over angular frequencies associated with both the donor and acceptor transitions it is reasonable to assume that the dielectric properties of the solid at frequency ω will now enter the formalism. What we need is a generalization of the expression for the dipole-dipole interaction, U_o. To obtain this we must first solve the general electrostatic problem presented by having two point dipoles in proximity to a spheroidal particle. The electrostatic potential inside the particle ($\xi < \xi_o$) may be expanded as

$$\Phi(\xi,\eta,\phi)=\sum_{n=0}^{\infty}\sum_{m=0}^{n}[A_{nm}\cos m\phi+B_{nm}\sin m\phi]\times P_n^m(\xi)P_n^m(\eta) \qquad (3.2.11a)$$

and the potential outside the particle($\xi > \xi_o$) as

$$\Phi(\xi,\eta,\phi)=\sum_{n=0}^{\infty}\sum_{m=0}^{n}[A_{nm}\cos m\phi+B_{nm}\sin m\phi]\times Q_n^m(\xi)P_n^m(\eta)+\Phi_d+\Phi_a\ . \tag{3.2.11b}$$

Here $P_n^m(\xi)$ and $Q_n^m(\xi)$ denote associated Legendre functions of the first and second kind, respectively. The dipolar potentials associated with isolated donor and acceptor molecules are denoted by Φ_d and Φ_a. Expansions for these potentials may be obtained starting with the Coulomb Green function

$$\frac{1}{|\vec{r}-\vec{r}'|}=\sum_{n=0}^{\infty}\sum_{m=0}^{n}F_{nm}P_n^m(\xi_<)Q_n^m(\xi_>)\times P_n^m(\eta)P_n^m(\eta')\cos m(\phi-\phi')\ , \tag{3.2.12}$$

where

$$F_{nm}=f^{-1}(-)^m(2-\delta_{m,0})(2n+1)[(n-m)!/(n+m)!]^2\ , \tag{3.2.13}$$

and $\xi_<=\min(\xi,\xi')$ and $\xi_>=\max(\xi,\xi')$. The potential due to a dipole $\vec{\mu}_d$ located at $\vec{r}_d$ is

$$\Phi_d=\frac{\vec{\mu}_d\cdot(\vec{r}-\vec{r}_d)}{|\vec{r}-\vec{r}_d|^3}=\vec{\mu}_d\cdot\nabla_d\frac{1}{|\vec{r}-\vec{r}_d|}\ . \tag{3.2.14}$$

The components of the gradient operator may be written as

$$\nabla_d=\frac{\hat{\xi}_d}{h_{\xi_d}}\frac{\partial}{\partial\xi_d}+\frac{\hat{\eta}_d}{h_{\eta_d}}\frac{\partial}{\partial\eta_d}+\frac{\hat{\phi}_d}{h_{\phi_d}}\frac{\partial}{\partial\phi_d}\ , \tag{3.2.15}$$

where $\hat{\xi}_d$, $\hat{\eta}_d$ and $\hat{\phi}_d$ are unit vectors and h_{ξ_d}, h_{η_d},

and h_{ϕ_d} are metric coefficients defined by

$$h_{\xi_d} = f[(\xi_d^2 - \eta_d^2)/(\xi_d^2 - 1)]^{1/2} \tag{3.2.16a}$$

$$h_{\eta_d} = f[(\xi_d^2 - \eta_d^2)/(1 - \eta_d^2)]^{1/2} \tag{3.2.16b}$$

$$h_{\phi_d} = f[(\xi_d^2 - 1)/(1 - \eta_d^2)]^{1/2} , \tag{3.2.16c}$$

so

$$\begin{aligned}\Phi_d = \sum_{n=0}^{\infty}\sum_{m=0}^{n} F_{nm} \Big\{ & (\mu_{\xi_d}/h_{\xi_d}) \frac{\partial}{\partial \xi_d}[P_n^m(\xi_>)Q_n^m(\xi_<)] \\ & \times P_n^m(\eta)P_n^m(\eta_d)\cos m(\phi - \phi_d) \\ & + (\mu_{\eta_d}/h_{\eta_d})P_n^m(\xi_>)Q_n^m(\xi_<) \\ & \times P_n^m(\eta)[P_n^m(\eta_d)]'\cos m(\phi - \phi_d) \\ & + m(\mu_{\phi_d}/h_{\phi_d})P_n^m(\xi_>)Q_n^m(\xi_<) \\ & \times P_n^m(\eta)P_n^m(\eta_d)\sin m(\phi - \phi_d)\Big\} .\end{aligned} \tag{3.2.17}$$

A similar formula holds for Φ_a with d replaced by a.

We now demand that Φ be continuous at the surface of the dielectric and also that the normal component of the electic displacement vector be continuous there. This allows us to solve for the unknown constants A'_{nm} and B'_{nm} appearing in Eq. (3.2.11b):

$$\begin{aligned}\begin{pmatrix} A'_{nm} \\ B'_{nm} \end{pmatrix} = & [1 - \epsilon]\Delta_{nm}^{-1} F_{nm} P_n^m(\xi_0)[P_n^m(\xi_0)]' \\ & \times \sum_{i=a,d} (\mu_{\xi_i}/h_{\xi_i})[Q_n^m(\xi_i)]' P_n^m(\eta_i) \\ & + (\mu_{\eta_i}/h_{\eta_i})Q_n^m(\xi_i)[P_n^m(\eta_i)]' \begin{pmatrix} \cos m\phi_i \\ \sin m\phi_i \end{pmatrix} \\ & + m(\mu_{\phi_i}/h_{\phi_i})Q_n^m(\xi_i)P_n^m(\eta_i)\begin{pmatrix} -\sin m\phi_i \\ \cos m\phi_i \end{pmatrix} ,\end{aligned} \tag{3.2.18}$$

where

$$\Delta_{nm}(\omega) = \epsilon(\omega) Q_n^m(\xi_0) P_n^m(\xi_0)' - P_n^m(\xi_0) Q_n^m(\xi_0)' \tag{3.2.19}$$

The interaction energy is obtained from the expression

$$U = -[\vec{\mu}_a \cdot \vec{E}_a + \vec{\mu}_d \cdot \vec{E}_d]/2 \quad . \tag{3.2.20}$$

Here $\vec{E}_a$ is the electric field at the position of the acceptor molecule and $\vec{E}_d$ is the corresponding field at the donor molecule. These fields are obtained from Eq. (3.2.11b) using

$$\vec{E} = -\nabla\Phi \quad , \tag{3.2.21}$$

and omitting the terms Φ_a of Eq.(3.2.11b) when computing $\vec{E}_a$ and Φ_d when computing $\vec{E}_d$. Thus we may write

$$U = U_o \ \Delta U(\omega) \quad , \tag{3.2.22}$$

where U_o is given by Eq. (3.2.3) and

$$\Delta U(\omega) = [\vec{\mu}_a \cdot \nabla\tilde{\Phi}\big|_{r=r_a} + \vec{\mu}_d \cdot \nabla\tilde{\Phi}\big|_{r=r_d}]/2, \tag{3.2.23}$$

where

$$\tilde{\Phi} = \sum_{n=0}^{\infty} \sum_{m=0}^{n} [A'_{nm} \cos m\phi + B'_{nm} \sin m\phi] \times Q_n^m(\xi) P_n^m(\eta) \quad . \tag{3.2.24}$$

Here $\tilde{\Phi}$ is the potential just due to the induced charges of the dielectric and $\Delta U(\omega)$ is the additional interaction energy between the donor and acceptor caused by the presence of the nearby particle. Thus

$$\Delta U(\omega)=0.5\sum_{j=d,a}\sum_{n=0}^{\infty}\sum_{m=0}^{n}\Big\{$$

$$m\frac{\mu_{j\phi}}{h_{\phi_j}}Q_n^m(\xi_j)P_n^m(\eta_j)$$

$$\times[-A'_{nm}\sin m\phi_j+B'_{nm}\cos m\phi_j]\Big\}$$

$$+\Big\{\frac{\mu_{j\xi}}{h_{\xi_j}}[Q_n^m(\xi_j)]'P_n^m(\eta_j)$$

$$+\frac{\mu_{j\eta}}{h_{\eta_j}}Q_n^m(\xi_j)[P_n^m(\eta_j)]'$$

$$\times[A'_{nm}\cos m\phi_j+B'_{nm}\sin m\phi_j]\Big\}\ .$$

(3.2.25)

Equation (3.2.25) contains three types of terms: terms bilinear in $\vec{\mu}_d$ and $\vec{\mu}_a$, terms quadratic in $\vec{\mu}_d$ and terms quadratic in $\vec{\mu}_a$. Only the terms bilinear in $\vec{\mu}_d$ and $\vec{\mu}_a$ cause energy transfer. The other terms, however, are responsible for modifying the decay rates of the donor and acceptor molecules and will be studied later. We will denote the bilinear terms collectively as $\Delta U_{da}(\omega)$.

When the spheroidal particle is in proximity to the donor-acceptor pair the transition rate is

$$K=(2\pi/\hbar)\sum_{i_a}\sum_{f_d}F_dF_a|(i_df_a|U_o+\Delta U_{da}|f_di_a)|^2$$
$$\times\delta(\epsilon_{f_d}+\epsilon_{i_a}-\epsilon_{i_d}-\epsilon_{f_d})\ . \qquad (3.2.26)$$

In place of Eq.(3.2.8) we now obtain

$$K=(9c^4/8\pi)\int_{-\infty}^{\infty} d\omega\,|A(\omega)|^2\,\sigma_a(\omega)\,\Gamma_d(\omega)/\omega^4 \,. \qquad (3.2.27)$$

The frequency dependent factor $A(\omega)$ replaces the factor A_o of Eq. (3.2.6) and is defined as

$$A=A_o+\Delta A \,, \qquad (3.2.28)$$

where

$$\Delta A=\hat{\mu}_d\cdot\Delta\overleftrightarrow{M}^{da}\cdot\hat{\mu}_a \,, \qquad (3.2.29)$$

and $\Delta\overleftrightarrow{M}^{da}$ is a tensor which may be written as

$$\Delta\overleftrightarrow{M}^{da}=\sum_{n=0}^{\infty}\sum_{m=0}^{n} T_{nm}\overleftrightarrow{E}^{da}(n,m) \,. \qquad (3.2.30)$$

Here

$$T_{nm}=[(1-\epsilon)/\Delta_{nm}]F_{nm}P_n^m(\xi_o)[P_n^m(\xi_o)]' \,, \qquad (3.2.31)$$

and the spheroidal components of the $\overleftrightarrow{E}^{da}$ tensor are

$$E^{da}_{\xi\xi}=[h_{\xi_d}h_{\xi_a}]^{-1}[Q_n^m(\xi_d)]'[Q_n^m(\xi_a)]' \times P_n^m(\eta_d)P_n^m(\eta_a)\cos m(\phi_d-\phi_a) \,, \qquad (3.2.32a)$$

$$E^{da}_{\eta\eta}=[h_{\eta_d}h_{\eta_a}]^{-1}Q_n^m(\xi_d)Q_n^m(\xi_a) \times[P_n^m(\eta_d)]'[P_n^m(\eta_a)]'\cos m(\phi_d-\phi_a) \,, \qquad (3.2.32b)$$

$$E^{da}_{\phi\phi}=[h_{\phi_a}h_{\phi_d}]^{-1}m^2Q_n^m(\xi_d)Q_n^m(\xi_a) \times P_n^m(\eta_d)P_n^m(\eta_a)\cos m(\phi_d-\phi_a) \,, \qquad (3.2.32c)$$

$$E^{da}_{\xi\eta} = [h_{\xi_d} h_{\eta_a}]^{-1} [Q^m_n(\xi_d)]' Q^m_n(\xi_a)$$
$$P^m_n(\eta_d)[P^m_n(\eta_a)]' \cos m(\phi_d - \phi_a) \qquad (3.2.32d)$$

$$E^{da}_{\xi\phi} = [h_{\xi_d} h_{\phi_a}]^{-1} m [Q^m_n(\xi_d)]' Q^m_n(\xi_a)$$
$$P^m_n(\eta_d) P^m_n(\eta_a) \sin m(\phi_d - \phi_a) , \qquad (3.2.32e)$$

$$E^{da}_{\eta\phi} = [h_{\eta_d} h_{\phi_a}]^{-1} m Q^m_n(\xi_d) Q^m_n(\xi_a)$$
$$[P^m_n(\eta_d)]' P^m_n(\eta_a) \sin m(\phi_d - \phi_a) \qquad (3.2.32f)$$

Expressions for $E^{da}_{\eta\xi}$, $E^{da}_{\phi\xi}$ and $E^{da}_{\phi\eta}$ are obtained from the last three equations by interchanging d and a. Similarly, we may express A_o in spheroidal coordinates by writing

$$A_o = \vec{\mu}_d \cdot \overleftrightarrow{M}_o \cdot \vec{\mu}_a , \qquad (3.2.33)$$

where

$$\overleftrightarrow{M}_o = \sum_{n=0}^{\infty} \sum_{m=0}^{n} F_{nm} \overleftrightarrow{W}(n,m) , \qquad (3.2.34)$$

and $\overleftrightarrow{W}$ is a tensor whose spheroidal components are

$$W_{\xi\xi} = [h_{\xi_d} h_{\xi_a}]^{-1} [P^m_n(\xi_<)]' [Q^m_n(\xi_>)]'$$
$$P^m_n(\eta_d) P^m_n(\eta_a) \cos m(\phi_d - \phi_a) \qquad (3.2.35a)$$

$$W_{\eta\eta} = [h_{\eta_d} h_{\eta_a}]^{-1} P^m_n(\xi_<) Q^m_n(\xi_>)$$
$$[P^m_n(\eta_d)]' [P^m_n(\eta_a)]' \cos m(\phi_d - \phi_a) , \qquad (3.2.35b)$$

$$W_{\phi\phi} = [h_{\phi_d} h_{\phi_a}]^{-1} m^2 P^m_n(\xi_<) Q^m_n(\xi_>)$$
$$P^m_n(\eta_d) P^m_n(\eta_a) \cos m(\phi_d - \phi_a) , \qquad (3.2.35c)$$

$$W_{\xi\eta} = [h_{\xi_d} h_{\eta_a}]^{-1} \frac{\partial}{\partial \xi_d}[P_n^m(\xi_<)Q_n^m(\xi_>)]$$
$$P_n^m(\eta_d)[P_n^m(\eta_a)]'\cos m(\phi_d - \phi_a) \qquad (3.2.35d)$$

$$W_{\xi\phi} = [h_{\xi_d} h_{\phi_a}]^{-1} m \frac{\partial}{\partial \xi_d}[P_n^m(\xi_<)Q_n^m(\xi_>)]$$
$$P_n^m(\eta_d)P_n^m(\eta_a)\sin m(\phi_d - \phi_a) \quad , \qquad (3.2.35e)$$

$$W_{\eta\phi} = [h_{\eta_d} h_{\phi_a}]^{-1} m P_n^m(\xi_<)Q_n^m(\xi_>)$$
$$P_n^m(\eta_d)[P_n^m(\eta_a)]'\sin m(\phi_d - \phi_a) \qquad (3.2.35f)$$

Expressions for $W_{\eta\xi}$, $W_{\phi\xi}$ and $W_{\phi\eta}$ are obtained from the last three equations by interchanging d and a. In the above,

$$\xi_< = \min(\xi_d, \xi_a) \quad \text{and} \quad \xi_> = \max(\xi_d, \xi_a).$$

The spheroidal components of the dipole unit vectors are related to the cartesian components by

$$\hat{\mu}_\xi = (\xi f/h_\eta)[\hat{\mu}_x \cos\phi + \hat{\mu}_y \sin\phi] + (\eta f/h_\xi)\hat{\mu}_z \, , \qquad (3.2.36a)$$

$$\hat{\mu}_\eta = (\eta f/h_\xi)[\hat{\mu}_x \cos\phi + \hat{\mu}_y \sin\phi] - (\xi f/h_\eta)\hat{\mu}_z \, , \qquad (3.2.36b)$$

$$\hat{\mu}_\phi = -\hat{\mu}_x \sin\phi + \hat{\mu}_y \cos\phi \quad . \qquad (3.2.36c)$$

A comparison of Eq. (3.2.27) to Eq. (3.2.8) shows that the integrands differ by a factor

$$R(\omega) = |A(\omega)/A_o|^2 \quad . \qquad (3.2.37)$$

We shall refer to this quantity as the enhancement factor. In addition to its frequency dependence it also depends on the locations of the molecules, their orientation and the size, shape and composition of the particle.

The present theory may be adapted somewhat so that it

may also apply to intramolecular energy transfer. Consider, for example, a molecule which is in some vibrational state associated with a given electronic state. Assume this molecule also possesses another electronic state associated with a given electronic tate. This level is embedded in the vibrational manifold associated with lower electronic states and if the latter are dense enough intramolecular radiationless transitions usually occur. Consider now the effect of the presence of the dielectric particle on such transitions. Since we now will be concerned with one molecule rather than two, we must talk in terms of donor modes and acceptor modes of that given molecule. The physical location of these modes are given by $\vec{r}_d = \vec{r}_a$ but there still can be independent transition dipole moments associated with the different electronic states.

Unlike the case of intermolecular energy transfer, the direct dipole-dipole interaction between the modes is no longer an appropriate concept. Since the modes are attached to the same molecule, the idea of representing them by point dipoles which will then interact is not very meaningful. Rather their direct interaction is already included in the Hamiltonian which will describe the internal dynamics of the isolated molecule. However, it is meaningful to talk about the donor and acceptor modes being represented by point dipoles when describing their

interaction with the solid particle and indirectly with each other through the presence of the solid. The interaction to be used in place of the dipole-dipole interaction is then simply $\Delta U(\omega)$ given by Eq. (3.2.25). One simply sets $(\xi_d, \eta_d, \phi_d) = (\xi_a, \eta_a, \phi_a)$.

The rate of energy transfer induced by the coupling is

$$K' = (9c^4/8\pi)\int_{-\infty}^{\infty} d\omega\, \omega^4 |\Delta A(\omega)|^2 \Sigma\, \sigma_a(\omega)\, \Gamma_d(\omega)\ , \tag{3.2.38}$$

where ΔA is given by Eq.(3.2.29) and σ_a is the absorption cross section for the acceptor band and Γ_d is the corresponding emission function for the donor band. This rate K' is in addition to the normal intramolecular energy rate that may be present for the isolated molecule. In Eq.(3.2.38) we have included now a summation over all intermediate electronic states, where $\sigma_a(\omega)$ and $\Gamma_d(\omega)$ are the line shapes related to virtual transitions involving these states. The reason for this summation becomes apparent if we compare the Förster-Dexter matrix element of Eq.(3.2.2) with the corresponding matrix element for the intramolecular case. In the former case the interaction is bilinear in the donor and acceptor dipole operators, so it only deexcited the donor molecule and excited the acceptor molecule. In the case of intramolecular energy transfer, where the donor and acceptor are the same molecule, the interaction

is quadratic in the dipole operator. Thus by inserting a complete set of states we see that we may first virtually excite the molecule and then virtually deexcite the molecule to some final electronic state.

3.3. Nonradiative decay

Let us now focus our attention on the other terms appearing in Eq. (3.2.25) which were previously neglected. These terms are quadratic in $\vec{\mu}_d$ or $\vec{\mu}_a$. We shall show that they are simply related to the nonradiative decay rates of the molecules. Let us consider one molecule at a time. Let

$$U_{dd} = -\frac{1}{2}\vec{\mu}_d^* \cdot \vec{E}_d \quad . \tag{3.3.1}$$

Note that $\vec{\mu}_d$ is assumed real, but we have written $\vec{\mu}_d^*$ in place of $\vec{\mu}_d$, for reasons which will soon become clear. Consider the quantity

$$\Gamma_d = \hbar^{-1} \mathrm{Im}(U_{dd}) \ , \tag{3.3.2}$$

which has the dimensions of a frequency. For a point dipole we may write the corresponding charge density as

$$\rho_d = -\vec{\mu}_d \cdot \nabla \ \delta(\vec{r} - \vec{r}_d) \ , \tag{3.3.3}$$

as may readily be seen by computing the first moment of the charge density:

$$\int \rho_d x_i d\vec{r} = -\int \nabla \cdot [\vec{\mu}_d x_i \delta(\vec{r}-\vec{r}_d)] d\vec{r} + \int \delta(\vec{r}-\vec{r}_d)(\vec{\mu}_d)_i d\vec{r} \tag{3.3.4}$$

The first integral vanishes so we obtain

$$\int \rho_d \vec{r}\, d\vec{r} = \vec{\mu}_d \ , \tag{3.3.5}$$

as conjectured. Consider next the integral

$$\int \phi \rho_d^* d\vec{r} = -\int_{out} d\vec{r}\, \nabla \cdot (\vec{\mu}_d^* \phi\, \delta(\vec{r}-\vec{r}_d)) + \int \delta(\vec{r}-\vec{r}_d)\, \vec{\mu}_d^* \cdot \nabla\phi \, d\vec{r} \ , \tag{3.3.6}$$

where the region of integration is outside the particle. Again the first integral vanishes and we obtain

$$\int_{out} \rho_d^* \phi \, dr = -\vec{\mu}_d^* \cdot \vec{E}_d \ . \tag{3.3.7}$$

Thus we have

$$\Gamma_d = \hbar^{-1} \mathrm{Im}[-(1/2)\, \vec{\mu}_d^* \cdot \vec{E}_d] = (1/2\hbar)\, \mathrm{Im} \int_{out} \rho_d^* \phi \, d\vec{r} \tag{3.3.8}$$

Using the Poisson equation, this becomes

$$\Gamma_d = (1/2\hbar)\, \mathrm{Im} \int_{out} \phi \nabla \cdot \vec{E}^* / (4\pi)\, d\vec{r} = (1/8\pi\hbar)\, \mathrm{Im} \int_{out} \nabla \cdot (\phi \vec{E}^*)\, d\vec{r} - (1/8\pi\hbar)\, \mathrm{Im} \int_{out} \vec{E}^* \cdot \nabla\phi \ d\vec{r}. \tag{3.3.9}$$

The last term vanishes while the first term can be converted to an integral over the particle's surface

$$\Gamma_d = (1/8\pi\hbar)\, \mathrm{Im} \int \hat{n}_{in} \cdot \vec{E}^* \phi \, dS \ , \tag{3.3.10}$$

where $\hat{n}_{in}$ denotes an inward pointing normal. Using the continuity of the normal component of $\vec{D}$, this may also be rewritten as

$$\Gamma_d = -(1/8\pi\hbar)\, \mathrm{Im} \int \hat{n}_{out} \cdot \vec{D}^* \phi \, dS \ , \tag{3.3.11}$$

where $\hat{n}_{out}$ is an outward pointing normal and the integral is now over a surface slightly inside the particle. Then converting the integral to one over the particle's volume we obtain

$$\Gamma_d = -(1/8\pi\hbar)\,\mathrm{Im}\int_{in}\nabla\cdot(\phi\,\vec{D}^*)\,d\vec{r}$$

$$= (1/8\pi\hbar)\,\mathrm{Im}\int_{in}\epsilon\,|\vec{E}|^2\,d\vec{r}\ . \qquad (3.3.12)$$

Finally we use the relation

$$\mathrm{Im}\,\epsilon = 4\pi\sigma/\omega\ , \qquad (3.3.13)$$

where σ is the phenomenological conductivity to obtain

$$\Gamma_d = (1/2\hbar\omega)\int_{in}\sigma\,|\vec{E}|^2\,d\vec{r}\ . \qquad (3.3.14)$$

The interpretation of the right hand side is that it is the power delivered to Ohmic heating divided by the photon energy. This is the nonradiative decay rate if the magnitude of the dipole is chosen to correspond to the molecule being excited with one quantum of energy.

The expression for the nonradiative decay rate becomes

$$\Gamma_d = \alpha\omega\,\mathrm{Im}\sum_{n=0}^{\infty}\sum_{m=0}^{n} T_{nm}\,\vec{\mu}_d\cdot\overleftrightarrow{E}^{dd}\cdot\vec{\mu}_d\ . \qquad (3.3.15)$$

Here $\overleftrightarrow{E}^{dd}$ is given by Eqs. (3.2.32) but with a replaced by d. A similar expression may be found for the nonradiative decay rate of the acceptor by replacing d by a in the above equation. We have expressed Γ_d in terms of the static polarizability, α, rather than in terms of the transition dipole so that the classical nature of the formula is manifest. Thus we have replaced $|\vec{\mu}_d|^2$ by $2\alpha\hbar\omega$.

We note in passing that the real parts of U_{dd} and U_{aa} are associated with the level shifts of the molecules due to the interaction with the solid state particle.

3.4. Radiative decay

Just as the nonradiative decay of a molecule near a particle may be enhanced, the same is true of the radiative decay. The donor molecule induces a dipole in the particle in response to its own dipole. The coherent sum of these dipoles is responsible for the net emission at the donor molecule frequency. (In addition a similar effect can occur at the acceptor molecule frequency). In previous work Gersten et al. have derived formulas for the enhanced dipole moment of the system for a collinear geometry. The generalizations of this formula is readily obtained from the previous formulas.

If we examine the system far away from the molecule or particle we can describe the system as consisting of a dipole located at the origin: $(\xi_1, \eta_1, \phi_1) = (1,0,0)$. The field due to such a dipole may be obtained from Eq.(3.2.17) and is

$$\Phi = f^{-1}\{F_{10}Q_1(\xi)P_1(\eta) + F_{11}Q_1^1(\xi)P_1^1(\eta)[\mu_\xi \cos\phi + \mu_\phi \sin\phi]\} . \tag{3.4.1}$$

On the other hand, an expression for Φ has been given in Eq.(3.2.11b). Substituting the values for A'_{nm} and B'_{nm} of Eq.(3.2.18) leads to an alternate expression for Φ in terms of the molecular dipole components. Equating the coefficients of terms with similar angular

behavior leads to the following

$$\begin{bmatrix} \mu_\xi \\ \mu_\eta \\ \mu_\phi \end{bmatrix} = \begin{bmatrix} F_{\xi\xi} & F_{\xi\eta} & F_{\xi\phi} \\ F_{\eta\xi} & F_{\eta\eta} & F_{\eta\phi} \\ F_{\phi\xi} & F_{\phi\eta} & F_{\phi\phi} \end{bmatrix} \begin{bmatrix} \mu_\xi \\ \mu_{\eta_d} \\ \mu_{\phi_d} \end{bmatrix} \qquad (3.4.2)$$

where μ_{ξ_d}, μ_{η_d} and μ_{ϕ_d} are the donor molecular coordinates and

$$F_{\xi\xi} = (f\cos\phi_d / h_{\xi_d}) P_1^1(\eta_d) \left\{ [P_1^1(\xi_d)]' + [(1-\epsilon)/\Delta_{11}] P_1^1(\xi_o) P_1^1(\xi_o) [Q_1^1(\xi_d)]' \right\} \qquad (3.4.3a)$$

$$F_{\xi\eta} = (f\cos\phi_d / h_{\eta_d}) [P_1^1(\eta_d)]' \left\{ P_1^1(\xi_d) + [(1-\epsilon)/\Delta_{11}] P_1^1(\xi_o) [P_1^1(\xi_o)]' Q_1^1(\xi_d) \right\} \qquad (3.4.3b)$$

$$F_{\xi\phi} = -(f\sin\phi_d / h_{\phi_d}) P_1^1(\eta_d) \left\{ P_1^1(\xi_d) + [(1-\epsilon)/\Delta_{11}] P_1^1(\xi_o) [P_1^1(\xi_o)]' Q_1^1(\xi_d) \right\} \qquad (3.4.3c)$$

$$F_{\eta\xi} = (f/h_{\xi_d}) P_1(\eta_d) \left\{ [P_1(\xi_d)]' + [(1-\epsilon)/\Delta_{10}] P_1(\xi_o) [P_1(\xi_o)]' [Q_1(\xi_d)]' \right\} \qquad (3.4.3d)$$

$$F_{\eta\eta} = (f/h_{\eta_d}) [P_1(\eta_d)]' \left\{ P_1(\xi_d) + [(1-\epsilon)/\Delta_{10}] P_1(\xi_o) [P_1(\xi_o)]' Q_1(\xi_d) \right\} \qquad (3.4.3e)$$

$$F_{\eta\phi} = 0 \qquad (3.4.3f)$$

$$F_{\phi\xi} = (f\sin\phi_d / h_{\xi_d}) P_1^1(\eta_d) \left\{ P_1^1(\xi_d) + [(1-\epsilon)/\Delta_{11}] P_1^1(\xi_o) [P_1^1(\xi_o)]' [Q_1^1(\xi_d)]' \right\} \qquad (3.4.3g)$$

$$F_{\phi\eta} = (f\sin\phi_d / h_{\eta_d}) [P_1^1(\eta_d)]' \left\{ P_1^1(\xi_d) + [(1-\epsilon)/\Delta_{11}] P_1^1(\xi_o) [P_1^1(\xi_o)]' Q_1^1(\xi_d) \right\} \qquad (3.4.3h)$$

$$F_{\phi\phi}=(f\cos\phi_d/h_{\phi_d})P_1^1(\eta_d)\left\{P_1^1(\xi_d)+[(1-\epsilon)/\Delta_{11}]P_1^1(\xi_0)[P_1^1(\xi_0)]'Q_1^1(\xi_d)\right\}. \tag{3.4.3i}$$

The decay rate due to radiation may be written as

$$\Gamma_{r,d}=\Gamma^0_{r,d}\left|\vec{\vec{F}}\cdot\vec{\mu}_d\right|^2 \tag{3.4.4}$$

Here $\Gamma^0_{r,d}$ is the radiative decay rate of the free molecule and $\Gamma_{r,d}$ is the rate in the presence of the particle.

3.5. results and discussion

In the previous sections we have developed a theory for the energy transfer between a donor and acceptor molecule in the presence of a small solid state particle in the shape of a spheroid. The energy transfer may be enhanced by having the particle actively assist in the transfer process. Secondly the presence of the particle opens up decay channels which would tend to compete with the energy transfer. A complete theory of energy transfer must take these two aspects into account.

In order to understand how energy transfer may be enhanced consider first the case of energy transfer in the absence of the particle. It is brought about by the dipole-dipole interaction. The dipole operator of the donor molecule deexcites the donor while the dipole operator of the acceptor molecule excites the acceptor.

The strength of the interaction falls off rapidly with distance, as r^{-3}, and the energy transfer rate, which is proportional to the square of the matrix element of this interaction, falls off as r^{-6}. If a solid state particle is in the presence of the molecules, however, the donor dipole will induce multipole moments on the particle. In particular, the dipole that is induced on the particle may be much larger than the donor dipole itself. This phenomenon, is partly responsible for the enhanced electrodynamic processes on rough surfaces or near small particles, including surface-enhanced Raman scattering, enhanced fluorescence, enhanced photochemistry and enhanced second-harmonic generation. The degree of enhancement of the dipole depends on the shape of the particle, the location of the molecular dipole and whether or not a resonance of the solid is excited. Once the dipole (and other multipoles) have been excited in the particle, the fields set up by the moment(s) can couple to the acceptor dipole and affect the energy transfer. Whereas in the absence of the particle the rate of energy transfer depends primarily on the molecule-molecule separation, now the energy transfer depends primarily on the molecule-solid distance. For a large particle size the molecules may be rather far apart and still have rapid energy transfer occur. However, if the molecules are far away from the solid, then the solid has little influence

on the transfer proce again. One of the main goals of this work is to define precisely how the location of the molecules influence transfer dynamics. We shall see the concept of 'activity zones' emerge.

We have developed side-by-side a theory for energy transfer and for nonradiative decay as well as for radiative decay. Just as the energy transfer depends sensitively on the location of the molecules relative to the particle, so do the decay losses. At those locations where there will be large internal fields in the solid, one would also expect large Ohmic losses to occur, as we shall see.

In Fig.3.1 we show the geometrical arrangement of the molecules and the particle. Figure 3.2 shows the dependence of the enhancement factor, R, of Eq.(3.2.37) on acceptor molecule location, $(r_a, \theta_d, \phi_d) = (125\ \text{Å}, 0^\circ, 0^\circ)$, $(\theta_a, \phi_a) = (180^\circ, 0^\circ)$, $(\theta_{\mu_d}, \phi_{\mu_d}) = (0^\circ, 0^\circ)$ and $(\theta_{\mu_a}, \phi_{\mu_a}) = (0^\circ, 0^\circ)$. The semi-major axis of the spheroid was a = 100 Å and the semi-minor axis of the spheroid was b=50 Å. The particle is made of silver and curves for several energies, $\hbar\omega$, are shown. We note that when the acceptor molecule is close to the particle the enhancement rate grows fairly large, i.e. by as much as five or more orders of mmagnitude. As the acceptor is moved away from the particle the fall-off is at first rapid, but tapers off to a slower fall-off at larger distances. Significant

enhancements persist out to r_a = 500 Å, corresponding to a donor-acceptor separation of 725 Å. There is also evidence in Fig.3.2 for a strong resonance at $\hbar\omega$ = 3.12 ev. This is close to the energy of the dipolar plasmon for a 2:1 prolate spheroidal silver particle.

In Fig.3.3 we study the effect of rotating the acceptor dipole orientation, still keeping everything else in a collinear geometry. Here $(r_d, \theta_d, \phi_d)=(125\text{Å}, 0^\circ, 0^\circ)$, $(r_a, \theta_a, \phi_a)=(125\ \text{Å}, 180^\circ, 0^\circ)$, $(\theta_{\mu_a}, \phi_{\mu_a})=(0^\circ, 0^\circ)$, $\phi_{\mu_a}=0^\circ$, and (a,b) = (100 Å, 50 Å). The energy is held fixed at $\hbar\omega$ = 3.0 ev. Two curves are drawn, the solid curve is $|A(\omega)|^2$, where $A(\omega)$ is the interaction energy associated with unit dipoles near a particle and is given by Eqs. (3.2.28) and (3.2.29). The dashed curve is A_o^2, where A_o is the interaction energy of two free unit dipoles. We note that in both cases the interaction energy is a maximum for a parallel alignment and falls to zero as the acceptor molecule is rotated to a perpendicular configuration. The interaction strengths are seen to differ by more than two orders magnitude. The enhancment ratio, $R=|A(\omega)/A_o|^2$ is found not to depend on the acceptor angle orientation, as is shown in Fig.3.4. The parameters are the same as in Fig.3.3, but curves are given for several energies, $\hbar\omega$.

In Fig.3.5 we plot the enhancement ratio as a function of the shape of the particle, keeping a collinear geometry.

ere a was held fixed at 100 Å but b was allowed to vary between 10 Å (a needle-like structure) to 90 Å (a nearly spherical structure). The donor and acceptor molecules had the same parameters as in Fig.3.3. Curves are drawn for several energies. We note the presence of resonance structure appearing in the optical region of the spectrum. As the particle's shape is varied the multipolar resonances of the particle sweep through the spectrum. Evidence for dipolar and quadrupolar resonances appear in this figure. Whenever the resonance peak overlaps with the donor emission band and the acceptor absorption band, we would expect strong energy transfer to occur, as should be clear from an examination of the integrand of Eq. (3.2.27). This should be kept in mind when attempting to design a particle to optimize the energy transfer.

In Fig.3.6 we vary both the angular location of the donor and acceptor molecules, keeping their orientations antiparallel to each other. The angular location is specified by giving the spheroidal coordinate η . The two are related by the formula

$$\tan\theta = (\xi\eta)^{-1}[(\xi^2-1)(1-\eta^2)]^{1/2} \quad . \qquad (3.5.1)$$

A plot is made of $R(\omega)$ vs η_a with $\eta_d = -\eta_a$. Here the molecules are allowed to move over the spheroidal surfaces which pass through the points $Z=\pm$ 125 Å along the symmetry axes. The molecules are oriented parallel to the normals to these spheroidal surfaces. Curves are drawn

r several values of b, keeping a fixed at 100 Å. We note that as the molecules are moved away from the vicinity of the sharp tips of the spheroid, the enhancement factor starts to fall off dramatically. In some cases, there may even be de-enhancement occuring. The largest degree of falloff occurs for the sharpest spheroid.

The general trends exhibited by Figs.3.2 and 3.6 are consistent with the existence of activity zones near the tips of the spheroid. If the donor and acceptor molecules lie within these activity zones they are able to couple to the solid effectively and efficient energy transfer ensues. If either or both of the molecules lie outside these zones the coupling is diminished and the energy transfer enhancement is quenched. This is in agreement with a lightning rod picture in which electric field lines tend to be concentrated near the sharpest features of a structure. The size of the activity zone may crudely be taken as the characteristic size of the sharpest feature on the solid. For the spheroid this is the radius of curvature of the tip: $r_c = b^2/a$. Thus, if the molecules both lie within a distance r_c of either tip strong energy transfer will occur. If the molecule is allowed to move out of the activity zone in the radial direction, as in Fig.3.2, or in an angular direction, as in Fig.3.6, the coupling drops off dramatically.

evertheless, there is still some remnant long range nature of the transfer due the presence of the particle, even when the activity zone is left. This is because it is the distances to the solid that are now more significant than the interparticle distances. It is not until the distance from the particle is large compared with the size of the particle that these will become unimportant.

In Fig.3.7 we keep the donor fixed along the symmetry axis and move the position of the acceptor over a spheroidal surface. The donor dipole is fixed parallel to the symmetry axis and the acceptor dipole is perpendicular to the spheroidal surface, so it varies as the acceptor molecule is moved. The geometry is shown in the inset. Here $(r_d, \theta_d, \Phi_d)=(125\ \text{Å}, 180^\circ, 0^\circ)$, $\Phi_a=0$, $(\theta_{\mu_a}, \Phi_{\mu_a})=(0^\circ, 0^\circ)$ and $r_a=125$ Å for $\eta_a=+1$, corresponding to $\theta_a=0^\circ$. Curves are shown for several values of the energy. As before, a=100 Å and b=50 Å. The results here are consistent with those of Fig.3.6, but the falloff with η_a is less dramatic. Since only one molecule is being taken out of the activity zone while the other molecule remains inside, this is to be expected.

In Fig.3.8 a graph is made of the enhancement ratio as a function of energy for spheroids of several different shapes. Here the molecules were held as in Fig.3.3. In addition to the resonance structure seen below the plasmon

energy we also see a region of de-enhancement. The curves are presented here for silver. Curves for other materials may be generated by using the corresponding optical properties of those materials. Having studied the energy transfer rate in some detail, let us now look at the behavior of the decay rate. This too we expect to depend strongly on such factors as the molecular location and orientation. In Fig.3.9 we present the nonradiative decay rate as a function of frequency for the same geometrical arrangements as were used in Fig.3.8. The dipole is taken to be of unit strength. We see that when there is a resonance in energy transfer there is also a peak in the decay rate. Since nonradiative decay is a competition mechanism, having a resonance situation is not a guarantor of efficient energy transfer. However, in affecting energy transfer we want the resonance to be located in the spectral region where there is the most overlap between donor and acceptor bands. This need not necessarily coincide, for example, with the donor emission band itself. Thus, to some extent, it is possible to 'tune' the structure to optimize energy transfer while not at the same time maximizing the nonradiative decay.

In Fig.3.10 the decay rate is presented as a function of molecular location on a spheroidal surface as in Fig.3.7. Curves are presented for several values of the molecular resonance energy. Some structure is seen as the

angular position is varied, which is probably due to the coupling of the molecule to the various multipolar modes of the solid. Associated with each mode is a particular angular pattern and, depending on the energy one of these patterns may tend to dominate the electrodynamics.

In Fig.3.11 the damping rate is plotted as a function of dipole orientation ϑ_μ for several locations on a spheroidal surface. Some sensitivity of the orientation of the dipole relative to the spheroid and its model structure are again noted. As in Fig.3.10, the spheroidal surface is taken as one which passes within 25 Å of the particle along the symmetry axis.

In addition to nonradiative decay there is also enhanced radiative decay. This comes about because the dipole that is induced in the particle adds coherently to the donor dipole and leads to a system dipole which may be much larger than the molecular dipole. Since the decay rate goes as the square of this dipole, radiative decay can be significant. These effects have been considered by Gersten et al. in a previous work for the case of a collinear geometry.

References

1. For a general view see V. M. Agranovich and M. D. Galanin, "Electronic Exitation Energy Transfer in Condensed Matter", (North-Holland, Amsterdam, 1982). For recent developments see " Energy Transfer Processes in Condensed Matter ", ed. by . D. Bartolo, (Plenum, New York, 198).
2. P. Y. Lu, Z. X. Yu, R. R. Alfano and J. I. Gersten, Phys. Rev. A 26, 3610(1982); 27, 2100(1983)
3. Th. Förster, Ann. Phys. 2, 55(1948); Zeits. Naturf. 19, 321(1949); Disc. Farady Soc. 27, 836(1959)
4. D. L. Dexter, J. Chem. Phys. 21, 836(1953); Phys. Status Solidi (b) 51, 571(1972)
5. D. L. Dexter, Th. Förster and R. S. Knox, Phys. Status Silidi 34, K159(1969)
6. S. I. Vavilov, Z. Phys. 31, 750(1925); 50, 52(1928); 53, 665(1929); Acta. Phys. Pol. 5, 417(1936)
7. F. Perrin, Ann. Phys. (N. Y.) 12, 169(1929)
8. J. Perrin, 2-me Conceil de Chimie Solvay, Bruxelles, 1924.
9. Ther are intensive literatures on SERS, for recent review see " Surface Enhanced Ramman Scattering", ed. by R. K. Chang and T. E. Furtak, (Plenum, NewYork, 1981).

10. M. Kerker, D. S. Wang and H. Chew, Appl. Opt. 19, 4159(1980).

11. J. I. Gersten and A. N. Nitzan, Chem. Phys. Lett. 104, 31(1984); J. Chem. Phys. 75, 1139(1981)

12. X. M. Hua, J. I. Gersten and A. Nitzan, J. Chem. Phys. 83, 3650(1985).

13. L. M. Folan and S. Arnold, Chem. Phys. Lett. 118, 322(1985).

14. J. I. Gersten, J. Chem. Phys. 72, 5779(1980); J. I. Gersten and A. Nitzan, J. Chem. Phys. 73, 3023(1980); S. L. McCall, P. M. Platzman and P. A. Wolff, Phys. Lett. A 77, 381(1980).

15. A. M. Stacy and R. P. Van Duyne, Chem. Phys. Lett. 102, 56(1983); D. A. Weitz, S. Garoff, J. I. Gersten and A. Nitzan, J. Chem. Phys. 78, 5324(1983); A. Bachackashvilli, S. Efrima, B. Katz and Z. Priel, Chem Phys. lett. 94, 571(1983).

16. A. Nitzan and L. E. Brus, J. Chem. Phys. 74, 5321(1981); 75, 2205(1981). G. M. Gonscher and C. B. Harris, J. Chem. Phys. 77, 3767(1982). C. J. Chen and R. M. Osgood, Phys. Rev. Lett. 50, 1705(1983). S. Garoff, D. A. Weitz and M. S. Alvarez, Chem. Phys. Lett. 93, 283(1982).

17. X. M. Hua and J. I. Gersten, Phys. Rev. B 33, 3756(1986).

18. See, for example, J. D. Jackson, " Classical

Electrodynamics ", 2nd ed., (Wiley, New York, 1975)

19. See, for example, E. Merzbacher, " Quantum Mechanics ", 2nd ed., (Wiley, New York, 1970).

20. See, for example, R. E. Collin, " Field Theory of Guided Waves ", (McGraw-Hill, New York, 1966).

Figure Captions

Fig.3.1. Geometrical arrangement of donor (d) and acceptor (a) molecules. The locations of d and a are specified by spherical coordinates (r_d, θ_d, ϕ_d) and (r_a, θ_a, ϕ_a), respectively. The donor and acceptor dipoles have orientations given by the polar angles ($\theta\mu_d$, $\phi\mu_d$) and ($\theta\mu_a$, $\phi\mu_a$), respectively.

Fig.3.2. Enhancement factor R as a function of acceptor location, r_a for a collinear geometry. The particle is a prolate silver spheroid with a 2:1 aspect ratio. Curves are drawn for several energies, $\hbar\omega$. The donor molecule is held fixed 25 Å from the tip of the particle.

Fig.3.3. Absolute square of the interaction energy as a function of acceptor dipole orientation for an otherwise collinear geometry. The solid curve is with the particle present and the dashed curve is with it absent. The donor and acceptor molecules are held 25 Å away from the opposite tips of a prolate 2:1 silver spheroid.

Fig.3.4 The enhancement ratio as a function of dipole orientation for the case of Fig. 3. Curves for several energies are shown.

Fig.3.5. The enhancement ratio as a function of semi-minor axis size, b, for the collinear geometrical arrangement of Fig. 3.3. Curves are presented for several energies.

Fig.3.6. The enhancement ratio plotted against the spheroidal coordinate associated with angular location of the donor and acceptor. The geometry is depicted in the inset. Curves are presented for several values of b, for fixed a.

Fig.3.7. Enhancement ratio as a function of acceptor location on a spheroidal surface. The acceptor dipole is perpendicular to the spheroid. The geometry is depicted in the inset. Curves are drawn for several energies.

Fig.3.8. Enhancement ratio as a function of energy for fixed donor and acceptor positions arranged in a collinear geometry. Curves are presented for several values of the semi-minor axis, b, for semi-major axis a=100 Å.

Fig.3.9. Damping rate as a function of energy of the molecular resonance for several shapes of the solid. Here a=100 Å and r_a=125Å, in a collinear arrangement.

Fig.3.10. Damping rate as a function of the molecular location on a spheroidal surface. Curves are shown for several energies.

Fig.3.11. Damping rate as a function of molecular dipole orientation angle for several locations on a spheroidal surface.

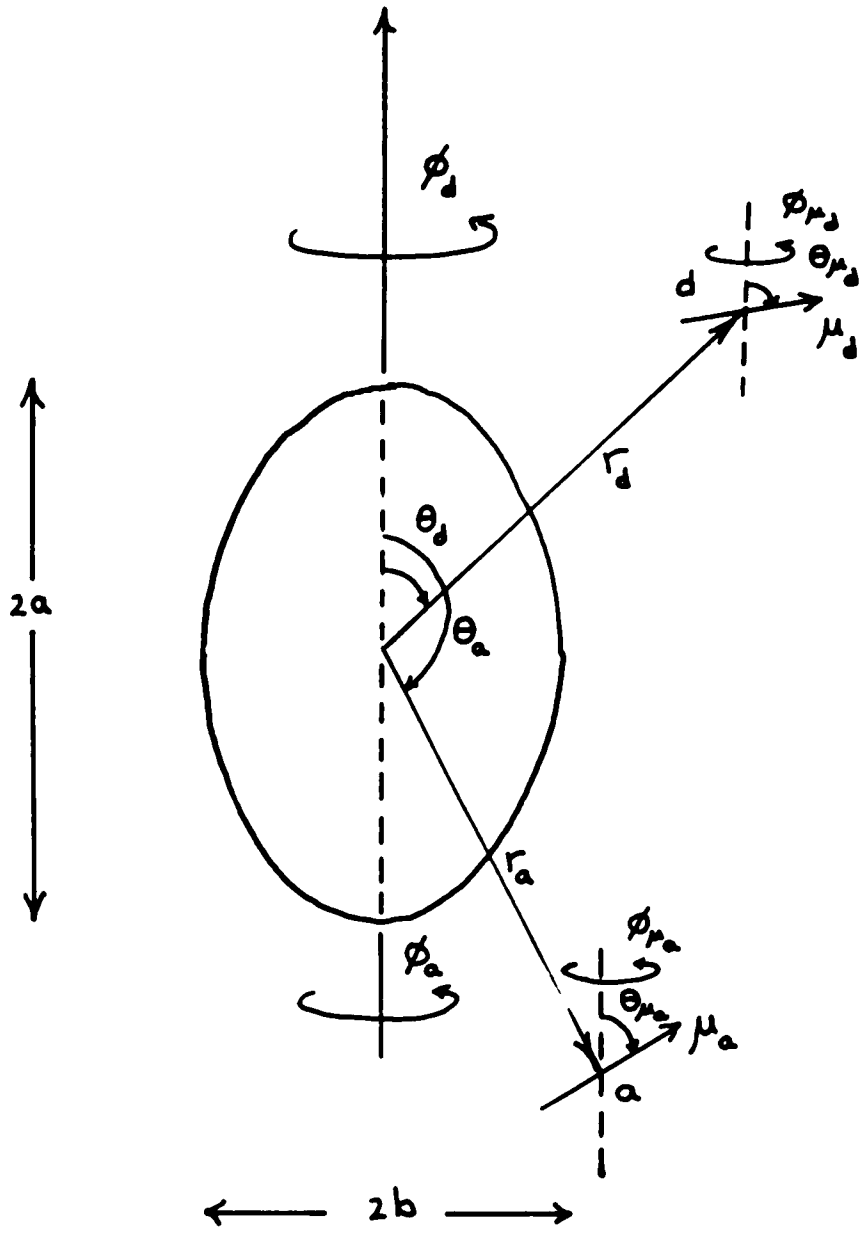
ϕ_d
ϕ_{μ_d}
θ_{μ_d}
d
μ_d
r_d
θ_d
θ_a
2a
r_a
ϕ_a
ϕ_{μ_a}
θ_{μ_a}
μ_a
a
2b

Fig.3.1

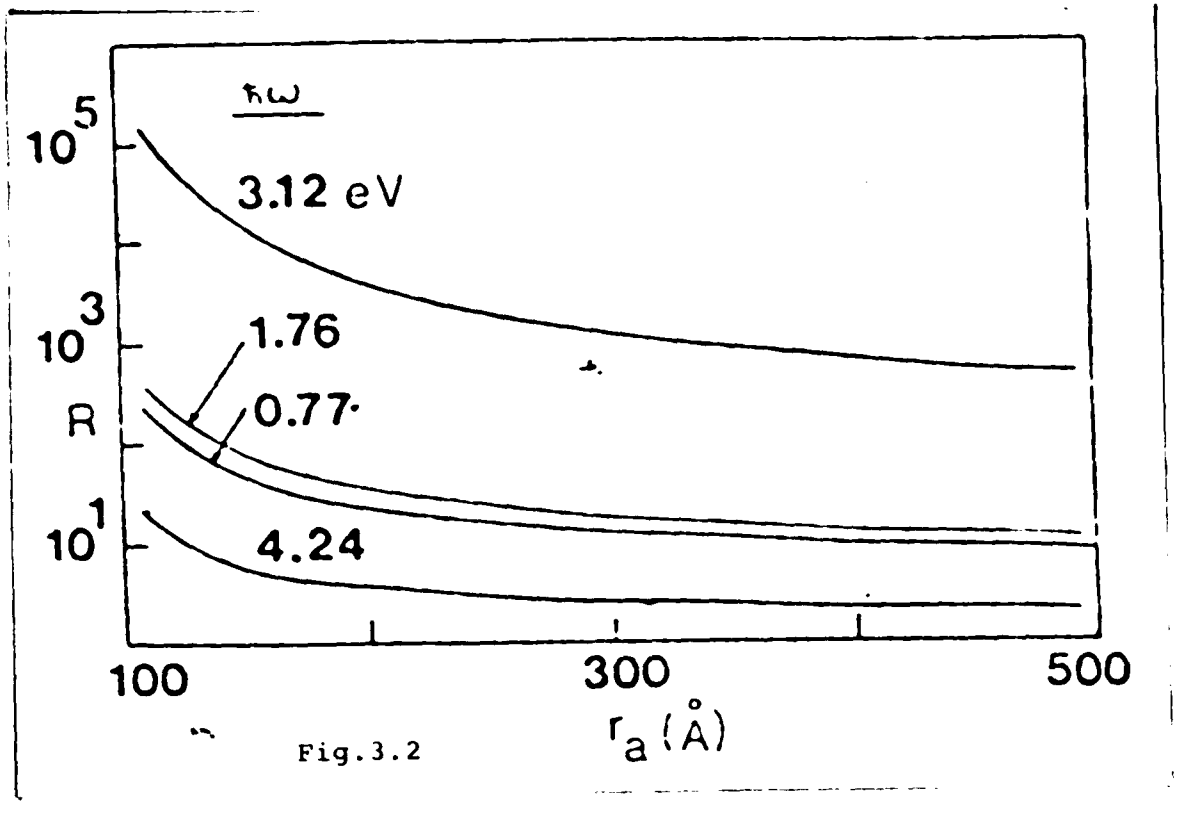

Fig.3.2

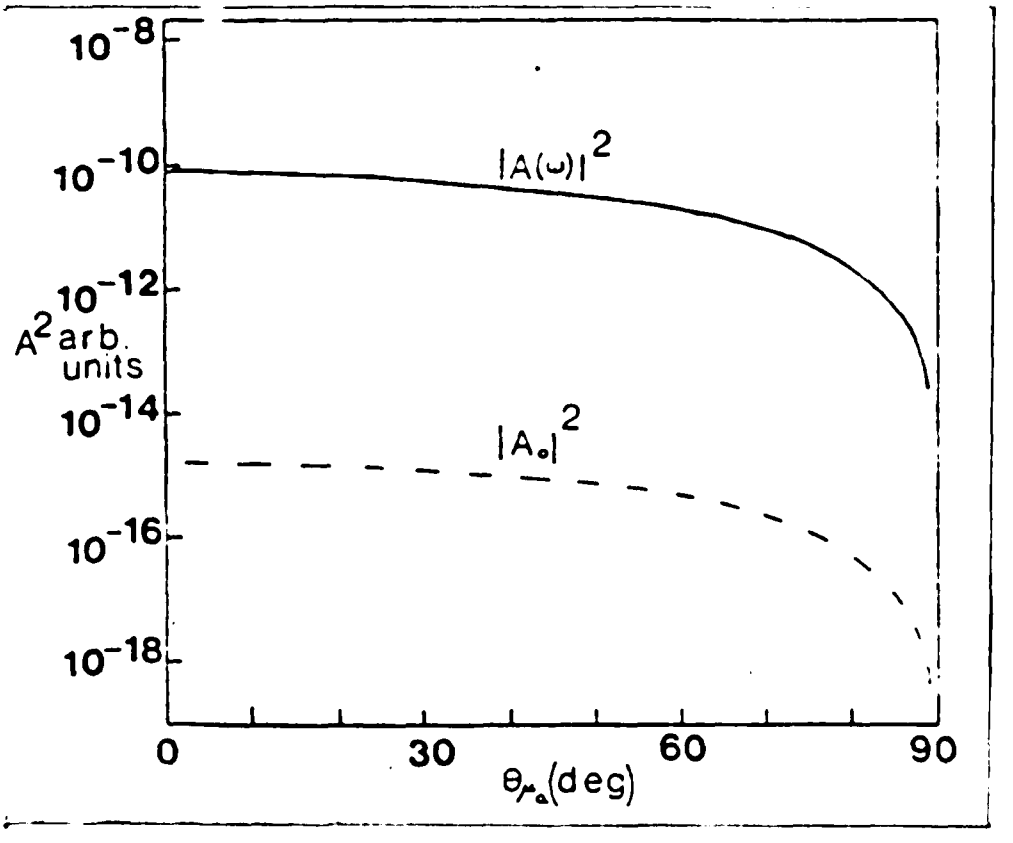
10^{-8}
10^{-10}
10^{-12}
A^2 arb. units
10^{-14}
10^{-16}
10^{-18}
$|A(\omega)|^2$
$|A_o|^2$
0
30
60
90
θ_{μ_a}(deg)

Fig.3.3

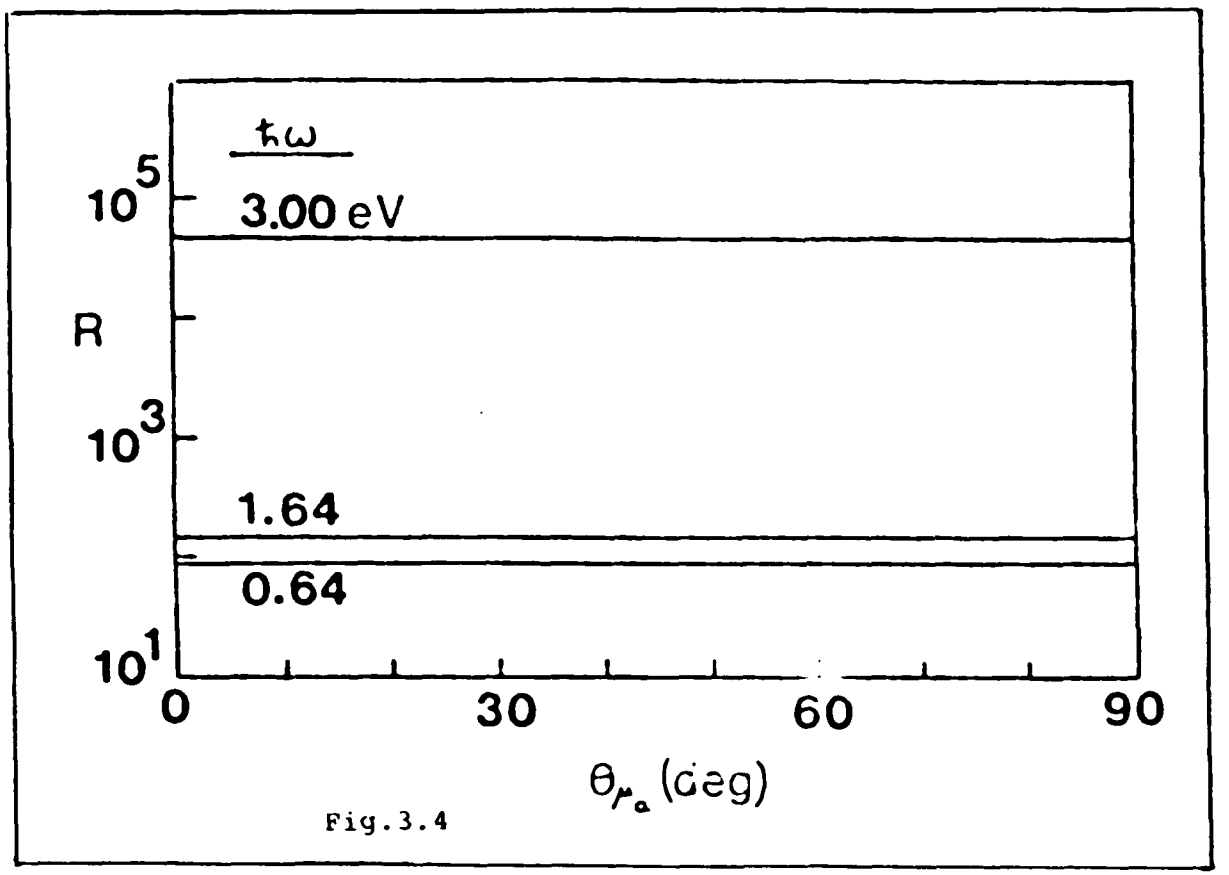

Fig.3.4

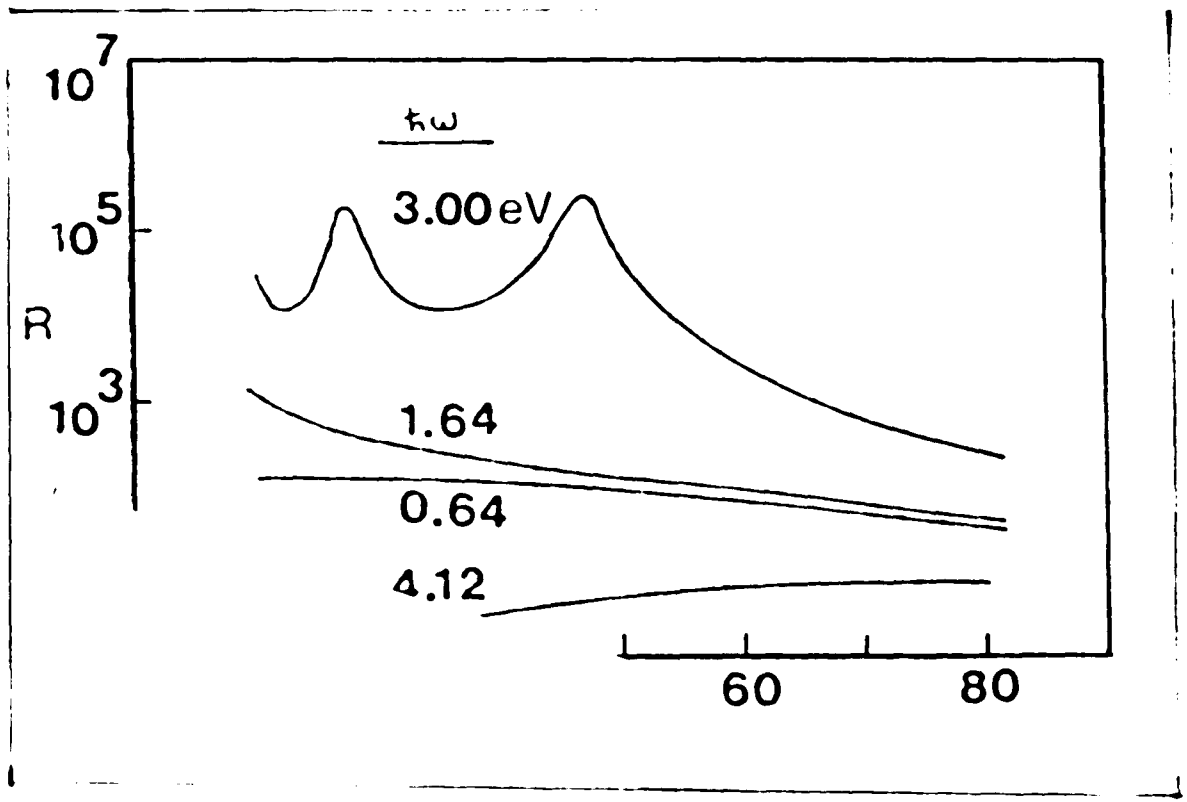

Fig.3.5

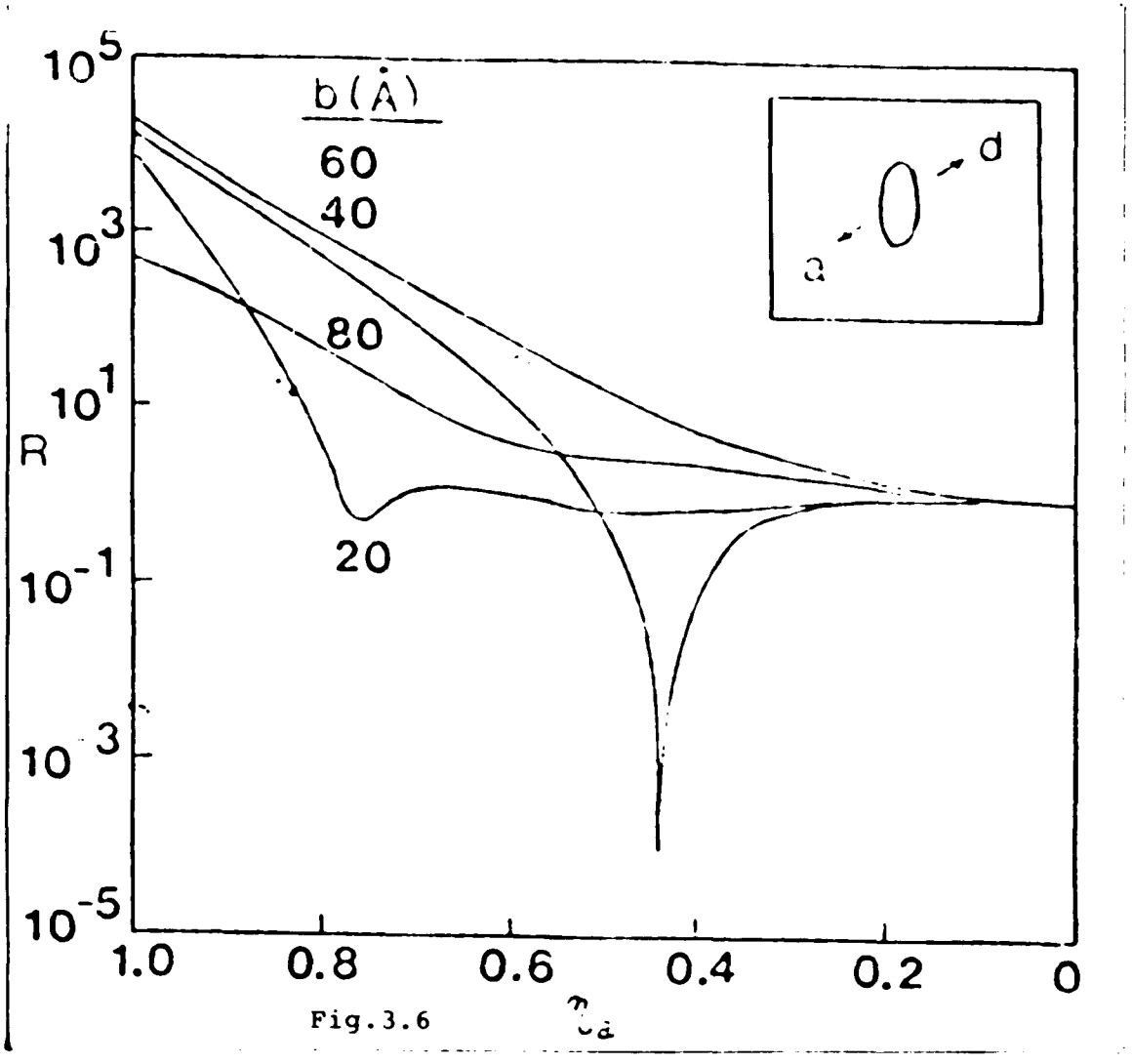

Fig.3.6

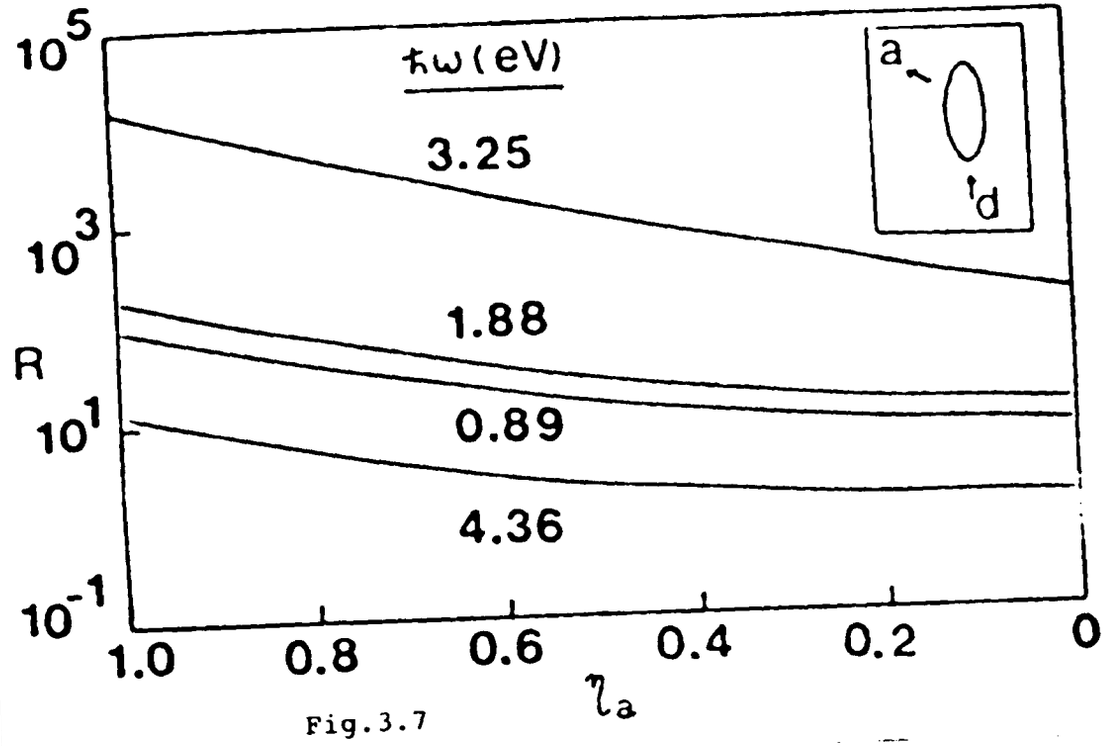

Fig.3.7

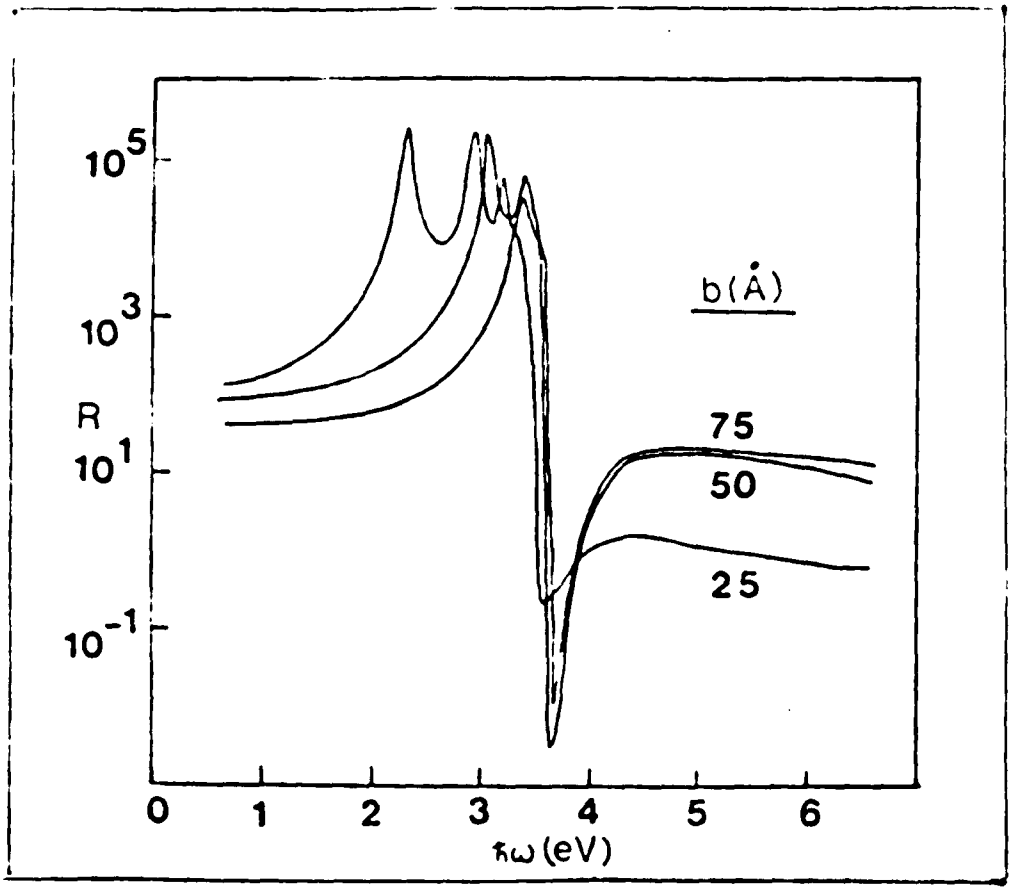

Fig.3.8

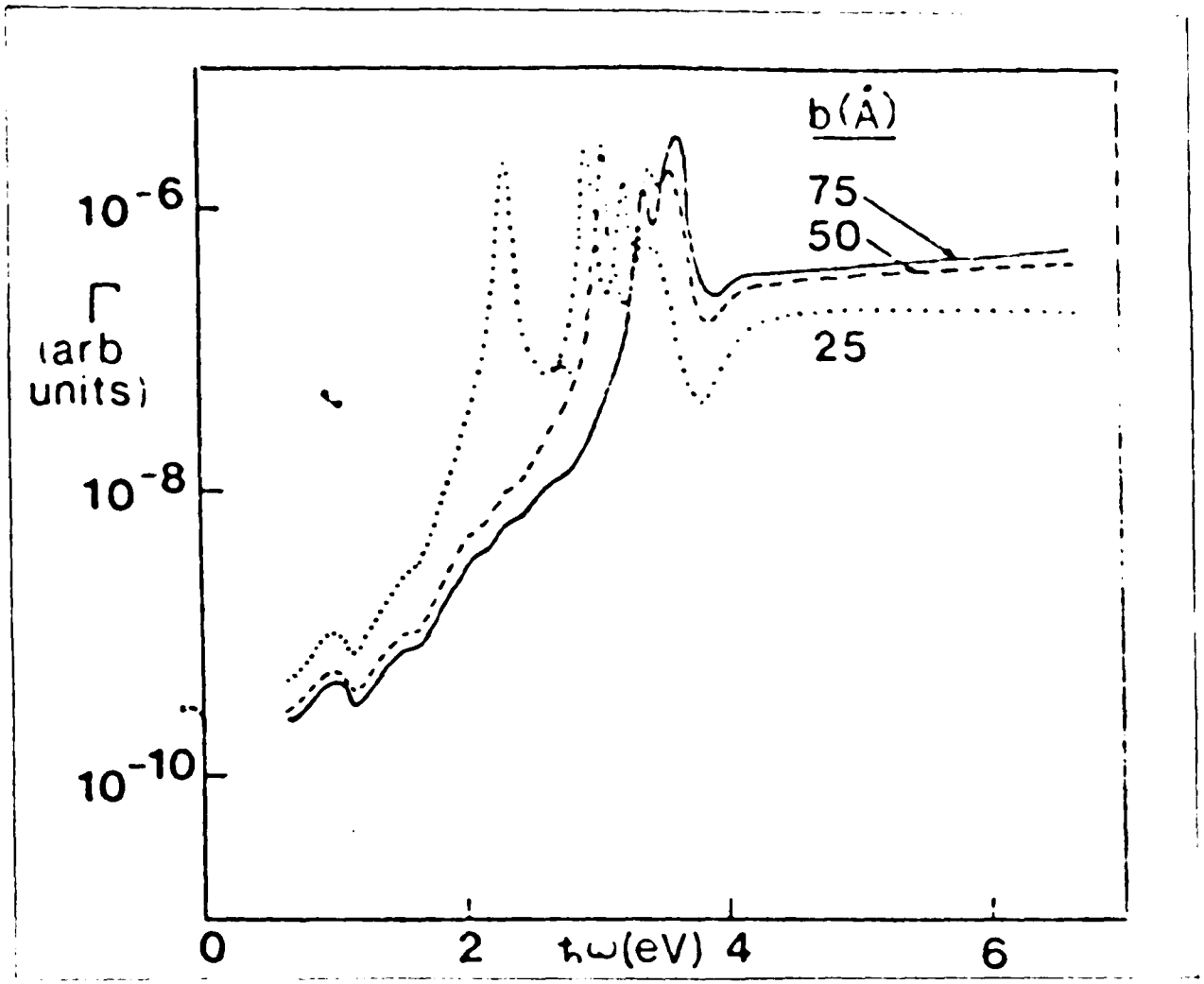

Fig.3.9

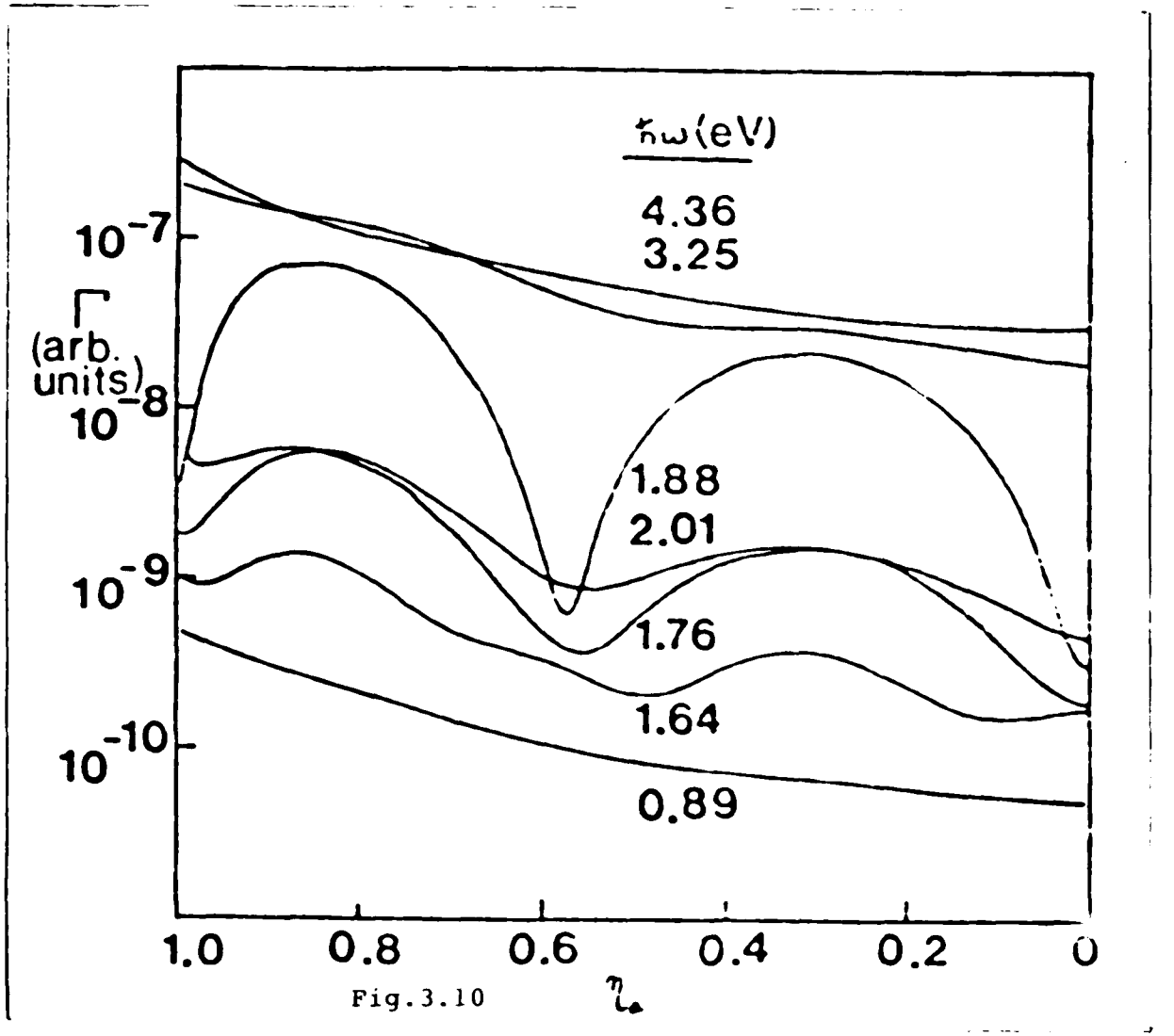
ħω(eV)
4.36
3.25
1.88
2.01
1.76
1.64
0.89
10^-7
(arb. units)
10^-8
10^-9
10^-10
1.0
0.8
0.6
0.4
0.2
0
η

Fig.3.10

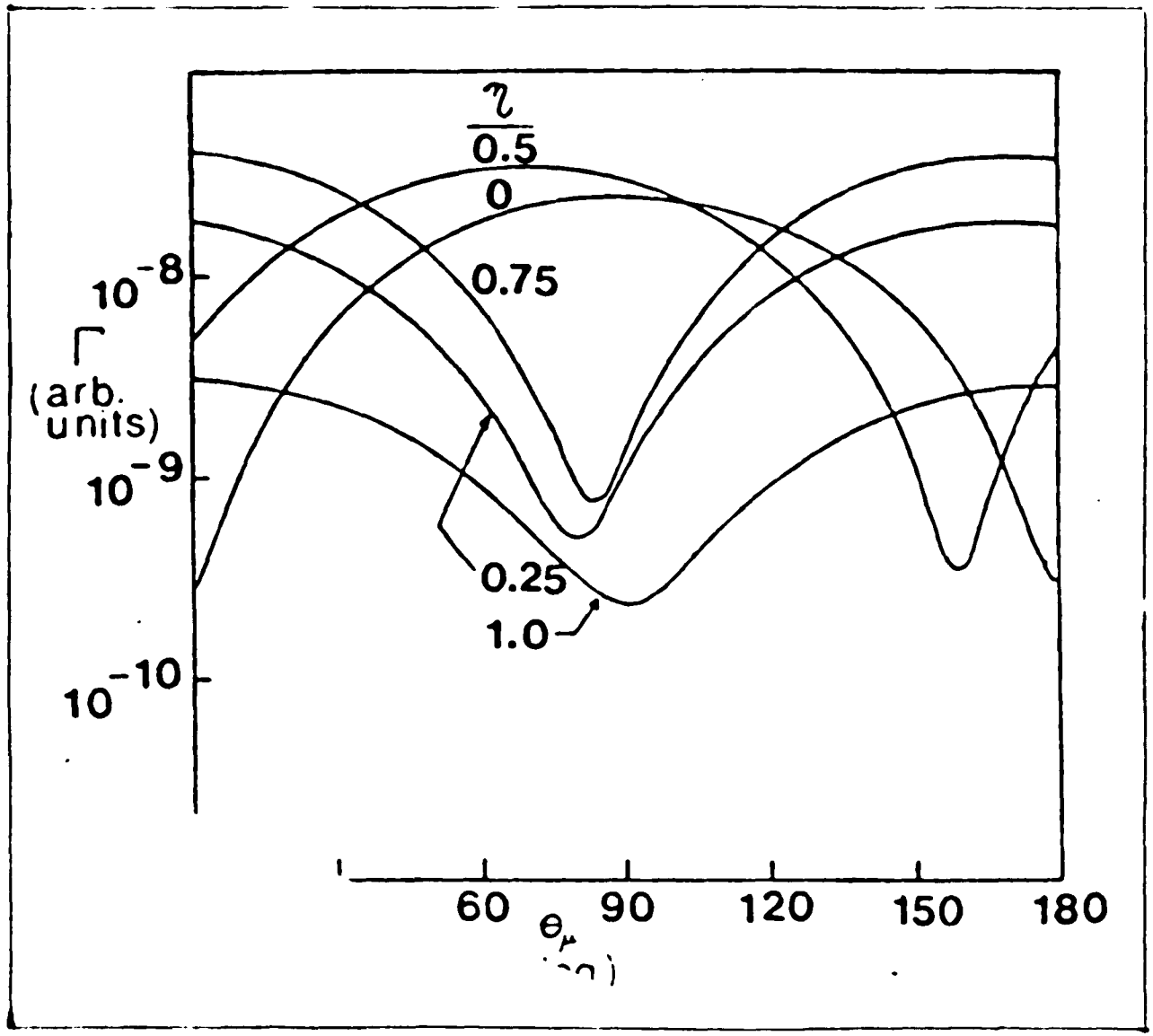
η
0.5
0
0.75
0.25
1.0
10^-8
10^-9
10^-10
(arb. units)
60
90
120
150
180

Chapter IV. Enhanced Energy Transfer Between Donor and Acceptor Molecules near Surface of Cylinder

4.1. Introduction

As antennas and waveguides have long been technologically important, there has been considerable interest in cylindrical configurations. Unlike small particles, which have a finite size, a long cylinder could be considered as a one-dimensionally infinite system. If the surface modes were excited a long-range coupling between the molecules adsorbed on the surface of the cylinder would be possible. Since the long wavelength approximation would fail at large intermolecular separations, a discussion of the full electrodynamic treatment is necessary.

As we described in Chapter III, the enhanced ratio of energy transfer is given by

$$R(\omega)=|A(\omega)/A_o|^2= 1+|\Delta A/A_o|^2 \ . \qquad (4.1.1)$$

where A_o is an angular-dependent factor

$$A_o=[\hat{m}_d\cdot\hat{m}_a-3\hat{r}_{ad}\cdot\hat{m}_a\hat{r}_{ad}\cdot\hat{m}_d]/\epsilon_h\, r_{ad}^3 \ , \qquad (4.1.2a)$$

in the long-wavelength approximation, and

$$A_o=[\hat{m}_a\cdot\hat{m}_d-3\hat{m}_a\cdot\hat{r}_{ad}\hat{m}_d\cdot\hat{r}_{ad}]$$
$$\times(r_{ad}^{-3}-ikr_{ad}^{-2})\exp(ikr_{ad})/\epsilon_h$$
$$-k^2[\hat{m}_a\cdot\hat{m}_d-\hat{m}_a\cdot\hat{r}_{ad}\hat{m}_d\cdot\hat{r}_{ad}]$$
$$\times\exp(ikr_{ad})/\epsilon_h r_{ad} \qquad (4.1.2b)$$

in the full electrodynamic treatment, and ΔA is a function of the geometry of the solids; $k=\frac{\omega}{c}\sqrt{\epsilon_h}$ with ω representing the circular frequency and c, the speed of light in vaccum. It is clear that if $kr_{ad} << 1$, the long wavelength approximation is good. The main task in this Chapter is therefore to find the closed-form solution for ΔA.

The Chapter is arranged as follows. In section II a long wavelength approximation is made for the cylindrical configuration, and a comparison with the flat plane configuration is presented. Section III is devoted to the full electrodynamic treatment for the energy transfer. The agreement of it and the long wavelength approximation in the limit $\omega \sim 0$ is checked. In section IV and V the expressions for nonradiative decay and radiative decay are formulated, respectively. In section VI the numerical results and discussion are presented. The emphasis will be on the long-range coupling between the molecules adsorbed on the surface of the cylinder.

4.2. Long Wavelength Approximation.

Consider a infinitely long cylinder with dielectric function ϵ , immersed in a homogeneous host with dielectric function ϵ_h . The axis of the cylinder is taken as the z axis in cylindrical coordinates. Consider a single charge Q, situated at (ρ', ϕ', z') with $\rho' > a$, where a is the radius of the cylinder.

In a static approach the Poisson equation s ould be satisfied both inside and outside the cylinder:

$$\nabla^2 \Phi = \theta(\rho - a) 4\pi Q/\epsilon_h \quad , \tag{4.2.1}$$

where Φ is the static electrical potential.

The solutions of (4.2.1) are well known[1]:

$$\Phi = Q/|\vec{r}-\vec{r}'|\epsilon_h + \sum_{m=-\infty}^{\infty} \int_{-\infty}^{\infty} dk\, \phi_m(k) K_m(k\rho) I_m(ka) e^{im\phi + ikz} \tag{4.2.2a}$$

for $\rho > a$; and

$$\Phi = \sum_{m=-\infty}^{\infty} \int_{-\infty}^{\infty} dk\, \psi_m(k) I_m(k\rho) K \quad <a) e^{im\phi + ikz} \quad , \tag{4.2.2b}$$

for $\rho < a$, where $\phi_m(k)$ and $\psi_m(k)$ are k-dependent coefficients that should be determined by boundary conditions.

The point charge potential $Q/|\vec{r}-\vec{r}'|\epsilon_h$ could be expanded in cylindrical coordinates as[1]

$$Q/|\hat{r}-\hat{r}'|\epsilon_h$$
$$=(Q/\pi\epsilon_h)\sum_{m=-\infty}^{\infty}\int_{-\infty}^{\infty}dk I_m(k\rho_<)K_m(k\rho_>)\quad \cdot\pi(\phi-\phi')+ik(z-z') \tag{4.2.3}$$

where $\rho_>$ ($\rho_<$) stands for max(ρ, ρ') [min(ρ, ρ')]. Since $\rho > a$ is the case we considered, when matching the boundary conditions we always take $\rho_< = a$, $\rho_> = \rho'$.

At the boundary the potential and the electric displacement should be continuous, this gives

$$\Phi_m(k)=\Delta_s(m)^{-1}(Q/\pi)(1-\epsilon/\epsilon_h)I_m'(ka)K_m(k\rho')$$
$$\times e^{-im\phi'-ikz} \tag{4.2.4a}$$
$$\Psi_m(k)=\Delta_s(m)^{-1}(Q/\pi)(K_m(k\rho')/K_m(ka))$$
$$\times[k_m'(ka)I_m(ka)-I_m'(ka)K_m(ka)]e^{-im\phi'-ikz'} \tag{4.2.4b}$$

where

$$\Delta_s(m)=\epsilon I_m'(ka)K_m(ka)-\epsilon_h K_m'(ka)I_m(ka)\ . \tag{4.2.5}$$

The normal modes would be excited when $\Delta_s(m) = 0$.

The electrostatic interactio is

$$U=\frac{1}{2}\mathrm{Re}[Q\tilde{\Phi}(\rho',\phi',z')]\ . \tag{4.2.6}$$

where $\tilde{\Phi}$ is the induced potential:

$$\tilde{\Phi}=\sum_{m=-\infty}^{\infty}\int_{-\infty}^{\infty}dk\,\Phi_m(k)K_m(k\rho)I_m(ka)e^{im\phi+ikz}. \tag{4.2.7}$$

Substitute (4.2.4a) into (4.2.7) and get

$$U=(Q^2/2\pi)\mathrm{Re}[(1-\epsilon/\epsilon_h)\sum_{m=-\infty}^{\infty}\int_{-\infty}^{\infty}dk \Delta_s^{-1}(m)I_m(ka)I_m(ka)K_m^2(k\rho')] \tag{4.2.8}$$

In the viewpoint of second quantization the Hamiltonian of the system including a single charge and a long cylinder is

$$H=\sum_{m=-\infty}^{\infty}\int_{-\infty}^{\infty}dk\hbar\omega_m(k)a_m^+(k)a_m(k)$$

$$+Q\sum_{m=-\infty}^{\infty}\int_{-\infty}^{\infty}dk[\gamma_m(k)a_m(k)K_m(k\rho')e^{im\phi'+ikz'}+\mathrm{h.c.}], \tag{4.2.9}$$

here $\omega_m(k)$ is the eigenfrequency of m^{th} normal mode, $a_m^+(k)$ and $a_m(k)$ are the creation and destruction operators of the m^{th} normal mode, and they obey the commutation of Bosons. The first term in (4.2.9) is the energy carried by the normal modes, the second term describes the coupling between the single charge Q and the normal modes. The induced potential has been expanded in terms of the normal modes with amplitude $\gamma_m(k)$ for m^{th} normal mode.

Based on a second order perpurbation calculation, the ground state energy of the system is

$$U=Q^2\sum_{m=-\infty}^{\infty}\int_{-\infty}^{\infty}dk\ |\gamma_m(k)|^2k_m^2(k\rho')/(-\hbar\omega_m(k)) . \tag{4.2.10}$$

Since (4.2.8) and (4.2.10) describe the same thing they should be equal, so

$$|\gamma_m(k)|^2/(-\hbar\omega_m(k))$$
$$=(1/2\pi)(1-\epsilon/\epsilon_h)\,\Delta_s^{-1}(m)I_m(ka)I_m'(ka) \qquad (4.2.11)$$

Note that $\omega_m(k)$ is determined by the condition

$$\Delta_s(m)=0,$$

this implies

$$\epsilon_m(k)I_m'(ka)K_m(ka)-\epsilon_h K_m'(ka)I_m(ka)=0, \qquad (4.2.12)$$

here, for simplicity, we assume that ϵ_h is not a frequency dependent quantity. Expanding ϵ around $\epsilon_m(k)$:

$$\epsilon = \epsilon_m(k)+(\omega-\omega_m(k))\frac{\partial\epsilon}{\partial\omega}\Big|_{\omega_m(k)}+\cdots, \qquad (4.2.13)$$

we would get

$$\Delta_s(m)=(\omega-\omega_m(k))\frac{\partial\epsilon}{\partial\omega}\Big|_{\omega_m(k)}I_m'(ka)K_m(ka)$$
$$\xrightarrow{\omega\sim 0} -\omega_m(k)\frac{\partial\epsilon}{\partial\omega}\Big|_{\omega_m(k)}I_m'(ka)K_m(ka)\ . \qquad (4.2.14)$$

Substituting (4.2.14) into (4.2.11) we obtain

$$|\gamma_m|^2$$
$$=(\hbar/2\pi)\mathrm{Re}[((\epsilon_h-\epsilon_m(k))/\epsilon_h\frac{\partial\epsilon}{\partial\omega}\Big|_{\omega_m(k)})I_m(ka)/K_m(ka)]$$
$$=(\hbar/2\pi)I_m(ka)[kaI_m'(ka)K_m^2(ka)]^{-1}[\mathrm{Re}\frac{\partial\epsilon}{\partial\omega}\Big|_{\omega_m(k)}]^{-1} \qquad (4.2.15)$$

In obtaining (4.2.15) we have assumed that $\epsilon=\epsilon_m(k)$ in (4.2.11) and used the condition (4.2.12).

So far we have only considered the second quantization

of the fields outside the cylinder. Now let us consider two molecules situated outside the cylinder. The donor molecule is located at position $\vec{r}_d=(\rho_d, \Phi_d, z_d)$ with orientation parameters $(\theta_{\mu_d}, \Phi_{\mu_d})$. In cylindrical coordinates we have

$$\vec{\mu}_d = \hat{\rho}\,\mu_{d,\rho}\cos(\Phi - \Phi_{\mu_d}) - \hat{\Phi}\,\mu_{d,\rho}\sin(\Phi - \Phi_{\mu_d}) + \hat{z}\,\mu_{d,z}, \qquad (4.2.16)$$

where $\mu_{d,\rho} = \mu_d \sin\theta_{\mu_d}$, $\mu_{d,z} = \mu_d \cos\theta_{\mu_d}$.

A similar formalism applies to $\vec{\mu}_a$ by replacing the subscripts d by a.

The Hamiltonian therefore could be expressed as

$$H=\sum_{m=-\infty}^{\infty}\int_{-\infty}^{\infty} dk\hbar\omega_m(k)a_m^+(k)a_m(k) + \vec{\mu}_a\cdot\nabla\tilde{\Phi}(r_a) + \vec{\mu}_d\cdot\nabla\tilde{\Phi}(r_d) + U_o, \qquad (4.2.17)$$

where U_o is t e dipole-dipole interaction , while

$$\tilde{\Phi}(r)=\sum_{m=-\infty}^{\infty}\int_{-\infty}^{\infty} dk[\,\gamma_m(k)a_m(k)K_m(k)e^{im\Phi+ikz}+h.c.] \qquad (4.2.18)$$

is the induced potential which has been quantized.

In cylindrical coordinates

$$\begin{aligned}\vec{\mu}_i\cdot\nabla\tilde{\Phi}(r_i)=\sum_{m=-\infty}^{\infty}\int_{-\infty}^{\infty} dk\,\{&\\ &\mu_{i,\rho}\cos(\Phi_i-\Phi_{\mu_i})k[\,\gamma_m a_m K_m'(k\rho_i)e^{im\Phi_i+ikz_i}+h.c.]\\ -&\mu_{i,\rho}\sin(\Phi_i-\Phi_{\mu_i})(im/\rho_i)[\,\gamma_m a_m K_m(k\rho_i)e^{im\Phi_i+ikz_i}-h.c.]\\ +&\mu_{i,z}(ik)[\,\gamma_m a_m K_m(k\rho_i)e^{im\Phi_i+ikz_i}-h.c.]\},\end{aligned} \qquad (4.2.19)$$

where i stands for d or a, respectively.

In second order perpurbation we have to calculate the quantity

$$\langle o|[\vec{\mu}_a\cdot\nabla\tilde{\Phi}(\vec{r}_a)+\vec{\mu}_d\cdot\nabla\tilde{\Phi}(\vec{r}_d)][\vec{\mu}_a\cdot\nabla\tilde{\Phi}(\vec{r}_a)+\vec{\mu}_d\cdot\nabla\tilde{\Phi}(\vec{r}_d)]^{\dagger}|o\rangle \ .$$

Note that the only terms with a combination of different kinds of dipole moments contribute to the energy transfer, the other terms will be related to nonradiative decay as we pointed out in Chapter III. Furthermore, the operators are all hermitian. This quantity could be written as

$$2\langle o|(\vec{\mu}_a\cdot\nabla\tilde{\Phi}(\vec{r}_a))(\vec{\mu}_d\cdot\nabla\tilde{\Phi}(\vec{r}_d))^{+}|o\rangle \ .$$

After some lengthy calculation, using (4.2.15) for $\gamma_m(k)$ and noting the properties for the Bessel functions:

$$K_m(-x)=\pm K_m(x) \ , \ (+ \text{ for m even, } - \text{ for m odd}) \ ,$$
$$K_m'(-x)=\pm K_m'(x) \ , \ (+ \text{ for m odd, } - \text{ for m even}) \ ,$$

we finally get the formula for ΔA_{da} as

$$\Delta A_{da}=\pi^{-1}\int_0^{\infty}dk\sum_{m=0}^{\infty}\frac{(2-\delta_{m,0})}{(\omega-\omega_m)\frac{\partial\epsilon}{\partial\omega}|_{\omega_m}}\hat{m}_a(\vec{r}_a)\cdot\overleftrightarrow{A}^m\cdot\hat{m}_d(\vec{r}_d) \ , \qquad (4.2.20)$$

where

$$\hat{m}_i(\vec{r}_i)$$
$$= \hat{\rho}_i \sin\theta_{\mu_i} \cos(\phi_i - \phi_{\mu_i}) - \hat{\phi}_i \sin\theta_{\mu_i} \sin(\phi_i - \phi_{\mu_i}) + \hat{z}_i \cos\theta_{\mu_i} \ , \tag{4.2.21}$$

and

$$A^m_{\rho\rho} = G_m k^2 K_m'(k\rho_a) K_m'(k\rho_d)[cm][ck] \tag{4.2.22a}$$

$$A^m_{\phi\phi} = G_m (m^2/\rho_a \rho_d) K_m(k\rho_a) K_m(k\rho_d)[cm][ck] \tag{4.2.22b}$$

$$A^m_{zz} = G_m k^2 K_m(k\rho_a) K_m(k\rho_d)[cm][ck] \tag{4.2.22c}$$

$$A^m_{\rho\phi} = -G_m (mk/\rho_d) K_m'(k\rho_a) K_m(k\rho_d)[sm][ck] \tag{4.2.22d}$$

$$A^m_{\rho z} = G_m k^2 K_m'(k\rho_a) K_m(k\rho_d)[cm][sk] \tag{4.2.22e}$$

$$A^m_{\phi z} = G_m (mk/\rho_a) K_m(k\rho_a) K_m(k\rho_d)[sm][sk] \tag{4.2.22f}$$

$$A^m_{\phi\rho} = A^m_{\rho\phi} \quad \text{with } a \leftrightarrow d \ , \tag{4.2.22g}$$

$$A^m_{z\rho} = A^m_{\rho z} \quad \text{with } a \leftrightarrow d \ , \tag{4.2.22h}$$

$$A^m_{z\phi} = A^m_{\phi z} \quad \text{with } a \leftrightarrow d \ . \tag{4.2.22i}$$

where

$$G_m = 2I_m(ka)[kaI_m'(ka)K_m^2(ka)]^{-1} \ .$$

and

$$[cm] = \cos m(\phi_a - \phi_d), \quad [sm] = \sin m(\phi_a - \phi_d) \ ,$$
$$[ck] = \cos k(z_a - z_d), \quad [sk] = \sin k(z_a - z_d) \ .$$

We could compare the cylindrical configuration with

the flat plane configuration. Consider two molecules $\vec{\mu}_a$ and $\vec{\mu}_d$ located at $\vec{r}_a$ and $\vec{r}_d$, respectively. A flat plane z=0 seperates the space into two semispaces, the dielectric function in the region $z < 0$ is ϵ ; while $\epsilon = 1$ for $z > 0$ (vaccume). A simple image method is applied. The image dipole

$$\vec{\mu}_i' = \frac{\epsilon - 1}{\epsilon + 1}\left[-\vec{\mu}_i + 2\,\vec{\mu}_i \cdot \hat{z}\,\hat{z}\right]$$

is located at $(x_i, y_i, -z_i)$, with i=a,d. The induced interaction energy would then simply be

$$\Delta U = \frac{\vec{\mu}_a' \cdot \vec{\mu}_d - 3\vec{\mu}_a' \cdot \hat{r}_{ad}'\, \vec{\mu}_d \cdot \hat{r}_{ad}'}{r_{ad}'^3} ,$$

where

$$\vec{r}_{ad}' = \vec{r}_a - \vec{r}_d - 2\,\hat{z}\,\hat{z}\cdot\vec{r}_a .$$

We could see clearly that the induced interaction would not be large except around the region $\epsilon \sim -1$. In using the Drude model,

$$\epsilon = 1 - \omega_p^2/\omega^2 ,$$

the peak would appear at $\omega^2/\omega_p^2 = 0.5$.

In the cylindrical configuration, according to (4.2.12), the normal modes would be excited if

$$\epsilon_m(k) = K_m'(ka) I_m(ka) / I_m'(ka) K_m(ka) .$$

In the Drude model this means

$$\omega_m^2/\omega_p^2=(ka)I_m'(ka)K_m(ka). \qquad (4.2.23)$$

In Fig. 4.1. we plot ω_m^2/ω_p^2 vs ka for first a few m's, this shows that at low frequencies only the m=0 mode could be excited, but as the frequency increases higher m modes could also be excited, at ω_m^2/ω_p^2 =0.5, all of the modes would be excited. The conclusion is therefore that the induced interaction spectrum would broaden in the cylindrical configuration, and so does the enhanced ratio of energy transfer compared to the flat plane configuration.

4.3. Full Electrodynamic Theory.

As the distance between the donor and the acceptor molecules is comparable with the wavelength retardation effects become important, and a full electrodynamic treatment is necessary.

Maxwell's equations inside and outside the cylinder are as follows:

$$\nabla\cdot\vec{E}=-(4\pi/\epsilon_h)[\vec{\mu}_a\cdot\nabla\delta(\vec{r}-\vec{r}_a)+\vec{\mu}_d\cdot\nabla\delta(\vec{r}-\vec{r}_d)], \qquad (4.3.1a)$$

$$\nabla\cdot\vec{B}=0\ , \qquad (4.3.1b)$$

$$\nabla\times\vec{E}=-c^{-1}\partial_t\vec{B}\ , \qquad (4.3.1c)$$

$$\nabla\times\vec{B}=c^{-1}\epsilon_h\partial_t\vec{E}\ , \qquad (4.3.1d)$$

for $\rho > a$, and

$$\nabla \cdot \vec{E}=0 \quad , \tag{4.3.2a}$$

$$\nabla \cdot \vec{B}=0 \quad , \tag{4.3.2b}$$

$$\nabla \times \vec{E}=-c^{-1}\partial_t \vec{B} \quad , \tag{4.3.2c}$$

$$\nabla \times \vec{B}=c^{-1}\epsilon\, \partial_t \vec{E} \quad , \tag{4.3.2d}$$

for $\rho < a$.

The Maxwell equations inside the cylinder are homogeneous, while outside the cylinder two dipoles exist. The solution of the fields outside the cylinder is the sum of the homogeneous fields and the dipole fields. The procedure to solve the Maxwell's equations are as follows. Firstly, we solve the homogeneous equations both inside and outside the cylinder, then expand the dipole fields in cylindrical coordinates, and finally determine the coefficients by the boundary conditions.

a). The Homogeneous Solutions.

Assuming the fields have $e^{-i\omega t}$ harmonic behavior, the wave equations are

$$(\nabla^2 + k^2)\begin{pmatrix}\vec{E}\\ \vec{B}\end{pmatrix}=0 \quad , \quad \rho > a \tag{4.3.3a}$$

$$(\nabla^2 + q^2)\begin{pmatrix}\vec{E}\\ \vec{B}\end{pmatrix}=0 \quad , \quad \rho < a \tag{4.3.3b}$$

where $k^2=\frac{\omega^2}{c^2}\epsilon_h$ and $q^2=\frac{\omega^2}{c^2}\epsilon$.

Furthermore we assume that the z-dependence and ϕ-dependence of the fields are through the factor

$e^{ipz+im\phi}$ with integer m (since the fields should be singlevalued), so the wave equations could be simplified as

$$(\nabla_t^2-Q'^2)\begin{pmatrix}\vec{E}\\ \vec{B}\end{pmatrix}=0 \quad , \qquad \rho > a \tag{4.3.4a}$$

$$(\nabla_t^2-Q^2)\begin{pmatrix}\vec{E}\\ \vec{B}\end{pmatrix}=0 \quad , \qquad \rho < a \tag{4.3.4b}$$

where $Q^2=q^2-p^2$, $Q'^2=p^2-k^2$, and ∇_t^2 is the transverse Laplacian:

$$\nabla_t^2=\frac{1}{\rho}\partial_\rho \rho \partial_\rho + \frac{1}{\rho^2}\partial_\phi^2 \quad . \tag{4.3.5}$$

It is obveous that the z components of the fields are satisfied by Bessel's equation for $\rho < a$, and the modified Bessel's equation for $\rho > a$. The natural boundary conditions at $\rho = 0$, and $\rho = \infty$ confirm that $J_m(Q\rho)$ and $K_m(Q'\rho)$ are suitable solutions for $\rho < a$ and $\rho > a$, respectively, to describe the fields. The symbols for cylindrical functions used through this chapter are the same as in [1].

With E_z and B_z in hand the other components of the fields could be obtained by the following relations[1],

$$\partial_z \vec{E}_t + i(\omega/c)\hat{z} \times \vec{B}_t = \nabla_t E_z \quad , \tag{4.3.6a}$$

$$\partial_z \vec{B}_t - i(\omega/c)\epsilon\, \hat{z} \times \vec{E}_t = \nabla_t B_z \quad , \tag{4.3.6b}$$

We list the homogeneous solutions as follows:

The solutions inside the cylinder, $\rho < a$, are

$$E_z=\int_{-\infty}^{\infty} dp \sum_{m=-\infty}^{\infty} PA_m J_m(Q\rho) \quad , \tag{4.3.7a}$$

$$B_z = \int_{-\infty}^{\infty} dp \sum_{m=-\infty}^{\infty} PB_m J_m(Q\rho) \ , \tag{4.3.7b}$$

$$E_\rho = \int_{-\infty}^{\infty} dp \sum_{m=-\infty}^{\infty} PQ^{-1}[ipA_m J_m'(Q\rho) - \frac{\omega}{c}\frac{m}{Q\rho} B_m J_m(Q\rho)] \tag{4.3.7c}$$

$$B_\rho = \int_{-\infty}^{\infty} dp \sum_{m=-\infty}^{\infty} PQ^{-1}[\frac{\omega}{c}\epsilon \frac{m}{Q\rho} A_m J_m(Q\rho) + ipB_m J_m'(Q\rho)] \tag{4.3.7d}$$

$$E_\phi = -\int_{-\infty}^{\infty} dp \sum_{m=-\infty}^{\infty} PQ^{-1}[\frac{mp}{Q\rho} A_m J_m(Q\rho) + i\frac{\omega}{c} B_m J_m'(Q\rho)] \tag{4.3.7e}$$

$$B_\phi = \int_{-\infty}^{\infty} dp \sum_{m=-\infty}^{\infty} PQ^{-1}[i\frac{\omega}{c}\epsilon A_m J_m'(Q\rho) - \frac{mp}{Q\rho} B_m J_m(Q\rho)] \tag{4.3.7f}$$

The homogeneous solutions outside the cylinder, a, are

$$E_z = \int_{-\infty}^{\infty} dp \sum_{m=-\infty}^{\infty} PC_m K_m(Q'\rho) \ , \tag{4.3.8a}$$

$$B_z = \int_{-\infty}^{\infty} dp \sum_{m=-\infty}^{\infty} PD_m K_m(Q'\rho) \ , \tag{4.3.8b}$$

$$E_\rho = -\int_{-\infty}^{\infty} dp \sum_{m=-\infty}^{\infty} PQ'^{-1}[ipC_m K_m'(Q'\rho) - (\omega m/cQ'\rho) D_m K_m(Q'\rho)] \ , \tag{4.3.8c}$$

$$B_\rho = -\int_{-\infty}^{\infty} dp \sum_{m=-\infty}^{\infty} PQ'^{-1}[(\omega \epsilon_h m/cQ'\rho) C_m K_m(Q'\rho) + ipD_m K_m'(Q'\rho)] \ , \tag{4.3.8d}$$

$$E_\phi = \int_{-\infty}^{\infty} dp \sum_{m=-\infty}^{\infty} PQ'^{-1}[(mp/Q'\rho) C_m K_m(Q'\rho) + i(\omega/c) D_m K_m'(Q'\rho)] \ , \tag{4.3.8e}$$

$$B_\phi = -\int_{-\infty}^{\infty} dp \sum_{m=-\infty}^{\infty} PQ'^{-1}[\,(\omega/c)\,\epsilon_n C_m K_m'(Q'\rho) - (mp/Q'\rho)D_m K_m(Q'\rho)\,] \,, \tag{4.3.8f}$$

where the phase factor P is

$$P = \exp[ipz + im\phi - i\omega t] \,,$$

and A_m, B_m, C_m, and D_m are coefficients to be determined by boundary conditions.

b). The Dipole Fields.

The dipole fields in a medium with dielectric function ϵ_h is given by[1]

$$\vec{B} = \nabla \times \vec{A} \,, \tag{4.3.9a}$$

$$\vec{E} = i\left(\frac{\omega}{c}\epsilon_h\right)^{-1} \nabla \times \vec{B} \,, \tag{4.3.9b}$$

$$\vec{A} = -ik\vec{\mu}' \exp[ik|\vec{r}-\vec{r}_o| - i\omega t]/|\vec{r}-\vec{r}_o| \,, \tag{4.3.9c}$$

where $\vec{A}$ is the vector potential, $k = \frac{\omega}{c}\sqrt{\epsilon_h}$, $\vec{\mu}' = \vec{\mu}/\sqrt{\epsilon_h}$ and $\vec{\mu}$ is the dipole moment, $\vec{r}_o$ is the position where the dipole sits. The Green's function could be expanded in cylindrical coordinates as[1]

$$e^{ik|\vec{r}-\vec{r}_o|}/|\vec{r}-\vec{r}_o|$$

$$= \pi^{-1}\int_{-\infty}^{\infty} dp \sum_{m=-\infty}^{\infty} e^{ip(z-z_o)+im(\phi-\phi_o)} I_m(Q'\rho_<) K_m(Q'\rho_>)$$

where $Q'^2 = p^2 - k^2$, and $\rho_<$ ($\rho_>$) stands for $\rho < \rho_o$ ($\rho > \rho_o$).

A straightforward calculation gives the dipole fields expanded in cylindrical coordinates as follows:

$$B_\rho = -i\frac{\omega}{c}\frac{1}{\pi}\int_{-\infty}^{\infty} dp \sum_{m=-\infty}^{\infty} S\left[i\frac{m}{\rho}\mu_z + ip\mu_\rho \sin(\phi - \phi_\mu)\right] \times I_m(Q'\rho_<)K_m(Q'\rho_>) \tag{4.3.10a}$$

$$B_\phi = -i\frac{\omega}{c}\frac{1}{\pi}\int_{-\infty}^{\infty} dp \sum_{m=-\infty}^{\infty} S \times \left[-Q'\mu_z\left(\frac{I_m'(Q'\rho)K_m(Q'\rho_\bullet)}{I_m(Q'\rho_\bullet)K_m'(Q'\rho)}\right) + ip\mu_\rho \cos(\phi - \phi_\mu) I_m(Q'\rho_<)K_m(Q'\rho_>)\right] \tag{4.3.10b}$$

$$B_z = i\frac{\omega}{c}\frac{\mu_\rho}{\pi}\int_{-\infty}^{\infty} dp \sum_{m=-\infty}^{\infty} S \times \left[Q'\sin(\phi - \phi_\mu)\left(\frac{I_m'(Q'\rho)K_m(Q'\rho_\bullet)}{I_m(Q'\rho_\bullet)K_m'(Q'\rho)}\right) + i\frac{m}{\rho}\cos(\phi - \phi_\mu) I_m(Q'\rho_<)K_m(Q'\rho_>)\right], \tag{4.3.10c}$$

$$E_\rho = -\frac{1}{\epsilon_h \pi}\int_{-\infty}^{\infty} dp \sum_{m=-\infty}^{\infty} S\left\{-\mu_\rho I_m(Q'\rho_<)K_m(Q'\rho_>) \times \left[i\frac{m}{\rho^2}\sin(\phi - \phi_\mu) + \left(\frac{m^2}{\rho^2} + p^2\right)\cos(\phi - \phi_\mu)\right] + Q'\left(\frac{I_m'(Q'\rho)K_m(Q'\rho_\bullet)}{I_m(Q'\rho_\bullet)K_m'(Q'\rho)}\right) \times \left[-ip\mu_z + im\frac{\mu_\rho}{\rho}\sin(\phi - \phi_\mu) + \frac{\mu_\rho}{\rho}\cos(\phi - \phi_\mu)\right]\right\} \tag{4.3.10d}$$

$$E_\phi = \frac{1}{\epsilon_h \pi}\int_{-\infty}^{\infty} dp \sum_{m=-\infty}^{\infty} S\left\{-I_m(Q'\rho_<)K_m(Q'\rho_>) \times \left[\frac{mp}{\rho}\mu_z + i\frac{m}{\rho^2}\mu_\rho \cos(\phi - \phi_\mu) + \mu_\rho\left(k^2 - \frac{m^2}{\rho^2}\right)\sin(\phi - \phi_\mu)\right] + Q'\frac{\mu_\rho}{\rho}\left(\frac{I_m'(Q'\rho)K_m(Q'\rho_\bullet)}{I_m(Q'\rho_\bullet)K_m'(Q'\rho)}\right) \times \left[im\cos(\phi - \phi_\mu) - \sin(\phi - \phi_\mu)\right]\right\}, \tag{4.3.10e}$$

$$E = \frac{1}{\epsilon_h \pi} \int_{-\infty}^{\infty} dp \sum_{m=-\infty}^{\infty} S \Big\{ I_m(Q'\rho_<) K_m(Q'\rho_>) \times [-\mu_z Q'^2 + \frac{mp}{\rho} \mu_\rho \sin(\phi - \phi_\mu)]$$

$$+ ipQ'\mu_\rho \begin{pmatrix} I'_m(Q'\rho) K_m(Q'\rho_\bullet) \\ I_m(Q'\rho_\bullet) K'_m(Q'\rho) \end{pmatrix} \cos(\phi - \phi_\mu) \Big\} . \qquad (4.3.10f)$$

where the phase factor S is

$$S = \exp[ip(z - z_0) + im(\phi - \phi_\bullet) - i\omega t] ,$$

and the upper lines in the parenthesis correspond to $\rho < \rho_\bullet$, while the lower lines to $\rho > \rho_\bullet$. For molecules outside the cylinder $\rho_\bullet$ is always larger than a, so when matching the boundary the upper lines are always used.

The sum of (4.3.8) and (4.3.10) would give the full solutions for the fields outside the cylinder.

c). The Boundary Conditions.

The boundary conditions are as usual, the tangential components of $\vec{E}$ and $\vec{B}$ are continuous, the radial components of $\vec{B}$ and $\vec{D}$ are continuous. These give us total 6 conditions of which only 4 are independent. The four coefficients determined by boundary conditions are the following.

$$D_i(m) = \Delta_i(D,m) / pK_m(Q'a) \Delta(m) , \qquad (4.3.11a)$$

$$B_i(m) = \Delta_i(B,m) / pJ_m(Qa) \Delta(m) , \qquad (4.3.11b)$$

$$C_i(m) = \Delta_i(C,m) / \frac{\omega}{c} K_m(Q'a) \Delta(m) , \qquad (4.3.11c)$$

$$A_i(m) = \Delta_i(A,m) / \frac{\omega}{c} J_m(Qa) \Delta(m) , \qquad (4.3.11d)$$

where the subcscript i denotes a (acceptor) or d (donor), and

$$\Delta(m)=(m/a)^2(\omega/c)^2p^2(\epsilon-\epsilon_h)^2(QQ')^{-4} -([J]+[K])(\epsilon[J]+\epsilon_h[K]) \quad , \tag{4.3.12}$$

where

$$[J]=J_m'(Qa)/QJ_m(Qa),\ [K]=K_m'(Q'a)/Q'K_m(Q'a). \tag{4.3.12'}$$

It is well-known[2] that $\Delta(m)=0$ corresponds to the excitation of the normal modes in the cylindrical, dielectric wave guide.

By introducing the folowing symbols

$$\Delta(I,m)=(m/a)^2(\omega/c)^2p^2(\epsilon-\epsilon_h)^2(QQ')^{-4} -([J]+[I])(\epsilon[J]+\epsilon_h[k]) \quad , \tag{4.3.13a}$$

$$\Delta(J,m)=(m/a)^2(\omega/c)^2p^2(\epsilon-\epsilon_h)^2(QQ')^{-4} -([J]+[K])(\epsilon[J]+\epsilon_h[I]) \quad , \tag{4.3.13b}$$

$$L_i(J,m)= (m/a)^2(\omega/c)^2(\epsilon-\epsilon_h)Q^{-2}Q'^{-4}K_m(Q'\rho_i)/K_m(Q'a) +(Q'/\epsilon_h)I_m(Q'a)K_m'(Q'\rho_i)\Delta(J,m) \quad , \tag{4.3.13c}$$

$$W_i(J,m)= (\omega/c)^2(\epsilon-\epsilon_h)(Qa)^{-2}Q'^{-3}K_m'(Q'\rho_i)/K_m(Q'a) +\frac{1}{\epsilon_h\rho_i}I_m(Q'a)K_m(Q'\rho_i)\Delta(J,m) \quad , \tag{4.3.13d}$$

$$L_i(I,m)= \frac{1}{\rho_i}(m/a)^2p^2(\epsilon-\epsilon_h)Q^{-2}Q'^{-4}K_m(Q'\rho_i)/K_m(Q'a) +Q'I_m(Q'a)K_m'(Q'\rho_i)\Delta(I,m) \quad , \tag{4.3.13e}$$

$$W_i(I,m)=(p/a)^2(\epsilon-\epsilon_h)Q^{-2}Q'^{-3}K_m'(Q'\rho_i)/K_m(Q'a)$$
$$+\frac{1}{\rho_i}I_m(Q'a)K_m(Q'\rho_i)\,\Delta(I,m)\ , \qquad (4.3.13f)$$

with $[I]=I_m'(Q'a)/Q'I_m(Q'a)$, (4.3.13')

we can write $\Delta_i(C,m)$ and $\Delta_i(D,m)$ in a compact way as

$$\Delta_i(C,m)=\pi^{-1}(\omega/c)e^{-i(pz_i+m\phi_i)}\Big\{$$
$$\mu_{i,z}Q'^2\,\epsilon_h^{-1}I_m(Q'a)K_m(Q'\rho_i)\,\Delta(J,m)$$
$$+\mu_{i,\rho}[ipL_i(J,m)\cos(\phi_i-\phi_{\mu_i})-mpW_i(J,m)\sin(\phi_i-\phi_{\mu_i})]\Big\} \qquad (4.3.14a)$$

$$\Delta_i(D,m)=(p/\pi)(\omega/c)e^{-i(pz_i+m\phi_i)}$$
$$-i\mu_{i,z}mp(\epsilon-\epsilon_h)(Qa)^{-2}Q'^{-3}K_m(Q'\rho_i)/K_m(Q'a)$$
$$+\mu_{i,\rho}[mW_i(I,m)\cos(\phi_i-\phi_{\mu_i})+iL_i(I,m)\sin(\phi_i-\phi_{\mu_i})]\Big\} \qquad (4.3.14b)$$

d). The Induced Interaction Energy.

The induced energy is

$$\Delta U=-0.5[\vec{\mu}_a\cdot\vec{E}_i(\vec{r}_a)+\vec{\mu}_d\cdot\vec{E}_i(\vec{r}_d)], \qquad (4.3.15)$$

where $\vec{E}_i$ is the induced electric field, and is the homogeneous solution presented in (4.3.8). Substituting (4.3.8d)-(4.3.8f) into (4.3.15) we get

$$\Delta U=\frac{1}{2}\sum_{i=a,d}\sum_{j=a,d}\int_{-\infty}^{\infty}dp\sum_{m=-\infty}^{\infty}\Big\{$$

$$Q'^{-1}\mu_{i,\rho}\cos(\phi_i-\phi_{\mu_i})[ipC_j(m)K_m'(Q'\rho_i)$$
$$-\frac{\omega}{c}\frac{m}{Q'\rho_i}D_j(m)K_m(Q'\rho_i)]$$

$$+Q'^{-1}\mu_{i,\rho}\sin(\phi_i-\phi_{\mu_i})\left[\frac{mp}{Q'\rho_i}C_j(m)K_m(Q'\rho_i)\right.$$
$$\left.+i\frac{\omega}{c}D_j(m)K_m'(Q'\rho_i)\right]$$

$$\left.-\mu_{i,z}C_j(m)K_m(Q'\rho_i)\right\}e^{i(pz_i+m\phi_i)} \quad . \qquad (4.3.16)$$

As we noted only the terms with i≠j contribute to the energy transfer, and the terms with i=j are responsible for the nonradiative decay. Thus the part of induced energy that contributes to energy transfer is

$$\Delta U_{da}=$$
$$\pi^{-1}\int_0^\infty dp\sum_{m=0}^{\infty}(2-\delta_{m,0})\vec{\mu}_a(\vec{r}_a)\cdot\overleftrightarrow{A}^{m}\cdot\vec{\mu}_d(\vec{r}_d)\ , \qquad (4.3.17)$$

and

$$\Delta A_{da}=$$
$$\pi^{-1}\int_0^\infty dp\sum_{m=0}^{\infty}(2-\delta_{m,0})\hat{m}_a(\vec{r}_a)\cdot\overleftrightarrow{A}^{m}\cdot\hat{m}_d(\vec{r}_d)\ , \qquad (4.3.18)$$

where

$$\hat{m}_i(\vec{r}_i)$$
$$=\hat{\rho}_i\sin\theta_{\mu_i}\cos(\phi_i-\phi_{\mu_i})-\hat{\phi}_i\sin\theta_{\mu_i}\sin(\phi_i-\phi_{\mu_i})+\hat{z}_i\cos\theta_{\mu_i} \qquad (4.3.19)$$

with i=a,d.

The elements of tensor $\overleftrightarrow{A}^{m}$ are

$$A^m_{\rho\rho}=$$
$$-2\Delta(m)^{-1}\left\{(m\omega p/acQ)^2Q'^{-4}(\epsilon-\epsilon_h)[Ka][Kd]([Ka']+[Kd'])\right.$$

$$+p^2\epsilon_h^{-1}\,[Ka][Kd][IK][Ka'][Kd']\,\Delta(J,m)$$
$$+(m\omega/c)^2[IK][Ka][Kd]\,\Delta(I,m)\Big\}\cosm(\phi_a-\phi_d)\cosp(z_a-z_d)$$

(4.3.20a)

$$A^m_{\phi\phi} =$$
$$-2\,\Delta(m)^{-1}\Big\{(m\omega\,p/acQ)^2Q'^{-4}(\epsilon-\epsilon_h)[Ka][Kd]([Ka']+[Kd'])$$
$$+(mp)^2\epsilon_h^{-1}\,[IK][Ka][Kd]\,\Delta(J,m)$$
$$+(\omega/c)^2[Ka][Kd][IK][Ka'][Kd']\,\Delta(I,m)\Big\}$$
$$\times\cosm(\phi_a-\phi_d)\cosp(z_a+z_d)$$

4.3.20b)

$$A^m_{zz} = -2\,\Delta(m)^{-1}\epsilon_h^{-1}\;Q'^2(Q'\rho_a\,Q'\rho_d)[IK][Ka][Kd]\,\Delta(J,m)$$
$$\times\cosm(\phi_a-\phi_d)\cosp(z_a+z_d)\ , \qquad (4.3.20c)$$

$$A^m_{\rho\phi} = m\,\Delta(m)^{-1}\Big\{(\omega/acQ)^2Q'^{-4}(\epsilon-\epsilon_h)(p^2+\tfrac{\omega^2}{c^2})$$
$$\times[Ka][Kd](m^2+[Ka'][Kd'])$$
$$+2\epsilon_h^{-1}\,[IK][Ka][Kd](p^2[Ka']+(\omega/c)^2\,[Kd'])\,\Delta(J,m)\Big\}$$
$$\times\sinm(\phi_a-\phi_d)\cosp(z_a-z_d)\ , \qquad (4.3.20d)$$

$$A^m_{\rho z} = -2p\,\Delta(m)^{-1}\Big\{$$
$$(m\omega/acQ)^2Q'^{-3}(\epsilon-\epsilon_h)(Q'\rho_d)[Ka][Kd]$$
$$+Q'\epsilon_h^{-1}\,(Q'\rho_d)[IK][Ka'][Ka][Kd]\,\Delta(J,m)\Big\}$$
$$\times\cosm(\phi_a-\phi_d)\sinp(z_a-z_d)\ , \qquad (4.3.20e)$$

$$A^m_{\phi z} = -2mp\,\Delta(m)^{-1}\Big\{$$
$$(\omega/acQ)^2Q'^{-3}(\epsilon-\epsilon_h)(Q'\rho_d)[Ka'][Ka][Kd]$$
$$+Q'\epsilon_h^{-1}\,(Q'\rho_d)[IK][Ka][Kd]\,\Delta(J,m)\Big\}$$
$$\times\sinm(\phi_a-\phi_d)\sinp(z_a-z_d)\ , \qquad (4.3.20f)$$

and

$$A^m_{\phi\rho} = A^m_{\rho\phi} \quad , \quad \text{with } a \leftrightarrow d \tag{4.3.20g}$$

$$A^m_{z\rho} = A^m_{\rho z} \quad , \quad \text{with } a \leftrightarrow d \tag{4.3.20h}$$

$$A^m_{z\phi} = A^m_{\phi z} \quad , \quad \text{with } a \leftrightarrow d \tag{4.3.20i}$$

where

$$[Ka] = K_m(Q'\rho_a)/Q'\rho_a K_m(Q'a) \quad , \tag{4.3.20'a}$$

$$[Kd] = K_m(Q'\rho_d)/Q'\rho_d K_m(Q'a) \quad , \tag{4.3.20'b}$$

$$[Ka'] = Q'\rho_a K_m'(Q'\rho_a)/K_m(Q'\rho_a) \quad , \tag{4.3.20'c}$$

$$[Kd'] = Q'\rho_d K_m'(Q'\rho_d)/K_m(Q'\rho_d) \quad , \tag{4.3.20'd}$$

and

$$[IK] = I_m(Q'a)K_m(Q'a) \quad . \tag{4.3.20'e}$$

The enhanced rate of energy transfer is, in accordance with definition,

$$R(\omega) = |1 + \Delta A_{da}/A_o|^2 \quad , \tag{4.3.21}$$

where A_o is given by (4.1.10b).

e). Long wavelength Limit.

We could check our main results (4.3.20) in the long wavelength limit. Note that, when $\omega \to 0$, $Q \to ip$, and $Q' \to p$; and from the property of the combination of Bessl's functions

$$xI_m'(x)/I_m(x) = ixJ_m'(ix)/J_m(ix) \quad .$$

We could find out that in $\omega \sim 0$ limit

$$\Delta(I,m) \to 0 \quad ,$$

and

$$\Delta(J,m) \to (\epsilon - \epsilon_h)[Ip]/(\epsilon[Ip] - \epsilon_h[Kp]),$$

where

$$[Ip]=I_m'(pa)/I_m(pa),$$

and

$$[Kp]=K_m'(pa)/K_m(pa).$$

Substituting these facts into Eq.(4.3.20) and expanding around $\epsilon_m(\rho)$ as we did in section II

$$(\epsilon-\epsilon_h)\Delta_s(m)^{-1}$$

$$\approx (\epsilon_m-\epsilon_h)/[(\omega-\omega_m)\frac{\partial\epsilon}{\partial\omega}\Big|_{\omega_m} I_m'(pa)K_m(Pa)]$$

$$=-\epsilon_h[(\omega-\omega_m)\frac{\partial\epsilon}{\partial\omega}\Big|_{\omega_m}(pa)I_m'^2(pa)K_m^2(pa)]$$

one could prove that Eq.(4.3.20) reduces to Eq.(4.2.22), i.e., the solution under static limit. Thus the full electrodynamic solution is checked under the long wavelength approximation.

4.4. Nonradiative Decay.

In Chapter III we have proved that the nonradiative decay rate is

$$\Gamma_d=-\hbar^{-1}ImU_{dd} \quad , \tag{4.4.1}$$

where

$$U_{dd}=-0.5\,\vec{\mu}_d\cdot\vec{E}(\vec{r}_d). \tag{4.4.2}$$

By using the same calculation as in section 4.3 we can formulate the nonradiative decay as follows.

$$\Gamma_d = (\hbar\pi)^{-1} \mathrm{Im} \int_0^\infty dp \sum_{m=0}^{\infty} (2-\delta_{m,0})\, \vec{\mu}_d(\vec{r}_d) \cdot \overleftrightarrow{N}^m \cdot \vec{\mu}_d(\vec{r}_d) \tag{4.4.3}$$

where $\overleftrightarrow{N}^m$ is diagonal with the elements

$$N^m_{\rho\rho} = \Delta(m)^{-1}\{2(m\omega p/acQ)^2 Q'^{-4}(\epsilon - \epsilon_h)[Kd]^2[Kd'] + p^2\, \epsilon_h^{-1}(Q'\rho_d)^{-2}[IK][Kd']^2\, \Delta(J,m) + (m\omega/c)^2[IK][Kd]^2\, \Delta(I,m)\}\ , \tag{4.4.4a}$$

$$N^m_{\phi\phi} = \Delta(m)^{-1}\{2(m\omega p/acQ)^2 Q'^{-4}(\epsilon - \epsilon_h)[Kd]^2[kd'] + (mp)^2\, \epsilon_h^{-1}[IK][Kd]^2\, \Delta(J,m) + (\omega/c)^2[IK][Kd]^2[Kd']^2\, \Delta(I,m)\} \tag{4.4.4b}$$

$$N^m_{zz} = \Delta(m)^{-1} Q'^2\, \epsilon_h^{-1}(Q'\rho_d)^2[IK][Kd]^2\, \Delta(J,m)\ . \tag{4.4.4c}$$

where [IK], [Kd], and [Kd'] are given in (4.3.20').

4.5. Radiative Decay

In considering the radiative decay we assume, as is usual in the liturature, that is a real quantity so that Q' is either pure real when $p \geq \frac{\omega}{c}\sqrt{\epsilon_h}$ or pure imaginary when $p < \frac{\omega}{c}\sqrt{\epsilon_h}$.

The complex Poynting vector is

$$(c/8\pi)\vec{E} \times \vec{B}^* \ .$$

So the power radiated by the s em is

$$P = (c/8\pi) \oint \mathrm{Re}(\vec{E} \times \vec{B}^*) \cdot \hat{\rho} \; d. \qquad (4.5.1)$$

where the int gral is defined on a big cylindrical surface encompassing the molecules and the solid cylinder, and $\hat{\rho}$ is the unit vector perpendicular to the surface and pointing outward.

We know that the fields include two parts, the dipole fields and the induced fields, so the radiated power could be written as

$$P = (c/8\pi) \oint \mathrm{Re}[\vec{E}_\mu \times \vec{B}_\mu^* + \vec{E}_i \times \vec{B}_i^* + \vec{E}_\mu \times \vec{B}_i^* + \vec{E}_i \times \vec{B}_\mu^*] \cdot \hat{\rho} \; dS. \qquad (4.5.2)$$

The first term in (4.5.2) is the dipole radiation power and it is well-known that

$$P_\mu = (ck^4/3\epsilon_h) |\vec{\mu}|^2 , \qquad (4.5.3)$$

where $k=(\omega/c)\sqrt{\epsilon_h}$.

The second term in (4.5.2) is the power radiated by the cylinder, the fields $\vec{E}_i$ and $\vec{B}_i$ are given in (4.3.8). Note that the integral element dS on a cylindrical surface is

$$dS = \rho \, d\phi \, dz ,$$

then the integral on ϕ would reduce the double sum on m and m' to a single sum and give a factor of 2π ; the integral on z would give a δ-function as $\delta(p-p')$. It would reduce the double integral on p and p' to a single integral and give another factor of 2π . Hence the power radiated by the cylinder is

$$P_c = (c/8\pi)\oint \mathrm{Re}(\vec{E}_i \times \vec{B}_i^{*}) \cdot \hat{\rho}\, s$$

$$= (c/8\pi)\int_0^{2\pi} d\phi \int_{-\infty}^{\infty} dz\, \rho\, \mathrm{Re}(\, \phi\, B_z^{*} - E_z B_\phi^{*}\,)$$

$$= (\pi\omega/2)\int_{-\infty}^{\infty} dp \sum_{m=-\infty}^{\infty} \mathrm{Re}\Big\{ \rho i[\,|D_m|^2 Q'^{-1} K_m'(Q'\rho) K_m(Q'\rho)^{*} - \epsilon_h |C_m|^2 Q'^{*-1} K_m(Q'\rho) K_m'(Q'\rho)^{*}\,]\Big\}$$

$$= -(\pi\omega/2)\int_{-\infty}^{\infty} dp \sum_{m=-\infty}^{\infty} (|D_m|^2 + \epsilon_h |C_m|^2) \times \mathrm{Im}[\,\rho\, Q'^{-1} K_m'(Q'\rho) K_m(Q'\rho)^{*}\,].$$

Using the asymptotic form of Bessel's function $K_m(x)$:

$$K_m(Q'\rho) \to (\pi/2Q'\rho)^{1/2} e^{-Q'\rho} \quad \text{, when } \rho \text{ is large,}$$

then

$$(\rho/Q')K_m'(Q')K_m(Q')^{*} \to$$

$$-(\rho/Q')(\pi/2Q'\rho)^{1/2} e^{-Q'\rho}\,(\pi/2Q'^{*}\rho)^{1/2} e^{-Q'^{*}\rho}$$

$$= -(\pi/2)(Q'|Q'|)^{-1} e^{-\rho(Q'+Q'^{*})}$$

$$= \begin{cases} 0, & \text{, when } Q' \text{ is real;} \\ -i\dfrac{\pi}{2Q_1^2} & \text{, when } Q' \text{ is pure imaginary.} \end{cases}$$

where $Q_1 = iQ' = [(\omega/c)^2 \epsilon_h - p^2]^{1/2}$. Finally,

$$P_c = \frac{\pi^2\omega}{2}\int_0^k dp \sum_{m=0}^{\infty} (2-\delta_{m,0})Q_1^{-2}(|D_m|^2+\epsilon_h|C_m|^2) \ . \tag{4.5.4}$$

As usual the term $|D_m|^2$ is interpreted as a magnetic response, and the term $\epsilon_h |C_m|^2$ is an electric response of the cylinder.

The cross terms in (4.5.2) is zero, this could be proven as follows

$$P_{cro}=(c/8\pi)\oint Re[\vec{E}_\mu \times \vec{B}_i^* + \vec{E}_i \times \vec{B}_\mu^*]\cdot \hat{\rho}\, dS$$
$$=(c/8\pi)Re\int_{out}\nabla\cdot[\vec{E}_\mu \times \vec{B}_i^* - \vec{B}_\mu^* \times \vec{E}_i]d\vec{r}$$

where "out" means outside the cylinder because the dipole fields $\vec{E}_\mu$ and $\vec{B}_\mu$ are defined only outside. A straightforward calculation gives

$$P_{cro}=(c/8\pi)\int_{out} Re[\vec{B}_i^*\cdot(\nabla\times\vec{E}_\mu)-\vec{E}_\mu\cdot(\nabla\times\vec{B}_i^*)$$
$$-\vec{E}_i\cdot(\nabla\times\vec{B}_\mu^*)+\vec{B}_\mu^*\cdot(\nabla\times\vec{E}_i)]d\vec{r}$$
$$=(c/8\pi)\int_{out} Re[\vec{B}_i^*\cdot i\tfrac{\omega}{c}\vec{B}_\mu - \vec{E}_\mu\cdot i\tfrac{\omega}{c}\epsilon_h\vec{E}_i^*$$
$$-\vec{E}_i\cdot i\tfrac{\omega}{c}\epsilon_h\vec{E}_\mu^* + \vec{B}_\mu^*\cdot i\tfrac{\omega}{c}\vec{B}_i]d\vec{r}$$
$$=(c/8\pi)\int_{out} Re\, i\tfrac{\omega}{c}[\vec{B}_i^*\cdot\vec{B}_\mu + \vec{B}_\mu^*\cdot\vec{B}_i$$
$$-\epsilon_h(\vec{E}_\mu\cdot\vec{E}_i^* + \vec{E}_i\cdot\vec{E}_\mu^*)]d\vec{r}.$$

Since the quantity in the brancket [ ] is purely real (we have assumed that ϵ_h is real) the intergrand is zero.

$$P_{cro}=0$$

In summary, the power radiated by the system is

$$P = P_\mu + P_c \ , \tag{4.5.5}$$

where P_μ is dipole radiation p er and is given in (4.5.3); P_c is the power radiated by the cylinder and is given in (4.5.4).

The radiative decay rate is defined as

$$\Gamma_r = P/\hbar\omega = \Gamma_o R_r(\omega) \quad , \tag{4.5.6}$$

where Γ_o is the radiative decay rate of a dipole in a homogeneous system, $\Gamma_o = P_\mu / \hbar\omega$, R_r is the enhanced rate of radiative decay,

$$R_r = 1 + P_c/P_\mu \quad . \tag{4.5.7}$$

4.6. Numerical Results and Discussion.

The general features of enhanced energy transfer and the competition between the energy transfer and the radiative and the nonradiative decay was discussed in Chapter III. Here we present some discussions about the energy transfer which occurs near a long fiber. Through this section the material of the cylinder is chosen to be the silver whose dielectric function was experimentally measured by Johnson and Christy[3]. Fig.4.2 shows the relation between the enhanced ratio $R(\omega)$ of energy transfer and the frequency (taking the units of $\hbar\omega$ to be ev). Here the radius of the cylinder is a=100 Å, the position of the molecules are

$$(\rho_a, \phi_a, z_a) = (105 \text{ Å}, 0^\circ, 0),$$

$$(\rho_d, \phi_d, z_d) = (105 \text{ Å}, 0^\circ, 100 \text{ Å}).$$

i.e., the distance between t molecules and the surface of the cylinder is 5 Å, the distance between two molecules is equal to the radius of the cylinder: $z_{ad}=a$, $\rho_a/a=\rho_d/a=1.05$. Three curves are presented in correspondance with three different orientations of the two molecules. The direction of the molecules is shown along with the graphs by the arrows. Curve 1 corresponds to the case that two molecules are parallel to the axis of the cylinder: $\hat{\mu}_a=\hat{\mu}_d=\hat{z}$; curve 2, two molecules are parallel to the surface of the cylinder but perpendicular to the axis of the cylinder: $\hat{\mu}_a=\hat{\mu}_d=\hat{\phi}$; curve 3, two molecules are both perpendicular to the surface and the axis of the cylinder: $\hat{\mu}_a=\hat{\mu}_d=\hat{\rho}$. It may be noted that a sharp peak, corresponding to the surface plasmon resonance, is present at $\hbar\omega=3.62$ ev in all three of three cases. It is consistent with the fact that the resonance would occur when $\epsilon=-1$ in long wavelength approximation as we discussed in section 4.2, and in Fig.4.1 also. The computation that leads to Fig.4.2 is based on the full electrodynamic formulas (4.3.20). We also calculate this configuration by using the long wavelength formulas (4.2.22). The results of these two calculations are close to each other, eventhough we do not present the curves obtained from the long wavelength calculation.

As the distance between two molecules, and between the

molecules and the surface of the cylinder, get larger and larger the wave picture of the process would become more and more obvious. Fig.4.3 shows that as the distance quantities related to the problem become larger, the enhanced ratio of energy transfer reveals oscillations, especially in the high frequency region. In Fig.4.3 two molecules are perpendicular to the surface of the cylinder, $\rho_a/a = \rho_d/a = 1.05$, and the distance between two molecules is $z_{ad}=a$. Curve 1 corresponds to the case that a=1000 Å, and curve 2, a=5000 Å. From the picture we see that as the relative distances get larger, and as the frequency gets higher, a single resonance at $\epsilon = -1$ would be replaced by a series of oscillations. To see this more clearly we present Fig.4.4. Here we keep the frequency $\hbar\omega$ =2.01 ev and vary the radius a of the cylinder. Again, we have $\rho_a/a = \rho_d/a = 1.05$ and $z_{ad}=a$. The orientations of the molecules are the same as in Fig.4.2. We see that in this situation the enhanced ratio of energy transfer is increasing as the radius is increasing for small a, and then it oscillates and decreases to 1 for large a. The wave picture presented in the last two Figs. is the result of the long distance coupling between two molecules near a long fiber. An excited surface mode offers a bridge for the energy transfer between the donor and the acceptor.

This mechanism becomes obvious when we look at Fig.4.5. Here the radius of the cylinder is a=1000 Å,

and $\rho_a/a = \rho_d/a = 1.05$. The distance between the two molecules varies from 100 Å to 15,000 Å, i.e., $z_{ad}/a = 0.1 \sim 15$. The frequency is $\hbar\omega = 3.62$ ev. A few interesting things should be noted, firstly the enhanced ratio R increases up to 10^5 as z_{ad} gets large, corresponding to the surface mode being excited. Secondly a series of periodic oscillations occur obviously with the period equal to $\lambda/2$, where λ is the wavelength, this corresponds to a standing wave picture. Thirdly we also see the saturation of $R(\omega)$ at some point. After that point $R(\omega)$ begin to decrease, corresponding to the decay of the surface modes that play a role in enhancing the energy transfer. Finally we see that two configurations, in which two molecules are perpendicular to the axis of the cylinder, have almost the same result for large a, corresponding to the fact that at large scales space really has only one special direction, $\hat{z}$, the other two directions are on an equal footing.

Let us turn to the other configurations. Fig.4.6 shows the relation between the enhanced ratio $R(\omega)$ and the frequency, but the positions of two molecules are different from Fig.4.2. Here we have

$$(\rho_a, \phi_a, z_a) = (105\ \text{Å}, 0^\circ, 0),$$

$$(\rho_d, \phi_d, z_d) = (105\ \text{Å}, 180^\circ, 0),$$

i.e., two molecules are on the opposite sides of the cylinder. The orientations of the molecules are shown in

the inset. We see that a sharp peak is presented again at $\hbar\omega$ =3.62 ev. The peculiar feature in this picture is that the enhanced ratio R is much higher than that in Fig.4.2. This could be understood from the fact that the enhanced ratio of energy transfer is due to the enhanced induced interaction between the real dipole and the image dipole in a static picture. In the configuration of Fig.4.2 the distance between the real dipole and the image dipole is larger than the one between two real dipoles; in Fig. 4.6 it is smaller than the distance between two real dipoles. Since the interaction is proportional to the inverse of the cube of the distance and the enhanced ratio is proportional to the inverse of the sixth order of the distance, the big difference between Fig.4.2 and 4.6 is understood. We also note that for the configuration that two dipoles are parallel to the surface but perpendicular to the axis of the cylinder the enhanced ratio in Fig.4.6 is not much higher than that in Fig.4.2. This is because the induced electric field, $E_\phi = \frac{1}{\rho}\partial_\phi \tilde{\Phi}$, is proportional to m, consequently there is no m=0 mode for E_ϕ.

The final picture for energy transfer is Fig.4.7. Here the two dipoles are again at opposite side of the cylinder as in Fig.4.6, but the distance between the molecules and the surface of the cylinder is varying from 5 Å to 200 Å. The enhanced ratio R is decreasing as the distance increases as expected.

We have discussed some properties of energy transfer. The characteristic property which differs from the one in Chapter III is the wave picture in long distance coupling. An excited surface wave, which is a standing wave for an infinitely long cylinder, plays a role for enhancing the coupling between two molecules and hence enhancing the energy transfer between them. This mechanism may find applications in technology.

To complete the discussion we present Fig.4.8, for nonradiative decay, and Fig.4.9, for radiative decay. We do see the resonance at $\hbar\omega = 3.62$ ev. This makes for a strong competition to the energy transfer. We have pointed out in Chapter III that in the case that the resonance frequency of the donor and the acceptor is different the competition may be weaker. On the other hand the decay rate of a single molecule has nothing to do with the distance between the two molecules, consequently the radiative and the nonradiative decay does not smear out the long distance coupling between two molecules.

References

For general references of energy transfer please see the references in Chapter III.

1. J. D. Jackson, "Classical Electrodynamics", 2nd edition, (Wiley, New York, 1975).
2. R. E. Collin, "Field Theory of Guided Waves", (McGraw-Hill, New York, 1966).
3. P. B. Johnson and R. W. Christy, Phys. Rev. B 6, 4370(1972).

Figure Captions

Fig.4.1 $(\omega_m/\omega_p)^2$ vs ka; based on the Eq.4.2.23. At low frequency only m=0 mode is excited, at $(\omega_m/\omega_p)^2=0.5$ all modes are excited.

Fig.4.2 Enhanced energy transfer ratio $R(\omega)$ vs. frequency $\hbar\omega$. The position of the donor is (105 Å, 0°,0), the position of the acceptor is (105 Å, 0°, a); the radius of the cylinder is a=100 Å. The distance between the two dipoles is z_{ad}=a. Three curves correspond to three different orientations of two dipoles as shown in the picture. Resonance occur at 3.62 ev for Ag corresponding to ϵ(3.62 ev)=-1.

Fig.4.3 Enhanced energy transfer ratio $R(\omega)$ vs. frequency. Same configuration as in Fig.4.2, curve 3, but the radius of the cylinder is different. curve 1 corresponds to a=1000 Å, and curve 2, a=5000 Å. The wave picture is obvious especially at high frequencies.

Fig.4.4 Enhanced energy transfer ratio $R(\omega)$ vs. a, the radius of the cylinder . $\hbar\omega$=2.01 ev, $\rho_a/a=\rho_d/a$=1.05, z_{ad}=a. Same configuration as in Fig.4.2. As radius a gets larger other relative distances also get larger, and the wave picture is more and more obvious. The distance between two peaks is $\lambda/2$.

Fig.4.5 Enhanced energy transfer ratio vs. the distance between two dipoles, z_{ad}. $\hbar\omega$=3.62 ev, $\rho_a/a=\rho_d/a$=1.05, a=1000Å. The standing wave picture of surface plasmon is quite clear.

Fig.4.6 Enhanced energy transfer ratio $R(\omega)$ vs. frequency. The position of the donor is (105 Å, 0°, 0), and the position of the acceptor is (105 Å, 180°,0). the radius of the cylinder is a=100 Å. Three orientations of the two dipoles are shown in the picture.

Fig.4.7 Enhanced energy transfer ratio $R(\omega)$ vs. the distances between the molecules and the surface of the cylinder. Same configurations as in Fig. 4.6, but $\rho_a = \rho_d$ is varying. $\hbar\omega = 3.62$ ev.

Fig.4.8 Nonradiative decay rate Γ_{nr} vs. frequency. The three curves correspond to three different orientations of the molecule as shown in the picture. The radius of the cylinder is a=100 Å, $\rho_d/a = 1.05$. The resonance occurs at 3.62 ev.

Fig.4.9 Enhanced radiative decay ratio vs. frequency. Same geometry as in Fig.4.8. The resonance occurs at 3.62 ev.

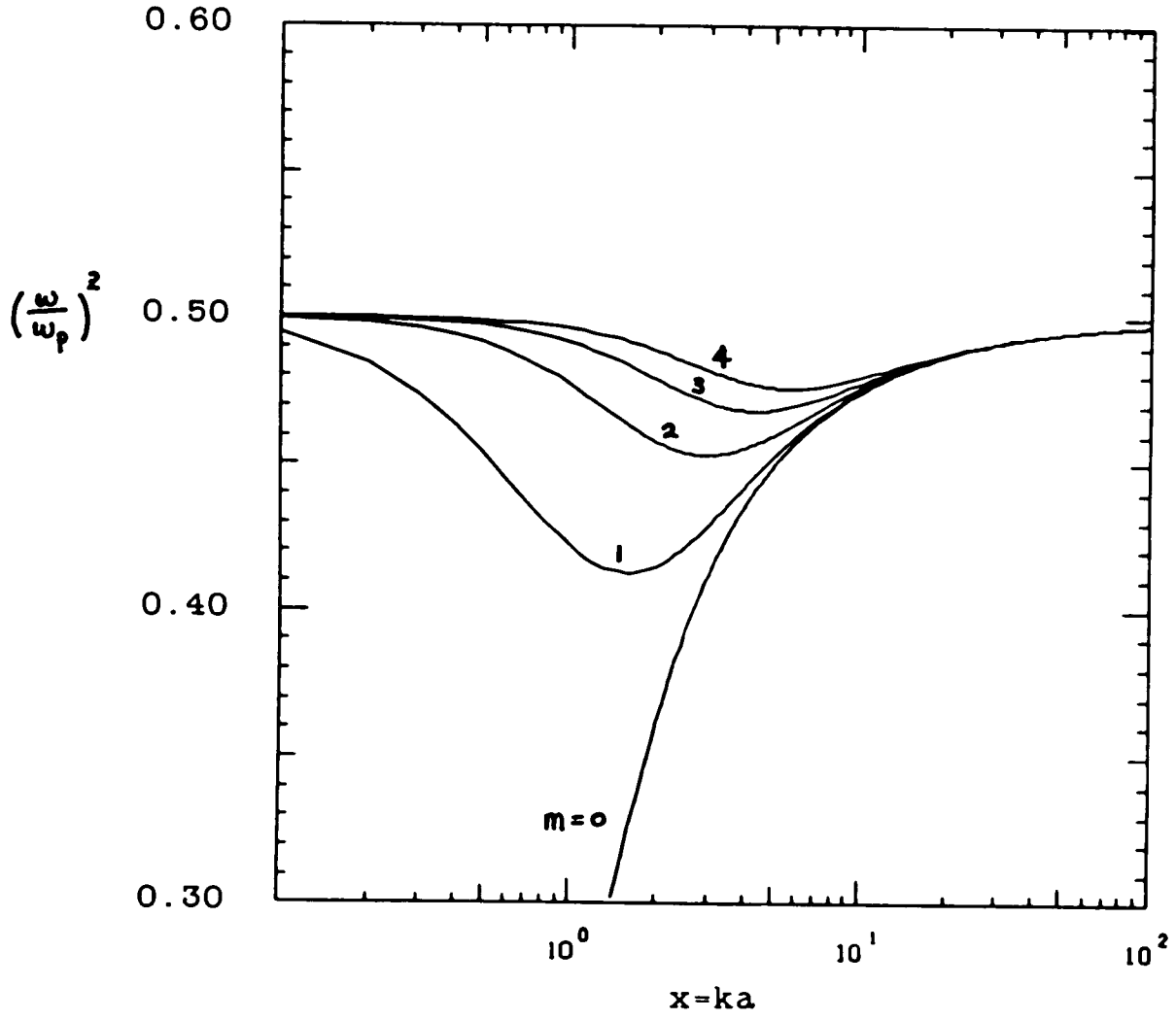
0.60
0.50
0.40
0.30
$\left(\frac{\omega}{\omega_p}\right)^2$
4
3
2
1
m=o
10^0
10^1
10^2
x=ka

Fig.4.1

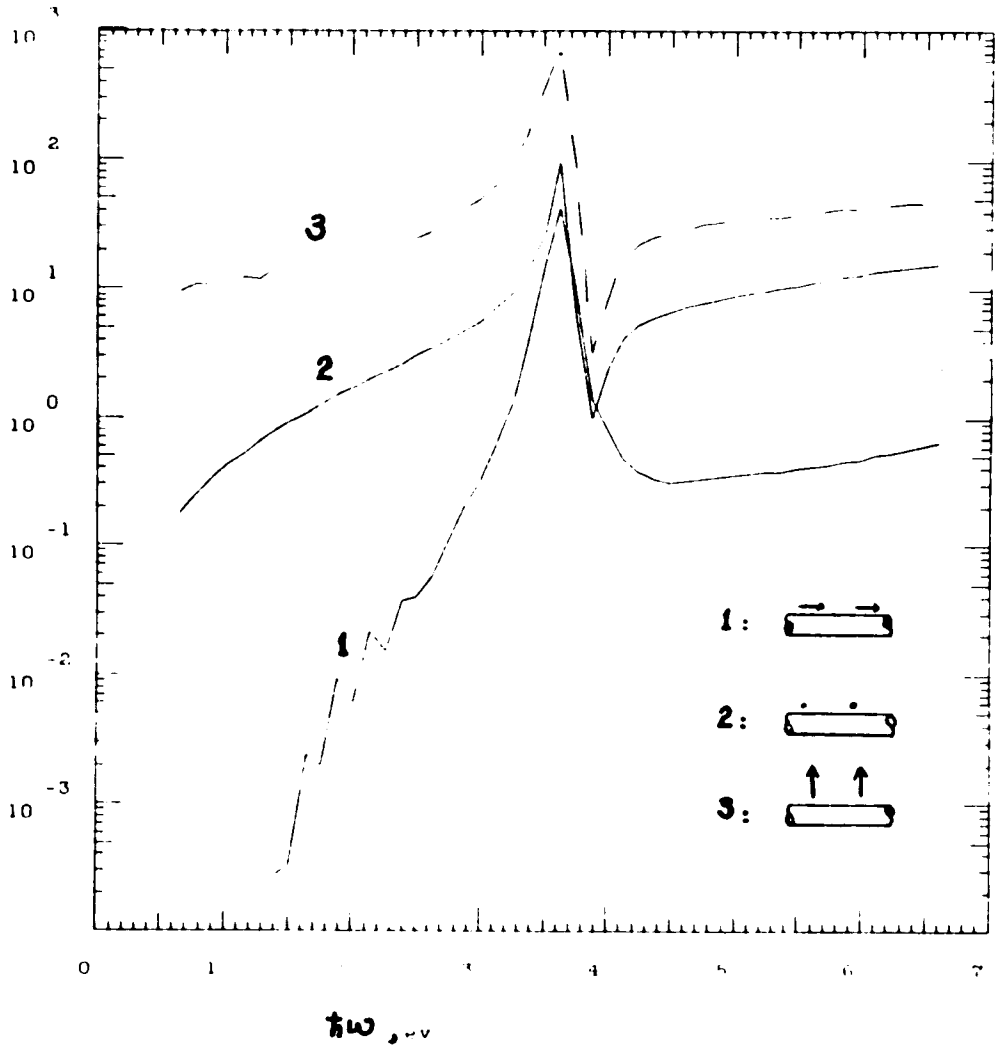

Fig. 4.2

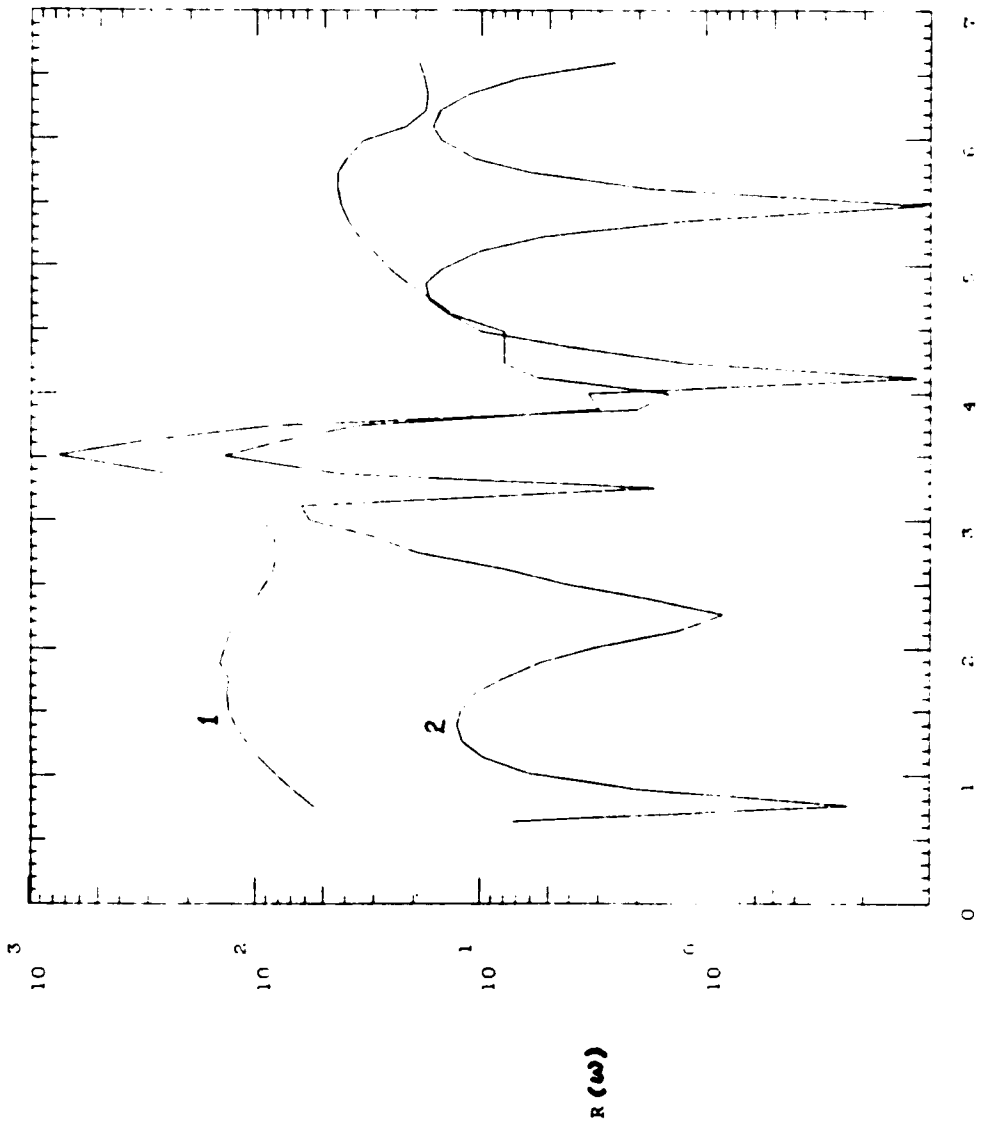

Fig. 4.3

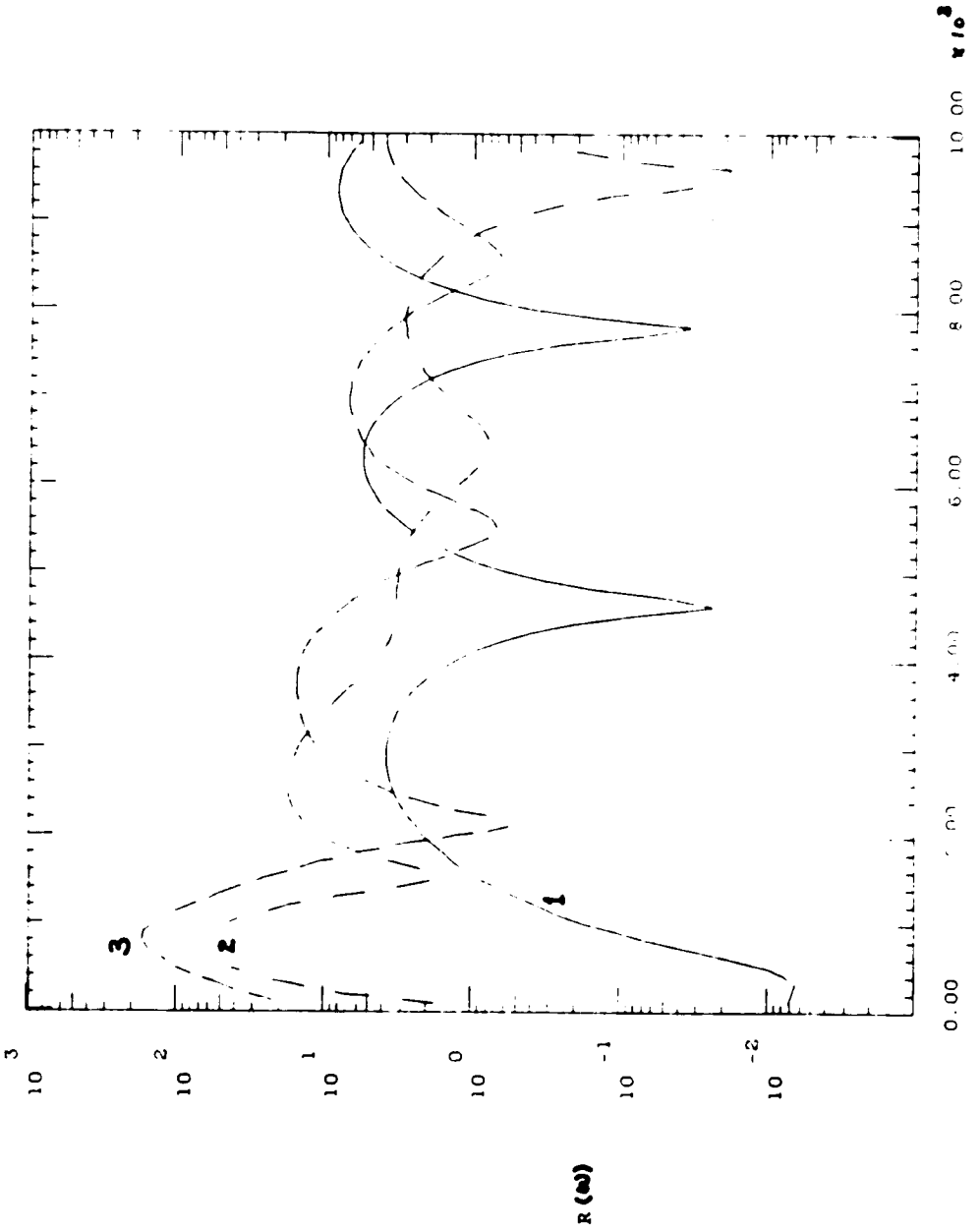

Fig. 4.4

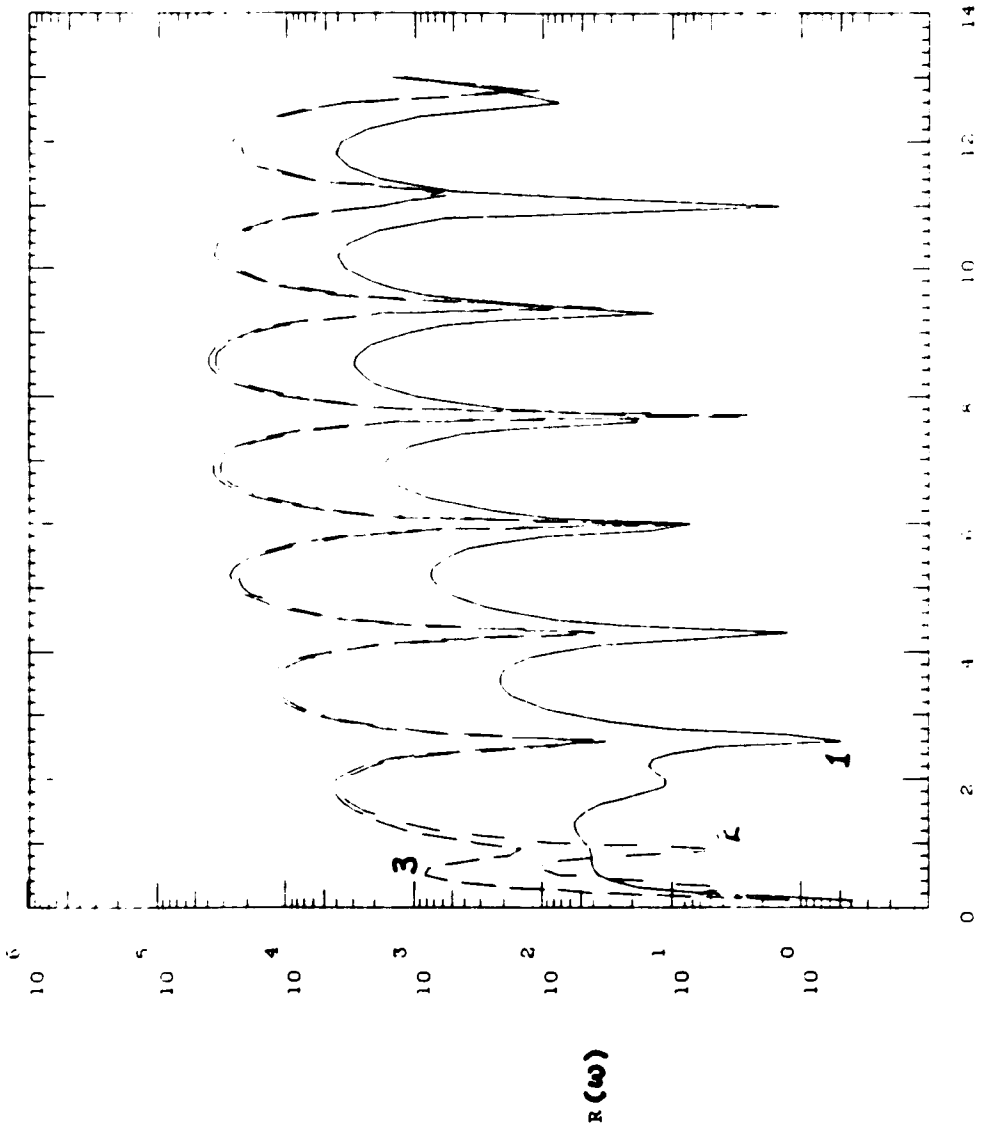

Fig.4.5

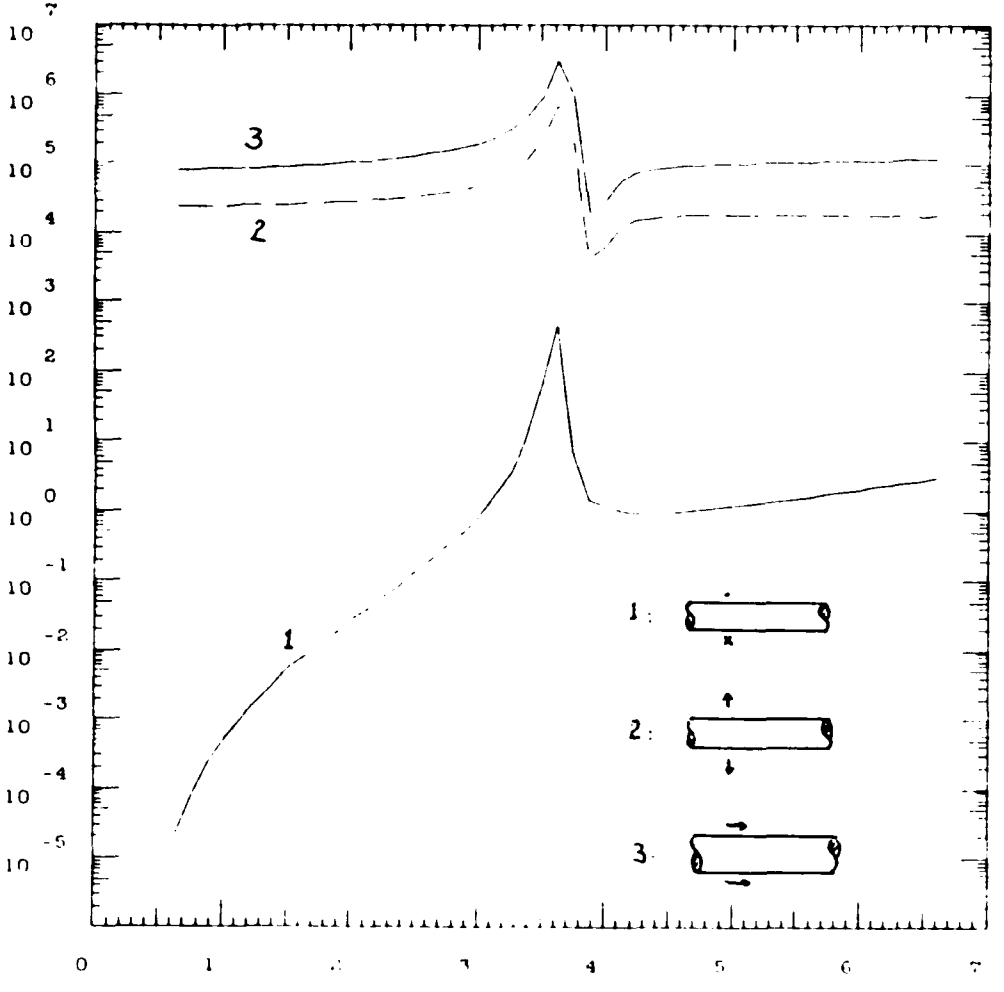
R(ω)
10^7
10^6
10^5
10^4
10^3
10^2
10^1
10^0
10^-1
10^-2
10^-3
10^-4
10^-5
0
1
4
5
6
3
2
1
1:
2:
3:
ħω ev

Fig.4.6

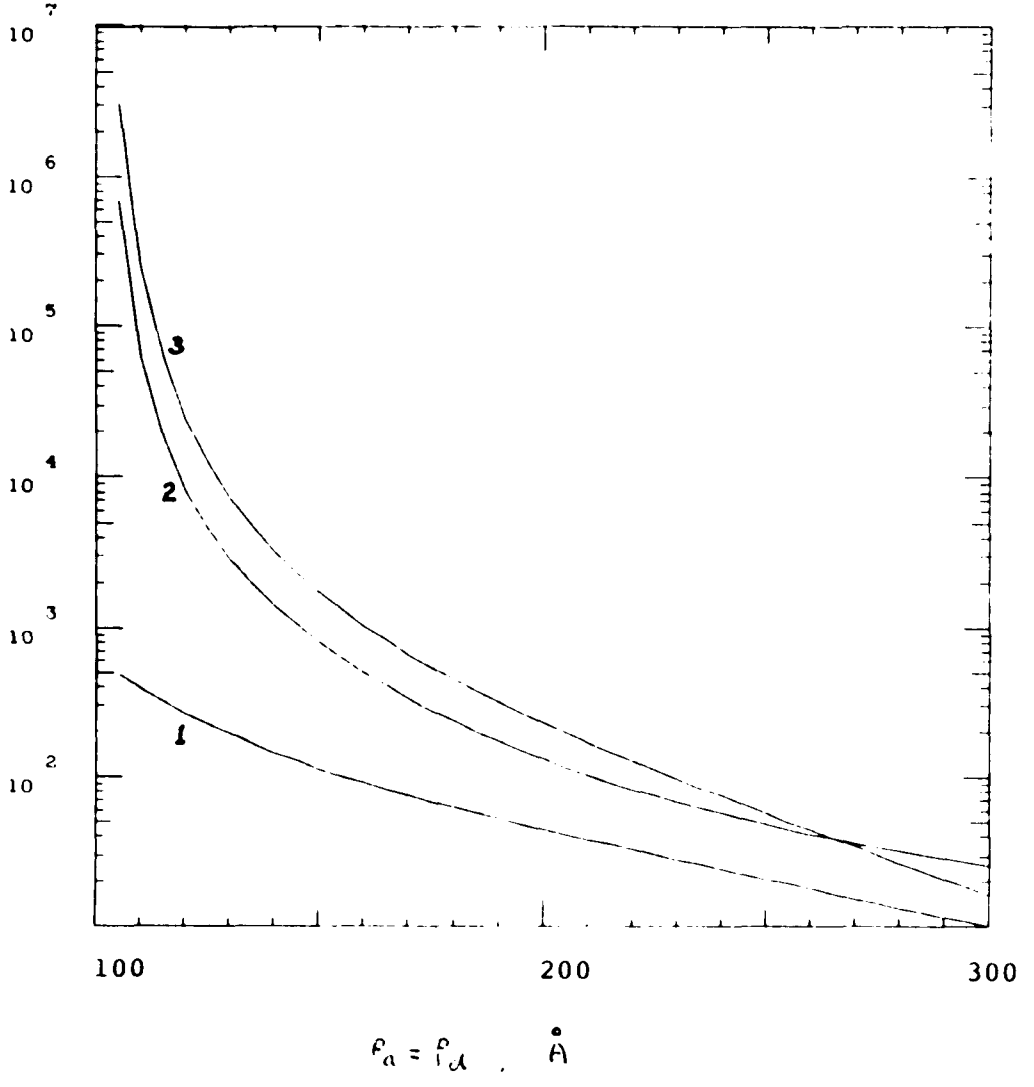

Fig. 4.7

Γ_{nr}, (arbitary units)
10^0
10^1
10^2
10^3
10^4
0
1
2
3
4
5
6
$\hbar\omega$, eV
1
2
3

Fig 1.8

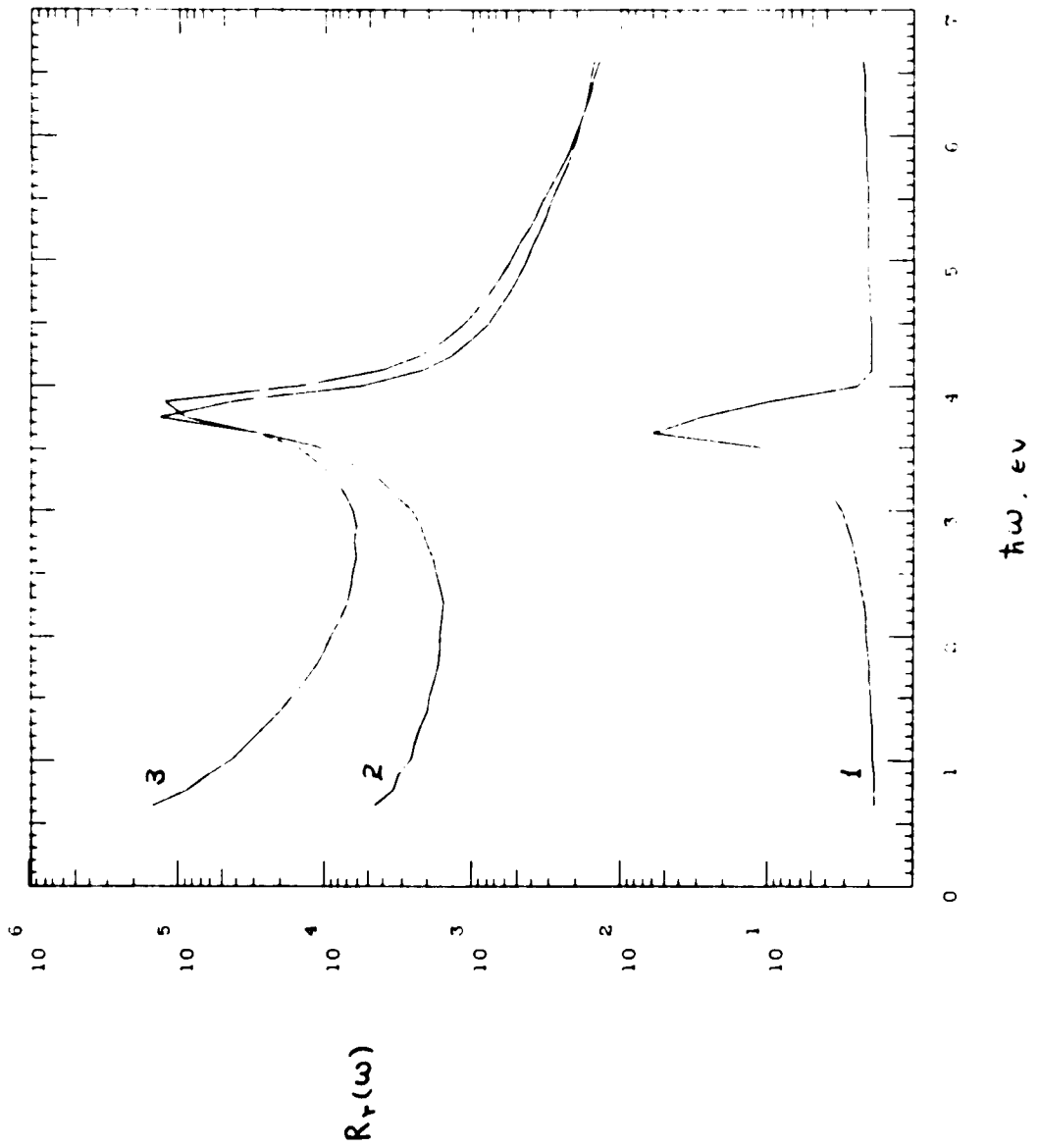

Fig. 4.9

Appendix. Program for Computing the Combinations of Bessel Functions

As is well-known one would be likely to encounter an overflow problem when computing a single Bessel function on a computer. One way to avoid the difficulty is to compute combinations of the Bessel functions. Fortunately, in some physics problems this is all we need. In this appendix a program for computing the combinations of Bessel functions $xJ_m'(x)/J_m(x)$, $xI_m'(x)/I_m(x)$, $xK_m'(x)/K_m(x)$, and $I_m(x)K_m(x)$ is presented for integer m. The output of the program has been checked with the PORT library, when it works, and also with the mathematical tables[1] for Bessel functions. The agreement between them is very good.

I. The principles for the program.

From the recursion relations of $J_m(x)$:

$$J_m'(x)=-(m/x)J_m(x)+J_{m-1}(x)=(m/x)J_m(x)-J_{m+1}(x),$$

and

$$J_{m-1}(x)+J_{m+1}(x)=(2m/x)J_m(x).$$

we could derive

$$[(m+1)/x+J_{m+1}'(x)/J_{m+1}(x)][(m/x)-J_m'(x)/J_m(x)]=1,$$

thus the recursion relation for computing $xJ_m'(x)/J_m(x)$ is

$$xJ_m'(x)/J_m(x)=m-x^2[m+1+xJ_{m+1}(x)/J_{m+1}(x)]^{-1}. \tag{1}$$

For $n >> x$, we have asymptotic form:

$$xJ_m'(x)/J_m(x)=m \quad . \tag{2}$$

Formulas (1) and (2) are the main principles needed in computing $xJ_m'(x)/J_m(x)$.

Since

$$xI_m'(x)/I_m(x)=ixJ_m'(ix)/J_m(ix) \ , \tag{3}$$

the same program could be used to compute $xI_m'(x)/I_m(x)$

The recursion relations for $K_m(x)$ are

$$K_m'(x)=-K_{m-1}(x)-(m/x)K_m(x)=-K_{m+1}(x)+(m/x)K_m(x)$$

and

$$-K_{m-1}(x)+K_{m+1}(x)=(2m/x)K_m(x).$$

From these one could get

$$[xK_m'(x)/K_m(x)-m][xK_{m+1}'(x)/K_{m+1}(x)+(m+1)]=1,$$

thus the recursion relation for $xK_m'(x)/K_m(x)$ is

$$xK_{m+1}'(x)/K_{m+1}(x)=-(m+1)+x^2[xK_m'(x)/K_m(x)-m]^{-1} \tag{4}$$

The formulas for $K_o(x)$, $K_1(x)$, $K_o'(x)$ and $K_1'(x)$ are available in a mathematical handbook[1]. With those and formula (4) one could program $xK_m'(x)/K_m(x)$.

Using the relation

$$I_m(x)K_m'(x)-I_m'(x)K_m(x)=-1/x,$$

one gets

$$[I_m(x)K_m(x)]^{-1}=xI_m'(x)/I_m(x)-xK_m'(x)/K_m(x) \tag{5}$$

Formula (5) is the principle used in computing $I_m(x)K_m(x)$.

II. The program.

```
      subroutine xdjoj( x0,m,xdjoj)
c     m=highest order of Jm(x) , xdjoj=xJ'(x)/J(x)
      complex x,x0 xdjoj(m+1),tj,cs,sj
      x=x0
      ax=cabs(x)
      a=ax/m
      pi=3.1415926
      if(a.ge.10.)goto 100
      if(a.le.0.1)goto 200
      if(a.gt.1.)goto 300
      if(a.le.0.1)goto 400
300   if(ax.lt.10.)goto 301
      n=2.*ax
      goto 302
301   n=ax+10
302   v=n
      tj=cmplx(v,0.)
10    tj=v-1.-x*x/(v+tj)
      v=v-1.
      n=v
      if(n.eq.-1)goto 41
      if(n.le.m)goto 11
      goto 10
11    xdjoj(n+1)=tj
      goto 10
400   if(m.lt.10)goto 401
      n=2*m
      goto 402
401   n=m+10
402   v=n
      tj=cmplx(v,0.)
      goto 10
200   n=m+20
      v=n
      tj=cmplx(v,0.)
      goto 10
100   if(m.gt.50)goto 101
      n=m+100
      v=n
      if(v.lt.ax)goto 102
```

```
      n=2*n
      v=n
      tj=cmplx(v,0.)
      goto 10
101   if(ax.gt.1000.)goto 102
      n=2.*ax
      v=n
      tj=cmplx(v,0.)
      goto 10
102   n=m+5
      v=n
      y=(0.5*v+0.25)*pi
      sj=cs(x)*cos(y)+sin(y)
      tj=-0.5+x*(-cos(y)+cs(x)*sin(y))/sj
      goto 10
41    continue
      return
      end

                complex function cs(x)
c     cs(x)=cos(x)/sin(x)
      complex x,cs,y,zx,xz,ui
      ui=cmplx(0.,1.)
      xi=aimag(x)
      y=2.*ui*x
      if(xi.gt.0.)goto 1
      if(xi.lt.0.)goto 2
      cs=ccos(x)/csin(x)
      goto 3
1     zx=cexp(y)
      cs=ui*(zx+1.)/(zx-1.)
      goto 3
2     xz=cexp(-y)
      cs=ui*(1.+xz)/(1.-xz)
3     continue
      return
      end
```

```
      subroutine xdioit(x0,m,xdioi)
c     m=highest order of Im(x), xdioi=xIm'(x)/Im(x)
      complex ui,x,x0,xdioi(m+1),dioim,xdjoj(1001),yy
      x=x0
      ui=cmplx(0.,1.)
      yy=ui*x
      call xdjojt(yy,m,xdjoj)
      do 1 n=1,m+1
      dioim=xdjoj(n)
1     xdioi(n)=dioim
      return
      end

      subroutine xdkokt(x0,m,xdkok)
c     m=highest order of Km(x), xdkok=xKm'(x)/Km(x)
      complex x,x0,xdkok(m+1),z,k1,k2,ui,i0,i1
      complex y,t,dkokm
      x=x0
      ui=cmplx(0.,1.)
      xr=real(x)
      ax=cabs(x)
      if(xr.lt.0.)goto 11
      goto 12
11    x=-x
12    y=x/2.
      z=2./x
      t=(x/3.75)**2
      if(ax.lt.2.)goto 10
      k1=1.25331414-.07832358*z+.02189568*z**2
      k1=k1-.01062446*z**3+.00587872*z**4
      k1=k1-.00251540*z**5+.00053208*z**6
      k2=1.25331414+.23498619*z-.03655620*z**2
      k2=k2+.01504268*z**3-.00780353*z**4
      k2=k2+.00325614*z**5-.00068245*z**6
      xdkok(1)=-x*k2/k1
      n=1
      goto 3
10    continue
      i0=1.+3.5156229*t+3.0899424*t**2
      i0=i0+1.2067492*t**3+.2659732*t**4
      i0=i0+.0360768*t**5+.0045613*t**6
```

```
      i1=0.5+.87890594*t+.51498869*t**2
      i1=i1+.15084934*t**3+.02658733*t**4
      i1=i1+.00301532*t**5+.00032411*t**6
      i1=x*i1
      k1=-clog(y)*i0-.57721566+.4227842*y**2
      k1=k1+.23069756*y**4+.0348859*y**6
      k1=k1+.00262698*y**8+.0001075*y**10
      k1=k1+.0000074*y**12
      k2=x*clog(y)*i1+1.+.15443144*y**2
      k2=k2-.67278579*y**4-.18156897*y**6
      k2=k2.01919402*y**8-.00110404*y**10
      k2=k2-.00004686*y**12
      xdkok(1)=-k2/k1
      n=1
3     continue
      v=n
      dkokm=-v+x*x/(xdkok(n)-v+1.)
      n=n+1
      if(n.gt.m+1)goto 41
      xdkok(n)=dkokm
      goto 3
41    if(xr.lt.0.)goto 42
      goto 43
42    x=-x
43    return
      end

                subroutine ikt(x0,m,ik)
c     m=highest order of I, K; ik=Im(x)Km(x)
      complex x,x0 ik(m+1),xdkok(1001),xdioi(1001),1f
      x=x0
      call xdkokt(x,m,xdkok)
      call xdioit(x,m,xdioi)
      do 1 n=1,m+1
      1f=xdioi(n)-xdkok(n)
1     ik(n)=1./1f
      return
      end
```

Reference

1. M. Abramowitz and I. Stegun, "Handbook of Mathematical Functions", (Dover, New York, 1965).